SOME RESONANCE CHARACTERISTICS OF LINEAR LEE WAVES IN A LAYERED ATMOSPHERE

by

Adrian Overton Pickersgill

A thesis submitted to the University of London for the degree of Master of Philosophy

January, 1976.

ABSTRACT

Emphasis has been given in the past in the study of lee waves on situations in which complete trapping occurs in the lower levels. More recently research has been conducted into models in which waves which are not completely trapped exist. This thesis describes some of the properties of a three layer stratosphere - troposphere model in which either type may exist. A comparison is made with a two layer tropospheric model when the stratospheric layer is very stable.

The object of this thesis is to investigate wave propagation in the atmosphere in terms of a linear theory of mountain lee waves, for varying degrees of stability in the troposphere and stratosphere.

Chapter one is a brief survey of some relevant theoretical work on the lee wave problem. In Chapter two a simple tropospheric model is considered, the waveguide problem. Chapter three is a lengthy discussion of the three layer troposphere-stratosphere model. When the stratosphere is very stable, a similarity exists with the waveguide problem of Chapter two. The fundamental properties of wave propagation into the stratosphere are discussed, and some attention is directed to wave propagation in the troposphere. Finally, Chapter four compares the results of this thesis with other predicted results, and with some lee wave observations.

The work of this thesis was conducted at the Mathematics Department, Imperial College of Science and Technology, under the supervision of Dr. F.H. Berkshire between October 1973 and January 1976. The author is indebted to him for his help and guidance. The author also wishes to thank Mr. P. Newton for his help with the computer programming,

which was performed on the Imperial College CDC 6400 machine.

CONTENTS

		Page
CHAPTER ONE	INTRODUCTION	
1.	A Survey of Relevant Theoretical Work	6
2.	Linear Two-dimensional Flows	11
CHAPTER TWO	A TWO-LAYERED TROPOSPHERIC MODEL WITH A RIGID LID AT THE TROPOPAUSE	
1.	The Equations of Motion	14
2.	The Eigenvalues in the Troposphere	22
3.	A Discussion of the Effects of Varying the Upper Scorer Parameter	24
4.	The Effects of a Variation in the Lower Tropospheric Depth	28
FIGURES		30
CHAPTER THREE	A THREE LAYER TROPOSPHERE-STRATOSPHERE MODEL FOR TWO-DIMENSIONAL FLOW OVER A MOUNTAIN	
1.	Introduction to Equations	31
2.	A consideration of the Amplitude Factor for $l_2 < l_3$ and $l_1 >> l_2$	33
3.	A Consideration of the Amplitude Factor for l_2 Greater than l_3 and $l_1 >> l_2$	39
4.	The Effects of Varying the Middle Scorer Parameter on the Amplitude Factor Beams when $l_1 >> l_2$	43
5.	A Discussion of the Amplitude Factor when S is large compared with $\mathcal{L}$.	49
6.	Some Numerical Results and the Influence of Complex Poles	52

Page

7. THE QUASI WAVE DRAG INTEGRAL 61

Tables 66

Figures 75

CHAPTER FOUR A DISCUSSION OF THE ADAPTATION OF SOME REALISTIC ATMOSPHERIC PROFILES INTO LAYERS IN WHICH THE ℓ PARAMETER IS CONSTANT

1. Introduction 125

2. Gales in Yorkshire 1962 127

3. Gales in Boulder 1972 130

4. The Colorado Lee-wave Program 1968 132

5. Conclusion 133

Tables 134

Figures 136

REFERENCES 143

CHAPTER ONE

INTRODUCTION

1. A Survey of Relevant Theoretical Work

When air flows over a mountain ridge stationary atmospheric waves are established which fall into one of three types.

1. Short waves of period much smaller than half a day are gravity waves.
2. Longer waves of period comparable with a half day are gravity-inertia waves.
3. The longest waves with periods much larger than this time interval are planetary waves of the Rossby-wave type.

Mountains of small extent in the direction of flow will excite only gravity waves, however, mountain ranges of continental scale will excite all types of waves.

The gravity-type waves were first examined by Lord Rayleigh (1883) and Lord Kelvin (1886, 1887). Kelvin considered the stationary waves produced on the surface of a running stream by either an elevation or depression of the stream bed. Both authors realised the uniqueness of the solution for speeds in excess of a critical velocity, but for speeds below this velocity they observed that a train of gravity waves existed. The authors considered a solution such that gravity waves should not appear upstream of the obstacle.

Atmospheric lee waves differ from lee waves on a running stream since the fluid is of infinite extent, because the vertical stratification of the basic flow is not abrupt. The first systematic observations of

ascending currents in the lee of hills were those sponsored by the German Glider Research Institute dating from 1928. However, the most extensive field study appears to have been the 'Sierra Wave Project' (Holmboe and Klieforth 1957) wherein lee-wave amplitude of 2,000 metres, and vertical currents of 25m/sec are reported. A survey of these and other observations from both a theoretical and observational point of view can be found in two technical notes by the World Meteorological Organization, Queney et al. (1960) and J. M. Nicholls (1973). An account of the damage caused locally in Sheffield by lee waves appears in Aanensen (1965).

The earliest theoretical work dealing with lee waves in a stratified flow was by Lyra (1943) and Queney (1947). Lyra used a Green's function method to evaluate the flow over a small ridge of rectangular cross-section, while Queney used a line disturbance on the ground. The results of these investigations give waves behind the ridge, with amplitudes which decrease with height, and disappear for large distances downstream. The type of solution in which the stability is constant will be referred to as the Lyra type solution.

Scorer (1949) was the first author to introduce a multi-layered atmosphere. He considered a two-layered atmosphere in each of which the parameter

$$\ell^2 = \frac{g\beta}{U^2} - \frac{U''}{U} \qquad (1.1)$$

was held constant. Here g is the acceleration due to gravity, U(z) is the air velocity, and β is the static stability parameter of the atmosphere defined by

$$\beta = \frac{\theta'}{\theta} \tag{1.2}$$

where θ is the potential temperature. Primes are used throughout to denote differentiation with respect to z. Scorer used the Fourier Transform method and discovered that a wave occurred which did not decay in the downstream direction provided.

$$l_1^2 - l_2^2 > \frac{\pi^2}{4h^2} \tag{1.3}$$

Here l_1 is the value of the parameter l in the upper layer which extends to infinity, while l_2 is its value in the lower layer of depth h. Scorer further noticed that two waves of differing wavelengths occurred provided

$$l_1^2 - l_2^2 > \frac{9\pi}{4h^2} \tag{1.4}$$

The type of layered atmosphere which is divided into two strata, the upper layer of which has infinite depth, in which l is constant in both layers, and such that l decreases with height is called the Scorer model. l is referred to as the Scorer parameter. Scorer did not recognize that significant decaying waves also exist in his model, which decay quickly downstream, but may increase in amplitude, and produce substantial wave motion in the stratosphere. Their importance was recognized by Berkshire and Warren (1970), among others. They discussed a two-layer model with the upper Scorer parameter greater than that near to the ground. l was kept constant in both layers. This model is sometimes referred to as the Berkshire model, in which no wholly trapped waves occur, but wave activity nevertheless exists.

The three-layer model atmosphere has been discussed by various authors. However, the equations involved are considerably more complicated than its two-layer counterpart, and it is usually necessary to

evaluate directly on the computer. Sawyer (1960) describes a method for the evaluation of a continuously stratified atmosphere on the computer using a finite difference method. A three layer model with an intermediate layer of neutral stability ($\ell = 0$) was discussed by Berkshire and Warren (1970), and some of the models discussed in this thesis can be considered as an extension to this work for atmospheres in which the intermediate layer has varying, non-zero, stability.

In Corby and Sawyer (1958) a four layer model is discussed and compared with a two layer model. However, all except three waves of long wavelength were of negligible amplitude. These three wavelengths were predicted by examining the corresponding two layer atmosphere. Two of these wavelengths were found by introducing a rigid lid near to the tropopause, while the third was found by examining the relevant two layer unbounded Scorer model.

An important discussion in the study of lee-waves has arisen because of the choice of upper boundary condition. The hypothesis of no upstream influence has been accepted by all writers on linearised atmospheric lee-waves. These waves generated by an obstacle transport momentum downstream. This momentum transport is compensated by a downwind drag on the obstacle. Scorer (1949, 1953, 1954, 1956, 1958) chose a solution which was subsequently shown to yield negative drag, and is consequently wrong. This solution requires the selection of a square root which determines whether the momentum is transported downstream or not, and will be referred to again in Chapter Three.

The lower boundary condition is determined by the shape of the ground. We limit our discussions to those aspects of the lee-wave

problem that fall within the lee-wave regime. This regime is determined by the parameter NH/U, where N(z) is the Brunt-Vaisala frequency, and H is a typical vertical length scale. The upper limit of the lee wave regime is determined by the appearance of local density inversions and flow reversals at some critical value. These regions are designated as rotors and tend to invalidate the lower boundary conditions. In other words when a rotor is formed at ground level in the leeward of a hill, the ground shape can be considered as incorporating the rotor. The lower limit of the regime is determined as $NH/U \rightarrow 0$, and corresponds to potential flow over an obstacle.

2. Linear Two-Dimensional Flows

In order to obtain tractable mathematical models of the stratified flow over mountain barriers, certain assumptions have to be made about the atmosphere. It was mentioned in section (1.1) that the parameter $\frac{NH}{U}$ which is in effect an inverse froude number must not be greater than a critical value, in order for lee waves to exist.

The Richardson number is defined by

$$Ri(z) = \left(N(z)/U'(z)\right)^2 \qquad (2.1)$$

and in order for shear to be negligible we assume that $Ri(z) \gg 1$. It was discussed by Miles (1961) that a sufficient condition for stability of the basic flow for very small disturbances is $Ri(z) > \frac{1}{4}$. However, no condition exists for finite amplitude disturbances.

A parameter involving rotational effects is the Rossby number, which we define by

$$R_o = \frac{U}{\Omega H} \qquad (2.2)$$

Here Ω is the Coriolis parameter, and is such that $\frac{1}{2}\Omega$ is the vertical component of the earth's angular velocity. We assume that $R_o \gg 1$ so that the earth's rotation may be ignored. The coriolis parameter is typically of the order 10^{-4} sec^{-1}, and it is not an unreasonable assumption for the lee-waves that will be considered in this thesis. However, for lee-wave trains on a continental scale, such as in the Sierra Nevada, rotation cannot be ignored.

The flow is idealised as being isentropic, in which the potential temperature of a fluid parcel remains constant. This assumption neglects the effect of condensation, which is not always true in the

atmosphere since clouds sometimes accompany lee-waves. It is possible to incorporate condensation into the model by defining the Brunt frequency in terms of the wet adiabatic lapse rate as in Miles (1969).

An important assumption to be made is that the velocities of the air motions are small compared with the velocity of sound. This is a reasonable assumption since the velocity of sound in air is about 330 m sec^{-1} and U is about 10m sec^{-1} at a height of five hundred metres above the ground. (Taken from Scorer 1949).

We proceed by deriving the relevant equation which describes the flow along the lines of linearized perturbation theory. This is the Helmholtz equation which for two dimensional flow is given by

$$\left(\frac{\partial^2}{\partial x^2} + \frac{\partial^2}{\partial z^2}\right)\overline{\mathcal{S}}(x, z) + \ell^2(z)\overline{\mathcal{S}}(x, z) = 0 \qquad (2.3)$$

The notation used is that x is the downstream coordinate, z is the vertical coordinate with the ground taken to be at $z = -1$, and $\overline{\mathcal{S}}$ is a modified streamline displacement related to the actual displacement by

$$\overline{\mathcal{S}}(x, z) = \left[\frac{\overline{\rho}(z)}{\overline{\rho}(-1)}\right]^{\frac{1}{2}} \frac{U(z)}{U(-1)} \mathcal{S}(x, z) \qquad (2.4)$$

Here $\overline{\rho}(z)$ is the air density at height z, and $\overline{\rho}(-1)$ is the air density at the ground.

A drawback of the linearised perturbation theory is that we need to relate the actual streamline displacement to the vertical perturbation velocity w(x, z) by

$$w(x, z) = U(z)\frac{\partial \mathcal{S}}{\partial x}(x, z) \qquad (2.5)$$

This implies that the streamline slope is small. However, Scorer (1955) has derived (2. 3) without the assumption of small displacements, and

indeed when U'/U is very small there is no restriction on the slope at all. We assume that U'/U is small so that it is possible to investigate the disturbances produced by a delta function mountain as discussed in the next chapter.

CHAPTER TWO

A TWO LAYERED TROPOSPHERIC MODEL WITH A RIGID LID AT THE TROPOPAUSE

1. The Equations of Motion

In theoretical studies of the atmosphere attention has been given to layered stratosphere-troposphere models consisting of two, three or even four layers, in which the top layer is unbounded. It is of important theoretical interest to investigate whether the main characteristics associated with these models are determined by tropospheric conditions alone, and only modified by the stratosphere. One of the aims of this thesis is to compare a three layer stratospheric model with a simpler tropospheric model consisting of either one or two layers, the top surface of which is a rigid lid situated at a finite height which designates the upper limit of the atmosphere. In this chapter we consider a two layer model, some attention will be given to a one layer model in Chapter Three.

The main assumptions which we make about the flow are linearised equations, isentropic and laminar flow, neglect of earth's rotation and viscosity and consideration of a time independent problem. The flow is two-dimensional, with x the downstream coordinate, z the vertical co-ordinate, and the notation:

basic unperturbed quantities (functions of height z only.)

$\overline{p}$	pressure
$\overline{\rho}$	density
$(U, 0)$	velocity

perturbation quantities

p	pressure
ρ	density
(u, w)	velocity

We neglect products of perturbation quantities in comparison with the products of unperturbed quantities.

The equations of motion are:

$$\bar{\rho}\, U \frac{\partial u}{\partial x} + \bar{\rho}\, U' w = -\frac{\partial p}{\partial x} \tag{1.1}$$

$$\bar{\rho}\, U \frac{\partial w}{\partial x} = -\frac{\partial p}{\partial z} - g\rho \tag{1.2}$$

The equation of continuity is:

$$\bar{\rho}\left(\frac{\partial u}{\partial x} + \frac{\partial w}{\partial z}\right) + U \frac{\partial \rho}{\partial x} + \bar{\rho}' w = 0 \tag{1.3}$$

We consider the entropy of a fluid parcel to remain constant. The equation of state is thus

$$U \frac{\partial p}{\partial x} + w\bar{p}' - c^2 \left(U \frac{\partial \rho}{\partial x} + w\bar{\rho}'\right) = 0 \tag{1.4}$$

A prime denotes that the quantity has been operated on by $\frac{d}{dz}$, g is the gravitational acceleration, and c is the speed of sound in the fluid.

In the derivation of (1.2) the pressure $\bar{p}$ has been related to its density $\bar{\rho}$ by the hydrostatic condition

$$\bar{p}' = -g\bar{\rho} \tag{1.5}$$

The quantities $\bar{p}$, ρ, u can be eliminated from (1.1) to (1.4) to obtain a single equation in terms of w,

$$\frac{\partial}{\partial z}\left\{\frac{U\bar{\rho}}{c^2-U^2}\left[c^2\frac{\partial w}{\partial z} - (UU' + g)w\right]\right\}$$

$$+\frac{g\bar{\rho}}{U(c^2-U^2)}\left[c^2\frac{\partial w}{\partial z} - (UU' + g)w\right] + \bar{\rho}\,U\frac{\partial^2 w}{\partial x^2}$$

$$-\frac{g}{U}\frac{\partial}{\partial z}(\bar{\rho}\,w) - \frac{\partial}{\partial z}(\bar{\rho}\,U'w) = 0 \qquad (1.6)$$

For typical values in the atmosphere we make the approximation $c^2 >> U^2$ $c^2 >> \left|UU'\frac{\bar{\rho}}{\bar{\rho}'}\right|$, $g >> \left|UU'\right|$ so that (1.6) becomes

$$\left(\frac{\partial^2}{\partial x^2} + \frac{\partial^2}{\partial z^2}\right) w + \frac{\bar{\rho}'}{\bar{\rho}}\frac{\partial w}{\partial z} + \left(\frac{g\beta}{U^2} - \frac{U''}{U}\right) w = 0 \qquad (1.7)$$

Here β is the stability parameter defined by

$$\beta = -\frac{\bar{\rho}'}{\bar{\rho}} - \frac{g}{c^2} = \frac{\theta'}{\theta} \qquad (1.8)$$

as was introduced in section (1.1). The restoring force on a parcel of air displaced vertically a distance $\mathcal{S}$ is $g\beta\mathcal{S}$, which means that $(g\beta)^{\frac{1}{2}}$ is the natural frequency with which it would oscillate if it were frictionless, and did not become deformed, i.e. the Brunt-Vaisala frequency as introduced in Chapter one.

We now transform (1.7) from an equation involving the perturbation velocity to the streamline displacement defined by

$$w(x,z) = U(z)\frac{\partial}{\partial x}\mathcal{S}(x,z) \qquad (1.9)$$

The limitations imposed by this equation were discussed in Section (1.2). It is more convenient to introduce the modified streamline displacement defined by

$$\bar{\mathcal{S}}(x,z) = \left[\frac{\bar{\rho}(z)}{\bar{\rho}(-1)}\right]^{\frac{1}{2}}\frac{U(z)}{U(-1)}\mathcal{S}(x,z) \qquad (1.10)$$

so that (1.9) becomes

$$w(x,z) = U(-1)\left[\frac{\bar{\rho}(-1)}{\bar{\rho}(z)}\right]^{\frac{1}{2}}\frac{\partial}{\partial x}\bar{\mathcal{S}}(x,z) \qquad (1.11)$$

On substituting for w into (1.7) we obtain a single equation in terms of $\overline{\mathcal{J}}$,

$$\frac{\partial}{\partial x}\left\{ \frac{\partial^2}{\partial x^2}\overline{\mathcal{J}} + \frac{\partial^2}{\partial z^2}\overline{\mathcal{J}} + \overline{\mathcal{J}}\left[\frac{g\beta}{U^2} - \frac{U''}{U} + \frac{1}{2}\overline{R}' - \frac{1}{4}\overline{R}^2\right]\right\} = 0 \qquad (1.12)$$

Here $\overline{R} = -\frac{\overline{\rho}'}{\overline{\rho}} = -\frac{d}{dz}(\log \overline{\rho})$ (1.13)

This parameter has the physical significance of being the Brunt Vaisala frequency for incompressible flow divided by the acceleration due to gravity. For the atmosphere it can be assumed that the coefficients of $\overline{R}$ and $\overline{R}'$ are negligible in comparison with the other terms involving $\overline{\mathcal{J}}$. It was discussed in the previous chapter that the terms in $\overline{\mathcal{J}}$ are referred to as the Scorer parameter defined by

$$\ell^2(z) = \frac{g\beta}{U^2} - \frac{U''}{U} \qquad (1.14)$$

We assume that $U(z) > 0$ at all levels, so that no critical levels exist at which ℓ would be infinite.

On integrating (1.12) and substituting from (1.14), we invoke the condition that $\overline{\mathcal{J}} = 0$ at large distances upstream of the mountain and we arrive at the Helmholtz equation given by:-

$$\frac{\partial^2}{\partial z^2}\overline{\mathcal{J}} + \frac{\partial^2}{\partial x^2}\overline{\mathcal{J}} + \ell^2(z)\overline{\mathcal{J}} = 0 \qquad (1.15)$$

The geometry of the model to be used (Fig. 1) has the zero of the z coordinate at the tropopause, and the height is scaled with the depth of the troposphere, so that the ground is situated at $z = -1$. In all the subsequent work, the length unit will be taken to be the tropopause depth, which is of order 10 kilometres for the atmosphere, and this length is used to non-dimensionalise all lengths, wavenumbers and ℓ parameters. In this chapter we consider a simple troposphere model

which is split into two layers. ℓ given by (1.14) is considered to be constant in each layer with a simple discontinuity at the interface, the upper layer is denoted by the suffix 2, and the lower layer is denoted by the suffix 3. (The reason for this notation is so that the equations can be transferred to Chapter Three, where we will introduce a stratosphere with suffix 1.) The axes are chosen so that the centre of the ridge is at x = 0.

We define the Fourier transform $\tilde{\bar{\psi}}$ of $\bar{\psi}$ by

$$\bar{\psi}(x, z) = \int_{-\infty}^{\infty} dk\, e^{ikx}\, \tilde{\bar{\psi}}(k, z) \tag{1.16}$$

so that

$$\tilde{\bar{\psi}}(k, z) = \frac{1}{2\pi} \int_{-\infty}^{\infty} dx\, e^{-ikx}\, \bar{\psi}(x, z) \tag{1.17}$$

Similar relations hold between the mountain shape f(x) and its transform $\tilde{f}(k)$. The significance of the parameter k is that it is the non-dimensionalised wave-number, related to the wavelength, λ, of a mode by $\lambda = \frac{2\pi}{k}$.

The lower boundary condition on $\bar{\psi}(x, z)$ is that the mountain shape should be a streamline. Thus $\tilde{\bar{\psi}}(k, -1) = \tilde{f}(k)$, and we can replace $\tilde{\bar{\psi}}(k, z)$ by $\frac{F(k, z)}{F(k, -1)}\, \tilde{f}(k)$, where F(k, z) satisfies the equation

$$F'' + (\ell^2 - k^2) F = 0 \tag{1.18}$$

On making the above substitution (1.16) becomes

$$\bar{\psi}(x, z) = \int_{-\infty}^{\infty} dk\, e^{ikx}\, \tilde{f}(k)\, \frac{F(k, z)}{F(k, -1)} \tag{1.19}$$

It is possible to rewrite (1.19) in terms of a Green's function $G(x, z:, \xi_3)$. We define this function by

$$G(x, z; \xi) = \mathrm{Re} \int_0^\infty dk\, e^{ik(x-\xi)} \frac{F(k, z)}{F(k, -1)} \tag{1.20}$$

so that its Fourier transform is given by

$$G(x, z; \xi) = \int_{-\infty}^{\infty} dk\, e^{ik\xi} \tilde{G}(x, z, k) \tag{1.21}$$

On applying Parsevals theorem, which can be written as

$$\int_{-\infty}^{\infty} d\xi\, f(\xi)\, G(x, z; \xi)$$

$$= 2\pi \int_{-\infty}^{\infty} dk\, \tilde{f}(k)\, \tilde{G}(x, z, -k) \tag{1.22}$$

it is possible to rewrite (1.19) as

$$\bar{\zeta}(x, z) = \frac{1}{\pi} \int_{-\infty}^{\infty} d\xi\, f(\xi)\, G(x, z, \xi) \tag{1.23}$$

If we consider the mountain shape given by a delta function then $f(x) = \delta(x)$ and $\tilde{f}(k) = \frac{1}{2\pi}$, then the function $G(x, z)$ where

$$G(x, z) \equiv G(x;\ z;\ 0) \tag{1.24}$$

can be envisaged as π times the modified displacement. The function $G(x, z)$ is termed the influence function.

Throughout most of this thesis we will consider a delta function mountain situated at the point $(0, -1)$, all wavenumber disturbances are excited equally. However, it is possible to excite certain waves unequally, when a more realistic mountain profile is introduced. For example if $f(x) = \frac{Ha^2}{(a^2+x^2)}$ then $\tilde{f}(k) = \frac{1}{2} Ha \exp(-|k|\, a)$. The small wavenumbers are excited more than the larger ones, and in particular, the wavenumber k, which is the inverse of the ridge half width a is stimulated the most.

As mentioned earlier ℓ is considered to be constant in each of the two layers. At the interface between the layers, there is an abrupt change in the stability parameter, β, but both the density and fluid velocity U are continuous. It is found that $F(k, z)$ and $\frac{\partial F(k, z)}{\partial z}$ are continuous across this interface at $z = -h$.

In the rigid lid tropopause model the perturbation velocity vanishes at the boundaries, so that (1.18) must satisfy

$$F(k, -1) = 0 \tag{1.25}$$

$$F(k, 0) = 0 \tag{1.26}$$

for discrete wavenumber solutions to (1.18).

The solution to (1.18) must be of the form

$$F(k, z) \propto \sin \nu_2 z \qquad 0 \geq z > -h \tag{1.27}$$

$$F(k, z) \propto \frac{-\sin \nu_2 h}{\sin \nu_3 (1-h)} \sin \nu_3 (z+1) \qquad -h \geq z > -1 \tag{1.28}$$

where the proportionality can include wavenumber k dependence. Since (1.25) is satisfied the following equation is derived:-

$$\frac{\tan \nu_3 (1-h)}{\nu_3} + \frac{\tan \nu_2 h}{\nu_2} = 0 \tag{1.29}$$

Here
$$\left.\begin{aligned} \nu_j &= (\ell_j^2 - k^2)^{1/2} \text{ if } k < \ell_j \\ &= i\mu_j = i(k^2 - \ell_j^2)^{1/2} \text{ if } k > \ell_j \end{aligned}\right\} \tag{1.30}$$

The parameter j takes the value 2 in the upper layer $z > -h$, and 3 in the lower layer. This choice of square root is immaterial for this model since reflection takes place from the rigid boundaries and wave motion which is both upward and downward propagating will occur. However, we choose it this way for consistency with the three layer unbounded

atmospheric model of the next chapter in which the choice of square root is determined by the upper boundary condition.

Equation (1.19) and (1.20) are not defined since $F(k,-1) = 0$ for discrete wavenumbers k. Consequently the integrand has singularities at these points, and needs to be evaluated by deforming the contour of integration into the complex k plane, see eg. Scorer (1949). A discussion of $\overline{\mathcal{G}}(x,z)$ and the related influence function will be postponed to Chapter Three where the function $|F(k,-1)|$ will be discussed in detail. We consider equation (1.29) for the rest of this chapter. This equation will be referred to as the eigenvalue equation and if we take $\ell_2 = 0$, it corresponds with equation 35 of Berkshire and Warren (1970).

2. The Eigenvalues in the Troposphere

Equation (1.29) is an eigenvalue equation which determines discrete wavenumbers, k, which may exist in the troposphere. The reality of k^2 with the boundary conditions of (1.25) and (1.26) will now be demonstrated. We multiply the complex conjugate of (1.18) by F, and (1.18) by F^*, and on subtracting we derive the equation

$$\frac{d}{dz}\left[F^* \frac{dF}{dz} - F\frac{dF^*}{dz}\right] + (k^{*2} - k^2)\,|F|^2 = 0 \qquad (2.1)$$

An asterisk is used to denote a complex conjugate in this section. On integrating (2.1) throughout the whole troposphere, since F and $\frac{\partial F}{\partial z}$ are differentiable near all the interfaces we obtain the equation

$$(k^{*2} - k^2)\left[\int_{-1}^{0} |F|^2\, dz\right] = 0 \qquad (2.2)$$

on utilising the boundary conditions. This implies that for non-identically zero F, k^2 must be real.

For simplicity of presentation we consider the Scorer parameter to decrease with height so that $\ell_3 > \ell_2$, and define two different types of real eigenvalue. An external mode in a layer is one in which the wavenumber, k, is greater than the Scorer parameter ℓ, in that layer. An internal mode in a layer is one in which the wave number, k, is less than the Scorer parameter ℓ, in that layer.

Wavenumbers which are internal to the bottom layer, but external to the upper layer are Scorer modes, so that these may exist for $\ell_2 < k < \ell_3$. No convenient name exists for modes which are external to the bottom layer and internal to the top layer, when $\ell_2 > \ell_3$.

For wavenumbers greater than both ℓ_2 and ℓ_3, equation (1.29)

can be written as

$$\frac{\tanh \mu_3 (1-h)}{\mu_3} + \frac{\tanh \mu_2 h}{\mu_2} = 0 \qquad (2.3)$$

No real wavenumber solutions exist for (2.3), consequently the largest wavenumbers that may exist are those which are external to one layer and internal to the other. In contrast, by Sturm Liouville analysis, it is found that there is an infinite set of negative k^2, i.e. imaginary wavenumbers.

When $\ell_3 > \ell_2$, the equation for Scorer modes becomes

$$\frac{\tanh \mu_2 h}{\mu_2} + \frac{\tan \nu_3 (1-h)}{\nu_3} = 0 \qquad (2.4)$$

The first solution occurs in the range $\frac{\pi}{2} < \nu_3 (1-h) < \pi$, while the second eigenvalue lies in the range $\frac{3\pi}{2} < \nu_3 (1-h) < 2\pi$. In consequence, the depth of the lower troposphere and the value of ℓ in this layer determine the number of Scorer modes that may exist. In particular if $\frac{1}{2}(1-h) \geq \pi$ then a Scorer type mode must exist satisfying (2.4), where

$$\frac{1}{2}^2 = \ell_3^2 - \ell_2^2 \qquad (2.5)$$

If $\frac{1}{2}(1-h) > \frac{\pi}{2}$, then a Scorer type mode may exist. This last result was obtained by Scorer (1949), although in his model, the upper layer was not bounded at the tropopause, and (1.29) is slightly modified.

3. A Discussion of the Effects of Varying the Upper Scorer Parameter

An important result can be found if we consider a variation in ℓ_2, with h and ℓ_3 kept constant. In order for the eigenvalue equation to be identically satisfied, (equation 1.29), the wavenumbers must depend critically on this parameter. The equation which relates the change in the Scorer parameter to ν, can be deduced from the definition (1.30) as

$$\nu_3^2 - \nu_2^2 = \ell_3^2 - \ell_2^2 = \$^2 \tag{3.1}$$

On differentiating (3.1) and (1.29) with respect to ℓ_2, and eliminating the terms in $\frac{d\nu_2}{d\ell_2}$ between these two differentiated equations, we obtain the following:-

$$\frac{d\nu_3}{d\ell_2}\left[\frac{(1-h)}{\nu_3}\left(\sec^2 X - \frac{1}{X}\tan X\right) + \frac{\nu_3 h}{\nu_2^2}\left(\sec^2 Y - \frac{\tan Y}{Y}\right)\right]$$

$$+ \frac{\ell_2 h}{\nu_2^2}\left(\sec^2 Y - \frac{\tan Y}{Y}\right) = 0 \tag{3.2}$$

where
$$\left.\begin{aligned}\nu_3(1-h) &= X\\ \nu_2 h &= Y\end{aligned}\right\} \tag{3.3}$$

For non zero real values of w, we use the relationship $\frac{\sin w}{w} < 1$ to obtain

$$\sec^2 w - \frac{\tan w}{w} > 0 \tag{3.4}$$

provided cos w $\neq$ 0, at which values equation (1.29) is singular. Equation (3.2) together with (3.4) imply that $\frac{d\nu_3}{d\ell_2}$ is negative, or that as ℓ_2 increases for constant ℓ_3 and h, the eigenvalues k, also increase.

The analysis is similar for wavenumbers greater than ℓ_3, if

we consider the effects of increasing ℓ_2 beyond the value ℓ_3. Equation (3.2) transposes into

$$\frac{d\mu_3}{d\ell_2}\left[\frac{(1-h)}{\mu_3}\left(\operatorname{sech}^2 X - \frac{\tanh X}{X}\right) + \frac{\mu_3 h}{\mu_2^2}\left(\operatorname{sech}^2 Y - \frac{1}{Y}\tanh Y\right)\right] - \frac{\ell_2 h}{\mu_2^2}\left(\operatorname{sech}^2 Y - \frac{\tanh Y}{Y}\right) = 0 \tag{3.5}$$

where
$$\left.\begin{aligned}\mu_3(1-h) &= X\\ \mu_2 h &= Y\end{aligned}\right\} \tag{3.6}$$

For non-zero values of w, the relationship

$$\operatorname{sech}^2 w - \frac{\tanh w}{w} < 0 \tag{3.7}$$

holds. Consequently we deduce from (3.5) that $\frac{d\mu_3}{d\ell_2}$ is positive, and as ℓ_2 increases the eigenvalues also must increase.

When k equals ℓ_3, the analysis fails. However (1.29) transforms into

$$\frac{\tan \nu_2 h}{\nu_2} + (1-h) = 0 \tag{3.8}$$

and this is true only for discrete values of ℓ_2 for constant h and k. Moreover, if we change ℓ_2 from such a solution by a small amount, then no solution will exist for that particular value of h and k satisfying (3.8).

A similar analysis can be applied to the differentials of (3.1) and (1.29) to obtain an equation in $\frac{d\nu_2}{d\ell_2}$, by eliminating $\frac{d\nu_3}{d\ell_2}$. It is found that $\frac{d\nu_2}{d\ell_2}$ is positive and $\frac{d\mu_2}{d\ell_2}$ is negative.

The conclusion is that as we increase ℓ_2 from zero to a value greater than ℓ_3, keeping ℓ_3 and h constant, the real eigenvalues

increase towards ℓ_3, but less rapidly than the increases in ℓ_2. A Scorer mode becomes internal to both layers when the eigenvalue equation (1.29) transposes into

$$\tan \$ (1-h) = -h \$ \tag{3.9}$$

When ℓ_2 increases to the value ℓ_3, all the real modes are internal to both layers and are found from the equation

$$\frac{\sin \nu}{\nu} = 0 \tag{3.10}$$

The solution of which is $\nu = n\pi$, $n = 1, 2, 3, \ldots$ These solutions will be referred to as an index ordered set. The solution corresponding to $n = 1$ is the first eigenvalue. When ℓ_2 increases beyond ℓ_3, internal modes become external to the lower troposphere for a solution of

$$\tan S (1-h) = -hS \tag{3.11}$$

where $$\nu_2^2 - \nu_3^2 = \ell_2^2 - \ell_3^2 = S^2 \tag{3.12}$$

As ℓ_2 increases from zero, the imaginary poles approach the origin. An eigenvalue is situated at the origin when (1.29) transposes into

$$\frac{\tan \ell_2 h}{\ell_2} + \frac{\tan \ell_3 (1-h)}{\ell_3} = 0 \tag{3.13}$$

When ℓ_2 increases beyond a value ℓ_{20} satisfying (3.13), a real eigenvalue increases in wavenumber from zero. The next imaginary pole reaches the origin if we increase ℓ_2 by approximately $\frac{\pi}{h}$. To be precise, when ℓ_2 has increased to the next solution of

$$\frac{\tan X}{X} = K \tag{3.14}$$

where $X = \ell_2 h$

$$K = -\frac{\tan \ell_3 (1-h)}{\ell_3 h} \tag{3.15}$$

and K is a constant. This function is tabulated in the National Bureau of Standards (1964) for K in the range $-1 \leq K \leq 0$ and K^{-1} in the range $-1 \leq K \leq 1.0$.

4. The Effects of a Variation in the Lower Tropospheric Depth

A result which is analogous to that derived in the last section can be obtained if we allow the intermediate tropospheric depth h to vary, keeping ℓ_2 and ℓ_3 constant. The wavenumbers, k, depend on h, and vary with a change in that parameter. We differentiate (1.29) and (3.1) with respect to h, and after eliminating terms in $\frac{d\nu_2}{dh}$, we obtain the relationship

$$\frac{d\nu_3}{dh}\left[\left(\frac{(1-h)}{\nu_3}\right)(\sec^2 X - \frac{\tan X}{X}) + \frac{h\nu_3}{\nu_2^2}\ (\sec^2 Y - \frac{\tan Y}{Y}) \right]$$

$$-\frac{\tan^2 X}{\nu_2^2 \nu_3^2}\left[\ell_3^2 - \ell_2^2 \right] = 0 \qquad (4.1)$$

where X and Y are defined by (3.3). Consequently $\frac{d\nu_3}{dh}$ has the same sign as $\ell_3^2 - \ell_2^2$, if ℓ_3 is greater than ℓ_2, the eigenvalues decrease, when the depth of the upper troposphere layer, h, is increased, and vice versa. A similar result is obtainable for Scorer modes in the range $\ell_2 < k < \ell_3$.

The conclusion is that it is possible to tune the eigenvalue model by varying ℓ_2 or h, keeping all other quantities except k constant, in order to produce eigenvalues at the origin which satisy (3.13), or eigenvalues which are neither internal or external in a given layer, i.e. $k = \ell$, which satisfies equation (3.9) or (3.11).

There is a duality in equation (1.29) which will be referred to again in the next chapter. If we interchange ℓ_2 and h with ℓ_3 and (1-h), (1.29) is unchanged, and the eigenvalues are unaltered. We can deduce that by varying ℓ_3 keeping ℓ_2 and h constant, the eigenvalues change in a similar fashion as that described in section three. However,

there seems to be enough scope in considering only one of the tropospheric Scorer parameters to vary, and in most of the numerical work of Chapter Three ℓ_3 is held constant, while graphs are drawn for a variation in ℓ_2 and h.

FIG. 1 The two-dimensional (x, z) tropospheric model with an upper layer between z = -h, and the tropopause z = 0, and a lower layer between z = -h, and the ground at z = -1. The x coordinate is positive downstream measured from the centre of the ridge in the lower troposphere.

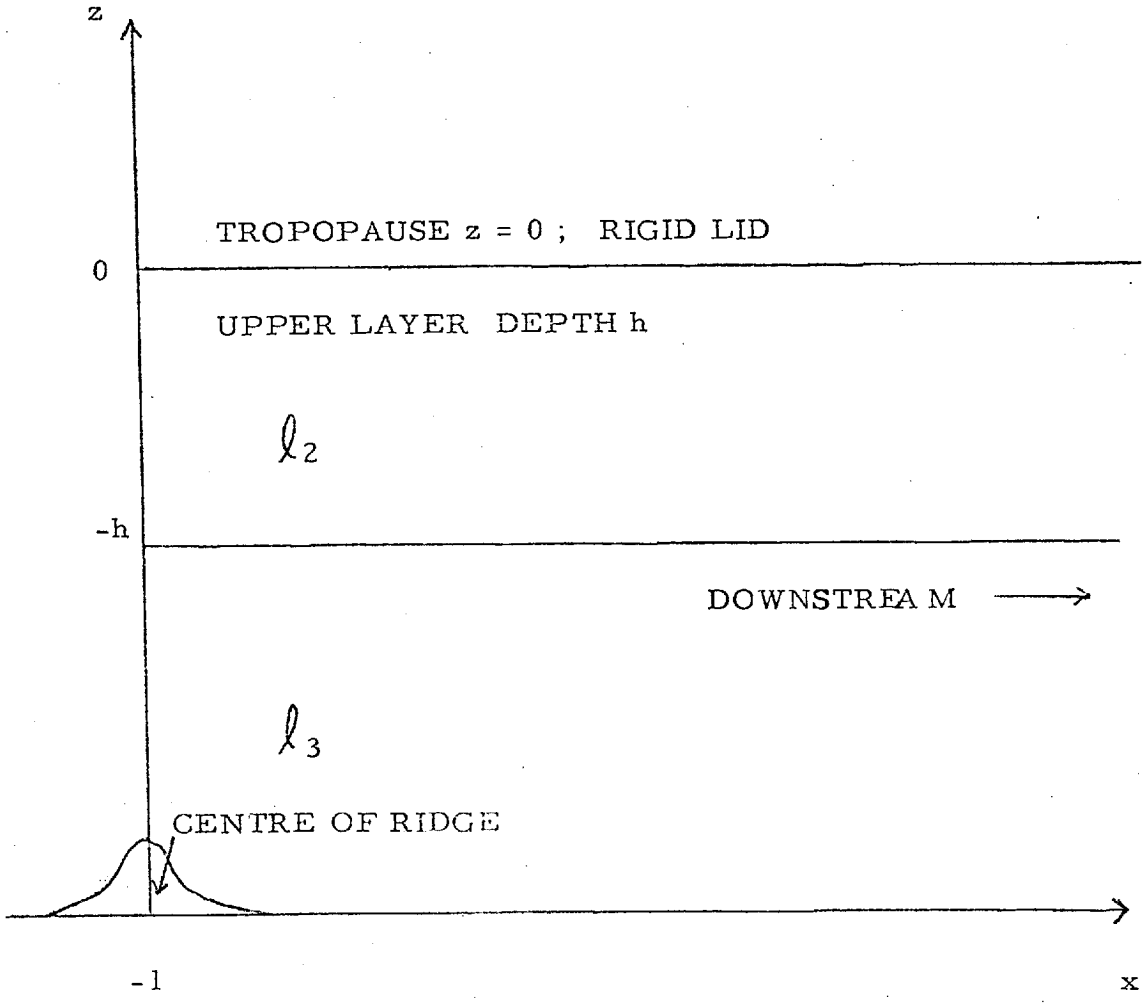

CHAPTER THREE

A THREE LAYER TROPOSPHERE-STRATOSPHERE MODEL FOR TWO-DIMENSIONAL FLOW OVER A MOUNTAIN

1. Introduction to Equations

The model (Fig. 1) that we consider in this chapter is structured in the troposphere in the same way as that considered in Chapter Two. The difference is the stratosphere which is modelled to extend to infinite height from the tropopause at z = 0. For most of this chapter, the Scorer parameter ℓ_1 is considered to be large compared with its value in the troposphere. A discussion for ℓ_1 smaller than ℓ_2 and for a value between ℓ_2 and ℓ_3 is given in section six of this chapter.

F is taken to be of the form

$$F = A \cos \nu z + B \sin \nu z \tag{1.1}$$

in the troposphere. In the stratosphere the condition for outward propagating energy implies that F is given by

$$\left.\begin{aligned} F &= \exp(i\nu_1 z) \qquad k < \ell_1 \\ F &= \exp(-\mu_1 z) \qquad k > \ell_1 \end{aligned}\right\} \tag{1.2}$$

This choice of the branch of the square root is that required by the radiation condition at the upper boundary (see chapter 1.1). As in the tropospheric model of Chapter Two, F(k, z) and $\frac{\partial F}{\partial z}(k, z)$ are considered continuous at the interfaces at z = h and z = 0. When $\ell_1 \gg \ell_2$ and $\ell_1 \gg \ell_3$, the zeros of F(k, -1) are all complex, and F(k, z) does not vanish at the ground for real wavenumbers.

The influence function for this model is given by

$$G(x, z) = \mathrm{Re} \int_0^\infty dk\, e^{ikx} \frac{F(k, z)}{F(k, -1)} \tag{1.3}$$

where $F(k, z)$ takes the following form for the three layers

$$F(k, z) = e^{i\nu_1 z} \qquad z > 0 \tag{1.4a}$$

$$F(k, z) = \cos \nu_2 z + \frac{i\nu_1}{\nu_2} \sin \nu_2 z \qquad 0 \geq z \geq -h \tag{1.4b}$$

$$F(k, z) = \cos \nu_2 h \cos \nu_3 (z+h) + \frac{\nu_2}{\nu_3} \sin \nu_2 h \sin \nu_3 (z+h)$$

$$- i\nu_1 \left\{ \frac{\sin \nu_2 h}{\nu_2} \cos \nu_3 (z+h) - \frac{\cos \nu_2 h}{\nu_3} \sin \nu_3 (z+h) \right\}$$

$$-1 \leq z < -h \tag{1.4c}$$

and $F(k, -1)$ is found by putting $z = -1$ in (1.4c). Here

$$\left.\begin{aligned} \nu_j &= (\ell_j^2 - k^2)^{\frac{1}{2}} \quad \text{for real } k < \ell_j \\ \nu_j &= i\mu_j = i\,(k^2 - \ell_j^2)^{\frac{1}{2}} \quad \text{for real } k > \ell_j \end{aligned}\right\} \tag{1.5}$$

In the following sections much attention will be given to the function

$$\left|F(k, -1)\right|^2 = (\ell_1^2 - \ell_2^2)\left[\frac{\sin \nu_2 h}{\nu_2} \cos \nu_3 (1-h) + \cos \nu_2 h \frac{\sin \nu_3 (1-h)}{\nu_3}\right]^2$$

$$+1 - \frac{(\ell_3^2 - \ell_2^2)}{\nu_3^2} \sin^2 \nu_3 (1-h) \tag{1.6}$$

which has similar but contrasting properties for the two cases of ℓ_2 greater or less than ℓ_3. The term $\frac{1}{|F(k, -1)|}$ is called the amplitude factor.

2. A Consideration of the Amplitude Factor for $\ell_2 < \ell_3$ and $\ell_1 >> \ell_2$

In this section we consider the solution of the influence function for large distances into the stratosphere. This expression is defined by

$$G(x,z) = \mathrm{Re} \int_0^\infty dk\, e^{ikx} \frac{F(k,z)}{F(k,-1)} \tag{2.1}$$

where in the stratosphere F takes the form

$$F(k,z) = e^{i\nu_1 z} \qquad z > 0 \tag{2.2}$$

and at the ground F is obtained from the following

$$F(k,-1) = \cos \nu_2 h \cos \nu_3(1-h) - \frac{\nu_2}{\nu_3} \sin \nu_2 h \sin \nu_3(1-h)$$

$$- i\nu_1 \left[\left\{ \frac{\sin \nu_2 h}{\nu_2} \cos \nu_3(1-h) \right\} + \frac{\cos \nu_2 h}{\nu_3} \sin \nu_3(1-h) \right] \tag{2.3}$$

We make the following substitution

$$\left.\begin{aligned} k &= \ell_1 \sin\theta \\ x &= r\cos\alpha \\ z &= r\sin\alpha \end{aligned}\right\} \tag{2.4}$$

so that $\nu_1 = \ell_1 \cos\theta$ and (2.1) transforms into

$$G(r,\alpha) = \mathrm{Re}\ \ell_1 \int_L \frac{d\theta \cos\theta\, e^{i r \ell_1 \sin(\theta+\alpha)}}{F(k)} \tag{2.5}$$

L is the path in the complex θ plane as shown in figure 2. Since ℓ_1 is large, the poles of $F(k,-1)$ are all complex, and by the method of stationary phase (2.5) transposes into

$$G(r,\alpha) \sim \mathrm{Re} \left\{ \left(\frac{2\pi \ell_1}{r}\right)^{\frac{1}{2}} \left(\frac{z}{r}\right) e^{i(r\ell_1 - \pi/4)} / F(k^*, -1) \right\} \tag{2.6}$$

where $k^{*} = \ell_1 \cos\alpha$ (2.7)

The function $F(k^{*}, -1)$ deserves further consideration and its properties will be analysed further. It is convenient to consider the amplitude factor $1/|F(k^{*}, -1)|$ given by

$$|F(k,-1)|^2 = \mathcal{L}^2\left[\frac{\sin\nu_2 h}{\nu_2}\cos\nu_3(1-h) + \cos\nu_2 h\ \frac{\sin\nu_3(1-h)}{\nu_3}\right]^2 + 1 - \frac{\$^2}{\nu_3^2}\sin^2\nu_3(1-h) \tag{2.8}$$

when k is less than ℓ_2, and its corresponding form for $\ell_2 < k < \ell_3$

$$|F(k,-1)|^2 = \mathcal{L}^2\left[\frac{\sinh\mu_2 h}{\mu_2}\cos\nu_3(1-h) + \cosh\mu_2 h\ \frac{\sin\nu_3(1-h)}{\nu_3}\right]^2 + 1 - \frac{\$^2}{\nu_3^2}\sin^2\nu_3(1-h) \tag{2.9}$$

Here
$$\left.\begin{aligned}\mathcal{L}^2 &= \ell_1^2 - \ell_2^2\\ \$^2 &= \ell_3^2 - \ell_2^2\end{aligned}\right\} \tag{2.10}$$

Examining $|F|$ instead of F introduces a phase factor which is a function of α. The motion has a radial wavelength of $\frac{2\pi}{\ell_1}$ and the amplitude of the solution is determined by the behaviour of $1/|F|$. The reciprocal of (2.8) and (2.9) is mostly small except near values which satisfy

$$\left.\begin{aligned}\frac{\tan\nu_2 h}{\nu_2} + \frac{\tan\nu_3(1-h)}{\nu_3} &= 0 \qquad k < \ell_2\\ \frac{\tanh\mu_2 h}{\mu_2} + \frac{\tan\nu_3(1-h)}{\nu_3} &= 0 \qquad \ell_3 > k > \ell_2\end{aligned}\right\} \tag{2.11}$$

These equations were discussed in Chapter Two and they determine the real or imaginary modes that exist in a tropospheric model with a rigid lid at the tropopause. When this occurs (2.8) contracts into

$$|F(k,-1)|^2 = 1 - \frac{\$^2}{\nu_3^2} \sin^2 \nu_3(1-h) \qquad (2.12)$$

which using (2.11) implies

$$\frac{1}{|F(k,-1)|^2} = 1 + \$^2 \frac{\sin^2 \nu_2 h}{\nu_2^2} \qquad (2.13)$$

Consequently the height of the beams of the amplitude factor is approximately given by (2.13).

If we take ℓ equal to zero, which is equivalent to considering a two strata atmosphere as first introduced by Scorer (1949), (2.9) transposes into (2.12). Consequently an important result is that for all wavenumbers less than ℓ_2, the peaks of the amplitude factor created by our three layer system have the same value as that produced by the Scorer model with ℓ_1 equal to ℓ_2. Examples on the variation of ℓ_1 of the amplitude factor are given in the numerical results section. The amplitude factor for wavenumbers which do not satisfy the eigenvalue relationship (2.11) is considerably smaller for this atmosphere than it would be for the corresponding Scorer model.

By changing the upper tropospheric depth, h, it is possible to 'tune' the amplitude factor beams so that their height reaches a maximum. There is a relationship between ν_2 and ν_3, which we obtain from (1.5) as

$$\nu_3^2 - \nu_2^2 = \$^2 \qquad (2.14)$$

On differentiating (2.14), (2.11) and (2.13) with respect to h and eliminating the terms in $\frac{d\nu}{dh}$ we acquire the following equation for a maximum in the height of the amplitude factor beams:-

$$\$^2 \left(-\frac{h}{\nu_2^2} + \frac{\tan \nu_2 h}{\nu_2^3} \right) = 1 \qquad (2.15)$$

When $\nu_2 \neq 0$ it can be alternatively written as

$$\frac{\tan \nu_2 h}{\nu_2 h} - 1 = \frac{\nu_2^2}{\$^2 h} \tag{2.16}$$

It is evident that (2.16) always has a solution for $\nu_2 h$ between $\nu_2^{\varkappa} h^{\varkappa} < \nu_2 h < n\pi + \frac{\pi}{2}$ where n is a positive integer and $\nu_2^{\varkappa} h^{\varkappa}$ satisfies $\tan \nu_2^{\varkappa} h^{\varkappa} = \nu_2^{\varkappa} h^{\varkappa}$. An analysis of the derivative of (2.16) with respect to h reveals that there is exactly one solution for $\nu_2 h$ in each of these ranges. The first of these solutions must satisfy

$$4.493 < \nu_2 h < 4.712.$$

When $\nu_2 h$ is large $\nu_2^{\varkappa} h^{\varkappa}$ tends to $n\pi + \frac{\pi}{2}$, and the beam is tuned to its maximum height for $\nu_2 h \approx (n + \frac{1}{2})\pi$. The square of the amplitude factor is then given by

$$\frac{1}{|F(k,-1)|^2} = 1 + \frac{\$^2 h^2}{((n+\frac{1}{2})\pi)^2} \tag{2.17}$$

to a good approximation. Equation (2.16) can be rewritten as

$$\$^2 \left(\frac{h}{\mu_2^2} - \frac{\tanh \mu_2 h}{\mu_2^3} \right) = 1 \tag{2.18}$$

for wavenumbers greater than ℓ_2. By a consideration of higher derivatives of (2.18) and (2.16) it can be shown that there is exactly one value of h (and subsequently k) which either satisfies (2.18) or (2.16) for $\nu_2 h < \frac{\pi}{2}$ or $k = \ell_2$. When this maximum occurs at $k = \ell_2$, (2.18) resolves into

$$h = \sqrt[3]{\frac{3}{\$^2}} \tag{2.19}$$

together with the eigenvalue relationship

$$\frac{\tan \$ (1-h)}{\$} = -h \tag{2.20}$$

Minima of the amplitude factor beams occur for values of h and k

which satisfy

$$\frac{\sin \nu_2 h}{\nu_2} = 0 \qquad (2.21)$$

together with (2.11). There is a minimum for h = 0 at which the beam height is unity, and for h = 1. Further minima exist for solutions of

$$\nu_2 h = n\pi \qquad (2.22)$$

where n is a positive integer. (2.22) implies that minima may occur for intermediate values of h, at all of which the amplitude factor has unit height.

It was discussed in Chapter Two that the effect of increasing h was to decrease the eigenvalues. We can now summarise the above results. As h increases from zero, all the amplitude factor beams increase from Unity. A beam which for small h is a Scorer mode, may produce its highest peak for wavenumbers less than, greater than or equal to ℓ_2. The first beam has exactly one maximum, whether it is a Scorer or internal mode, since when h equals one, $\nu_2 h$ which is an increasing function with h, has only increased to π. The second beam will have one minimum for a value of h not equal to zero or one, and two maxima, at least one of which is for a wavenumber which is internal to ℓ_2. In general the nth peak will have n maxima, at least (n-1) occurring for k less than ℓ_2, and (n+1) values of h which include zero and one, at which the peak is a minimum.

If we consider the Scorer parameters and the upper tropospheric depth as constant, (2.13) may be used to compare the height of the different beams produced by the model. Equation (2.13) transforms for

wavenumbers greater than ℓ_2, into

$$\frac{1}{|F(k,-1)|^2} = 1 + \phi^2 \frac{\sinh^2 \mu_2 h}{\mu_2^2} \tag{2.23}$$

This is a positive and monotonically increasing function with k such that $\frac{1}{|F(k,-1)|^2} \geq 1 + \phi^2 h^2$, and the beams with larger wavenumbers have taller peaks. This is true also for $0 < k < \ell_2$ when $\ell_2 h < \pi$. Equation (2.13) is a positive and monotonically increa sing function with k such that $1 < \frac{1}{|F(k,-1)|^2} < 1 + \phi^2 h^2$. If $\ell_2 h > \pi$ then it is possible in the range $0 < k < \ell_2$, for beams with smaller wavenumbers to have taller peaks than beams with larger wavenumbers. These beams will not be as tall as those for $\ell_2 < k < \ell_3$.

When $k > \ell_3$, no beams exist, and the amplitude factor is everywhere small. The amplitude factor $\frac{1}{|F|}$ given by (2.9) with ν_3 replaced by $i\,\mu_3$ is a monotonically decreasing and positive function with k for $\ell_3 < k < \ell_1$.

To summarize this section the amplitude factor exhibits several high level beams in the stratosphere outside of which little lee wave activity exists. The height of the beams is greater than or equal to one, the height obtainable for the lyra one layer model, and is less than that obtainable with $\ell_1 = \ell_2$ except at the peak of the beams which are approximately determined by the waveguide. The physical interpretation for the wave field is that bits of the lyra solution are left intact by the waveguide, some are amplified. The wave activity is in discrete directions due to fundamental wave properties of the waveguide.

3. A Consideration of the Amplitude factor for ℓ_2 greater than ℓ_3 and $\ell_1 >> \ell_2$

In this section consideration is given to the amplitude factor, when the Scorer parameter piecewise increases with height in three layers. It was discussed in section two that for large distances into the stratosphere, the influence function evaluation depends critically on the amplitude factor $\frac{1}{|F|}$.

$$G(r,\alpha) \sim \mathrm{Re}\left\{ \left(\frac{2\pi \ell_1}{r}\right)^{\frac{1}{2}} \left(\frac{z}{r}\right) \frac{e^{i(r\ell_1 - \pi/4)}}{|F(k^*, -1)|\, P(\alpha)} \right\} \tag{3.1}$$

where $F(k^*, -1) = P(\alpha)\left|F(k^*, -1)\right|$ (3.2)

and $k^* = \ell_1 \cos\alpha$. $P(\alpha)$ is a phase factor dependent upon α. For $\ell_1 >> \ell_2 > \ell_3$, (2.8) transposes into

$$\left|F(k,-1)\right|^2 = \mathcal{L}^2\left(\frac{\sin \nu_2 h}{\nu_2} \cos \nu_3(1-h) + \cos \nu_2 h \, \frac{\sin \nu_3(1-h)}{\nu_3}\right)^2 + 1 + \frac{S^2}{\nu_3^2} \sin^2 \nu_3(1-h) \tag{3.3}$$

where

$$S^2 = \ell_2^2 - \ell_3^2 \tag{3.4}$$

Equation (3.3) implies that the amplitude factor is small except near the wavenumbers satisfying the eigenvalue relationship

$$\frac{\tan \nu_2 h}{\nu_2} + \frac{\tan \nu_3(1-h)}{\nu_3} = 0 \tag{3.5}$$

As earlier described, the lee waves exist in beams which propagate far into the stratosphere at angles given by (2.7). When a wavenumber satisfies (3.5), the square of the amplitude factor is given by

$$\frac{1}{|F(k,-1)|^2} = 1 - \frac{S^2 \sin^2 \nu_2 h}{\nu_2^2} \tag{3.6}$$

A comparison of (3.6) and (3.3) shows that the amplitude factor

at the peak of the beam is the same in the three layer atmosphere as it is in the two strata model with $\ell_1 = \ell_2$ (the Berkshire model, 1970), and is everywhere less than the amplitude factor produced for the lyra atmosphere except when (3.4) is satisfied with $\nu_2 h = n\pi$. $n = 1, 2, 3\ldots$ when the peaks have unit height.

Using (3.5) and (3.6) we obtain the following:-

$$\frac{1}{|F(k,-1)|} = \frac{\cos \nu_2 h}{\cos \nu_3 (1-h)} \tag{3.7}$$

It is an important property of (3.5) that if ℓ_2 is interchanged with ℓ_3 and h with (1-h) the eigenvalues remain the same,

If we establish the same interchanges in (3.7) we obtain

$$\frac{1}{|F(k,-1)|} = \frac{\cos \nu_3 (1-h)}{\cos \nu_2 h} \tag{3.7a}$$

which is the reciprocal of (3.7). Consequently the peaks of the beams with ℓ_2 greater than ℓ_3 are the reciprocal values of a configuration with ℓ_3 greater than ℓ_2.

When $\ell_3 < k < \ell_2$, we can rewrite (3.6) using (3.5) as

$$\frac{1}{|F(k,-1)|^2} = \frac{1}{1 + \frac{S^2}{\mu_3^2} \sinh^2 \mu_3 (1-h)} \tag{3.8}$$

This function is a monotonically decreasing function for increasing k. Thus beams for wavenumbers begween ℓ_3 and ℓ_2 have successively smaller peaks for increasing wavenumbers. The beams in this range all have values of $\frac{1}{|F(k,-1)|^2} < \frac{1}{1+S^2(1-h)^2}$. For $0 < k < \ell_3$, the beams have values of $\frac{1}{|F(k,-1)|^2} > \frac{1}{1+S^2(1-h)^2}$. No procession of decreasing peaks exists for this range of k. The peak with the longest wavelength may be greater or less than the next peak provided $k < \ell_3$.

No beams may exist in the amplitude factor for wave numbers shorter than ℓ_2, and this function monotonically decreases.

It was discussed in section two of this chapter that it was possible to tune the beams to reach a maximum when the upper troposphere depth h was varied keeping the Scorer parameters constant. A similar equation can be derived to tune the beams to a minimum. When (3.3) satisfies (3.5) we obtain

$$\left|F(k,-1)\right|^2 = 1 + \frac{S^2}{\nu_3^2} \sin^2 \nu_3(1-h) \tag{3.9}$$

We differentiate (2.14), (3.5) and (3.9) treating h as the variable (k must also be considered to vary), and eliminate the terms involving $\frac{d\nu}{dh}$ between these equations to derive the condition for a minimum beam as

$$\frac{\tan \nu_3(1-h)}{\nu_3^3} - \frac{(1-h)}{\nu_3^2} = \frac{1}{S^2} \tag{3.10}$$

There is a direct analogy between (3.10) and (2.15) if we substitute ℓ_2 for ℓ_3 and (1-h) for h. The minimum just defined transposes into the equation for a maximum beam which was discussed in the last section.

As we decrease h from one, the function $\nu_3(1-h)$ increases, and for large ℓ_3, several minima will exist. The solutions to (3.10) satisfy

$$\nu_3^{\kappa}(1-h)^{\kappa} < \nu_3(1-h) < n\pi + \frac{\pi}{2} \tag{3.11}$$

where n is a positive integer, and $\nu_3^{\kappa}(1-h)^{\kappa}$ is defined by $\tan \nu_3(1-h^{\kappa}) = \nu_3^{\kappa}(1-h^{\kappa})$. The first solution exists in the range

$$4.493 < \nu_3(1-h) < 4.712 \tag{3.12}$$

and is unique. When $\nu_3(1-h)$ is large, the solutions to (3.11) are close to $n\pi + \frac{\pi}{2}$. With this approximation the minimum amplitude factors are obtainable from

$$\frac{1}{|F|} = \frac{(n+\frac{1}{2})\pi}{\sqrt{(n+\frac{1}{2})^2\pi^2 + S^2(1-h)^2}} \tag{3.13}$$

For wavenumbers larger than ℓ_3, (3.10) becomes

$$\frac{(1-h)}{\mu_3^2} - \frac{\tanh \mu_3(1-h)}{\mu_3^3} = \frac{1}{S^2} \tag{3.14}$$

One solution exists for (3.14) or for (3.10) when $\nu_3(1-h) < \frac{\pi}{2}$. Alternatively the minimum can exist at $k = \ell_3$ when (3.14) reduces to the special form $(1-h) = \sqrt[3]{\frac{3}{S^2}}$ together with the eigenvalue relationship

$$\frac{\tan Sh}{S} + (1-h) = 0 \tag{3.15}$$

The maxima of the beams (unity), occur when $\nu_3(1-h) = n\pi$, where n is a positive integer, and for h = 0 or h = 1. As we decrease h from one to zero, the beams will oscillate between the values determined by (3.13) and unity. The beam with the largest value of k will generate one minimum, the next beam will produce two, and in general the nth beam creates n minima, where all except the first must be for wavenumbers less than ℓ_3.

4. The Effect of Varying the Middle Scorer Parameter on the Amplitude Factor Beams when $\ell_1 \gg \ell_2$

It was discussed in section two of this chapter that when ℓ_1 is very large the beams produced by the amplitude factor occur very near to the wavenumbers determined by the eigenvalue equation

$$\frac{\tan \nu_3(1-h)}{\nu_3} + \frac{\tan \nu_2 h}{\nu_2} = 0 \qquad (4.1)$$

At these wavenumbers, the square of the amplitude factor is obtained from

$$\frac{1}{|F(k,-1)|^2} = 1 + \$^2 \frac{\sin^2 \nu_2 h}{\nu_2^2} \qquad (4.2)$$

when ℓ_2 is smaller than ℓ_3. In this section the behaviour of the beams will be discussed when ℓ_2 is varied. This variation will create a change in the wavenumbers satisfying (4.1). All the other parameters are kept constant. The zeroes of the differential of (4.2) are equivalent to the turning points of (4.2), these certainly occur when $\sin \nu_2 h = \sin \nu_3(1-h) = 0$ i.e. $\nu_2 h = n\pi$, where n is a positive integer. At these points, the amplitude factor is unity. When ℓ_2 is smaller than ℓ_3, this solution corresponds to a minimum in the amplitude factor beams. However, the opposite is true for ℓ_2 larger than ℓ_3. The other turning points can be obtained by differentiating with respect to ℓ_2

$$|F(k,-1)|^2 = 1 - \$^2 \frac{\sin^2 \nu_3(1-h)}{\nu_3^2} \qquad (4.3)$$

When ℓ_2 is smaller than ℓ_3, the maximum in the amplitude factor beams occurs when

$$\frac{\tan \nu_3(1-h)}{\nu_3(1-h)} - 1 = \frac{\nu_3^2}{\nu_2^2} \left(\frac{\tan \nu_2 h}{\nu_2 h} - 1\right) \tag{4.4}$$

If ℓ_2 is larger than ℓ_3, (4.4) determines the minima.

Since the analysis falls neatly into two parts, we will begin by considering ℓ_2 to be smaller than ℓ_3. Equation (4.4) can be rewritten using (4.1) as

$$\frac{\tan \nu_2 h}{\nu_2 h} = 1 - \frac{\nu_2^2}{(1-h)\,\$^2 + \nu_2^2} \tag{4.5}$$

the solutions of which determine the maxima of the amplitude factor beams. The eigenvalues of (4.5) satisfy

$$n\pi < \nu_2 h < \nu_2^{*} h^{*} \tag{4.6}$$

where $\tan \nu_2^{*} h^{*} = \nu_2^{*} h^{*}$ and n is a positive integer. The first root lies in the range $3.142 < \nu_2 h < 4.49$.

An analysis of the derivative of (4.5) reveals that the solutions of (4.6) are unique between successive integer values for n. When k is greater than ℓ_2 (4.5) transforms into

$$\frac{\tanh \mu_2 h}{\mu_2 h} = 1 + \frac{\mu_2^2}{(1-h)\,\$^2 - \mu_2^2} \tag{4.7}$$

No roots occur for this expression. This implies that as ℓ_2 increases from zero towards ℓ_3, the amplitude factor beams for wavenumbers greater than ℓ_2 decrease monotonically, provided $\ell_1 >> \ell_2$ and $\ell_1 >> \ell_3$. When ℓ_2 equals ℓ_3, the eigenvalues satisfying (4.1) take the form $\nu = n\pi$, the first beam in the amplitude factor occurs for n = 1. It was shown in Chapter Two that the wavenumber roots of (4.1) increase more slowly than ℓ_2 as this parameter is changed. Consequently, the

greatest value obtainable for ν_2 is ν, provided ℓ_2 is not greater than ℓ_3. The term $\nu_2 h$ is thus always less than π, when h is less than unity, for the first beam.

If $\ell_3(1-h)$ is greater than π, (the condition that a beam exists for real wavenumbers when ℓ_2 equals zero) the first beam will monotonically decrease in height, and grow in wavenumber as ℓ_2 increases from zero to ℓ_3 in both the ranges when the beam is internal and external to ℓ_2. When $\ell_3(1-h)$ is greater than 2π and h is larger than a half, the second beam will generate one minimum-maximum pair for intermediate values of ℓ_2 between zero and ℓ_3. In the range for which ℓ_2 is less than k, the beam will monotonically decrease in height. If h is less than a half, the second beam will monotonically decrease as ℓ_2 approaches ℓ_3. In general when $\ell_3(1-h)$ is greater than $m\pi$, the mth beam will decrease monotonically if $h < \frac{1}{m}$ as ℓ_2 approaches ℓ_3. There will be n intermediate beam maxima-minima pairs if $\frac{n}{m} < h < \frac{n+1}{m}$, and there are m-1 of them for values ℓ_{2m}, such that $0 < \ell_{2m} < \ell_3$ if $h > \frac{m-1}{m}$. All beams decrease as ℓ_2 grows from zero, until they attain a minimum, which occurs for wavenumbers less than ℓ_2. At a minimum, the amplitude factor has the value one.

When ℓ_2 is greater than ℓ_3, the minima of the amplitude factor beams are furnished by solutions to (4.4), which using (4.1) transforms into

$$\frac{\tan \nu_3(1-h)}{\nu_3} = 1 - \frac{\nu_3^2}{hS^2 + \nu_3^2} \tag{4.8}$$

where

$$S^2 = \ell_2^2 - \ell_3^2 \tag{4.9}$$

We assume that as ℓ_2 increases beyond ℓ_3, the assumption $\ell_1 >> \ell_2$ is still valid. These roots exist for $n\pi < \nu_3(1-h) < \nu_3^*(1-h)^*$ where n is a positive integer and $\nu_3^*(1-h)^*$ satisfies tan x = x. The first solution exists for $3.14 < \nu_3(1-h) < 4.49$. A consideration of the derivative of (4.8) reveals that there is only one eigenvalue in each of these ranges described above. No solution satisfies (4.8) for wavenumbers in the range $\ell_3 < k < \ell_2$.

As ℓ_2 increases beyond ℓ_3, at which the beams have unit height, all the beams decrease until they attain a minimum, if any, for which k is less than ℓ_3. Since k increases with ℓ_2, the largest attainable value of $\nu_3 = \nu = n\pi$, when ℓ_2 equals ℓ_3, and ν_3 decreases monotonically to zero, with growing ℓ_2. If ℓ_3 is greater than π, (the condition for the first beam to exist for a real wavenumber when ℓ_2 equals ℓ_3), the first beam will decrease monotonically with increasing ℓ_2. The second beam if $\ell_3 > 2\pi$, will decrease monotonically if $(1-h) < \frac{1}{2}$, and will generate a minimum-maximum pair if $(1-h) > \frac{1}{2}$ when $Sh = 2\pi$, (the condition for the second eigenvalue to have become larger than ℓ_3), this beam will shrink with increasing ℓ_2. In general if $\ell_3 > m\pi$, the mth beam will shrink monotonically as ℓ_2 increases if $(1-h) < \frac{1}{m}$. If $\frac{n}{m} < (1-h) < \frac{n+1}{m}$ there will be n maxima-minima pairs in the beam size, before $Sh = m\pi$. When $(1-h) > \frac{m-1}{m}$, there are m-1 maxima-minima pairs, for the beam for values ℓ_{2m}, such that $\ell_3 < \ell_{2m} < \frac{m^2\pi^2}{h^2} + \ell_3^2$. If $\ell_2 > \frac{m^2\pi^2}{h^2} + \ell_3^2$ the beam height shrinks with growing ℓ_2.

When the wavenumber, k, is greater than ℓ_3, (4.3) transforms into

$$\frac{1}{|F|^2} = \frac{1}{1+S^2 \dfrac{\sinh^2 \mu_3 (1-h)}{\mu_3^2}} \tag{4.10}$$

which is a decreasing function as k increases. Consequently, if ℓ_2 is greater than $\frac{m^2\pi^2}{h^2} + \ell_3^2$, the first m beams increase in size from the first to the last, provided $\ell_1 >> \ell_2$.

In order to complete the analysis, the case when ℓ_2 equals ℓ_3 will be discussed. The solution of (4.1) take the form $\nu = p\pi$, where p is a positive integer. The derivative of (4.2) with respect to ℓ_2 has a zero when $\ell_2 = \ell_3$ if $\frac{\sin \nu_2 h}{\nu_2} = 0 = \frac{\sin \nu_3 (1-h)}{\nu_3}$. Consequently, the solution is $\nu_2 h = n\pi$, together with $\nu_3 (1-h) = m\pi$ where m and n are positive integers. Consequently we derive the following constraints on these integers as

$$h = \frac{n}{p} \tag{4.11}$$

and

$$(1-h) = \frac{m}{p} \tag{4.12}$$

adding we obtain

$$n + m = p \tag{4.13}$$

Equation (4.13) implies that $p \geq 2$, so the first beam height cannot have a turning point. That is, as ℓ_2 is increased from zero to a value greater than ℓ_3, the first beam monotonically decreases in height. The second beam, p = 2, has a point of inflexion if ℓ_3 is greater than 2π, and n equals 1. This occurs when $h = \frac{1}{2}$. In general the Ith beam has a point of inflexion at $\ell_2 = \ell_3$ when $h = \frac{1}{I}, \frac{2}{I} \ldots \frac{I-1}{I}$. When $h = \frac{1}{2}$, and $\ell_3 > m\pi$, where m is even, the $\frac{m}{2}$ even numbered beams will have a point of inflexion at $\ell_2 = \ell_3$ at which the amplitude factor beams have a height of unity.

Lastly, if we treat ℓ_3 as the variable Scorer parameter then (4.4) is the condition governing the turning points and the analysis is identically to that already discussed.

The conclusion of this section is that, provided $\ell_2 \ll \ell_1$, as ℓ_2 increases from zero to a value much greater than ℓ_3, the beams grow in wavenumbers and decrease in size except for a set of minimum-maximum pairs, the number of which is one less than the index of the beam. The value of h which is chosen determines whether these pairs occur when ℓ_2 is less or greater than ℓ_3. For particular values of h, a point of inflexion occurs when ℓ_2 is equal to ℓ_3, at which the number of minima-maxima pairs is two fewer than the beam index. Numerical examples appear in section six of this chapter. Figures 3 and 8 show examples on the variation of ℓ_2.

5. A Discussion of the Amplitude Factor when S is large Compared with ℓ

In this section, for completeness of results, the Scorer parameter, ℓ_2, in the upper troposphere is taken to be almost as large as its value in the stratosphere, whereas it is considerably smaller in the lower troposphere. The amplitude factor, $\frac{1}{|F|}$, is given by

$$|F(k,-1)|^2 = \ell^2\left[\frac{\sin \nu_2 h}{\nu_2}\cos \nu_3(1-h) + \cos \nu_2 h \frac{\sin \nu_3(1-h)}{\nu_3}\right]^2 + 1 + \frac{S^2}{\nu_3^2}\sin^2 \nu_3(1-h) \qquad (5.1)$$

when S^2 is large compared with ℓ^2, the amplitude factor beams will occur near to wavenumbers, k, which satisfy

$$\frac{\sin \nu_3(1-h)}{\nu_3} = 0 \qquad (5.2)$$

at which $\nu_3(1-h) = n\pi \qquad (5.3)$

This is the condition for k to be an eigenvalue for a model with a rigid lid at the mid tropospheric depth, h. It is assumed that the lower troposphere has finite thickness, so that h is not equal to one, and n is a positive integer.

When (5.3) is substituted into (5.1), the value of the beam amplitude is acquired from

$$|F(k,-1)|^2 = \ell^2 \frac{\sin^2 \nu_2 h}{\nu_2^2} + 1 \qquad (5.4)$$

If the Scorer parameters are held constant and the intermediate thickness, h, is varied, the positions of resonance of the beams may be found by differentiating (5.4) and (5.3). The condition for turning points is

$$0 = \mathcal{L}^2 \frac{\sin \nu_2 h}{\nu_2} \left[\frac{\cos \nu_2 h}{\nu_2} \left(\nu_2 + h \frac{\nu_3^2}{(1-h)\nu_2} \right) - \frac{\sin \nu_2 h}{\nu_2^2} \frac{\nu_3^2}{(1-h)\nu_2} \right] \tag{5.5}$$

Since ℓ_2 is smaller than ℓ_1, $\mathcal{L}$ is non zero. A resonant beam will occur when $\frac{\sin \nu_2 h}{\nu_2} = 0$, at which $\frac{1}{|F|}$ equals one, its maximum value for the chosen Scorer parameters. When this occurs $\nu_2 h = m\pi$, where m is a positive integer. This resonance occurs when k is an eigenvalue for a model with rigid lids at the mid troposphere and the tropopause, and the air motion is confined between the ground and first lid, and between the two lids.

The minima of the beams occur when

$$\frac{\tan \nu_2 h}{\nu_2 h} - 1 = \frac{(1-h)}{h} \frac{\nu_2^2}{\nu_3^2} \tag{5.6}$$

for non zero h. Condition (5.3) implies that $\nu_2 h$ is an increasing function with h, and using this equation, (5.6) can be written as

$$\frac{1}{\nu_2^2} \left(\frac{\tan \nu_2 h}{\nu_2 h} - 1 \right) = \frac{(1-h)^3}{h\, n^2 \pi^2} \tag{5.7}$$

There is exactly one solution to (5.7) in the range

$$\nu_2^{\varkappa} h^{\varkappa} < \nu_2 h < p\pi + \frac{\pi}{2} \tag{5.8}$$

where $\nu_2^{\varkappa} h^{\varkappa}$ satisfies $\tan x = x$, zero being the first solution.

The condition for real wavenumbers satisfying (5.3) is that the largest value that h may take, $h^{\varkappa}$, is given by

$$h^{\varkappa} = 1 - \frac{n\pi}{\ell_3} \tag{5.9}$$

consequently the solutions of (5.7) have a restriction on the values $\nu_2 h$ may take which is

$$0 \leq \nu_2 h \leq \ell_2 (1 - \frac{n\pi}{\ell_3}) \tag{5.10}$$

When h equals zero a beam maximum exists since $\frac{1}{|F|}$ equals one when (5.3) is satisfied.

If the intermediate thickness, h, is kept constant, and ℓ_2 is varied over a range for which $S^2 \gg \mathcal{L}^2$, (5.4) and (5.3) are the relevant equations. By differentiating both these equations, with respect to ℓ_2, the condition for turning points is found to be

$$0 = \ell_2 \frac{\sin \nu_2 h}{\nu_2} \left(- \frac{\sin \nu_2 h}{\nu_2} + \mathcal{L}^2 \left(h \frac{\cos \nu_2 h}{\nu_2^2} - \frac{\sin \nu_2 h}{\nu_2^3} \right) \right) \tag{5.11}$$

Since ℓ_2 is greater than ℓ_3, ℓ_2 cannot equal zero, and the stipulation for beam resonance becomes

$$\nu_2 h = m\pi \tag{5.12}$$

where m is a positive integer. A minimum in the beam amplitude occurs when

$$\frac{\tan \nu_2 h}{\nu_2^3} - \frac{h}{\nu_2^2} = - \frac{1}{\mathcal{L}^2} \frac{\tan \nu_2 h}{\nu_2} \tag{5.13}$$

Roots of (5.13) lie in the range

$$n\pi < \nu_2 h < \nu_2^{\varkappa} h^{\varkappa} \tag{5.14}$$

where $\nu_2^{\varkappa} h^{\varkappa}$ satisfies $\tan x = x$. The first root is in the range $3.14 < \nu_2 h < 4.49$. There is exactly one root in each range determined by (5.14).

A consequence of (5.3) is that for constant h, the eigenvalues, k, for which this theory is valid, remain unchanged as ℓ_2 varies. It is evident from Fig. 8 that the comparison with a model with a rigid lid at $z = -h$ is sound for values of ℓ_2 which are considerably smaller than ℓ_1, provided the upper troposphere has small thickness.

6. Some Numerical Results and the Influence of Complex Poles

Figures 3 to 13 are plots of the amplitude factors against wavenumber, k. Amplitude factors greater than one are produced when ℓ_2 is smaller than ℓ_3. In figure 3, the effect of increasing ℓ_2 from 3.16 to 4.74 is to produce a shorter, sharper beam with smaller area under the curve. These values of ℓ_1 and ℓ_3 were chosen to compare with Berkshire thesis 1970, Berkshire and Warren 1970, and Sawyer 1960. For such a value of ℓ_1, the beam maxima coincide to a good approximation, to the wavenumbers, k, determined by (2.11), when ℓ_2 is less than ℓ_3. This equation specifies the wavenumbers for infinite ℓ_1. (The rigid lid model as discussed in Chapter 2). In the example $\ell_2 = 3.16$, the actual beam wavenumber is 1.99, whereas that for infinite ℓ_1 is 1.989. When ℓ_2 is larger than ℓ_3, the beams have height less than unity. When $\ell_2 = 9.48$, the beam wavenumbers are still close to where they would be for infinite ℓ_1. The beam on the right, associated with the complex pole with the smallest imaginary part has the sharpest peak. The beam at k = 8.87 is external to ℓ_3, and agrees with the theoretical result for large ℓ_1, that it is the shortest. A broad beam for small wavenumbers corresponds to the Gamow pole with the large imaginary part. A comparison between $\ell_2 = 18.96$ and $\ell_2 = 700^{1/2}$ reveals there is little difference. The beams for $\ell_2 = 18.96$ have almost negligible amplitude. The sharpest 'beams' for $\ell_2 = 18.96$ are still close to the value one would obtain for infinite ℓ_1. For $\ell_1 = 700^{1/2}$, the beams are at 5.25, 12.05, 15.45, 17.49 and 18.60 whereas those for infinite ℓ_1 are at 6.16, 12.21, 15.49, 17.49 and 18.60.

Figure five portrays that the effect of increasing h is to decrease the wavenumber k. The beams which are internal to ℓ_2 are considerably broader than those which are external, the beam for small values of h is at its broadest when it is close to the value k = 0. A comparison between the case h = 0 (as in Berkshire thesis 1970) and h = 0.4 reveals that the beam for larger wavenumbers changes by a relatively small amount i.e. between k = 6.72 and k = 6.244, but more than trebles in height. Equation (2.15) predicts that the beam is tallest for a value of h given by h = 0.57.

In figure six it can be seen that the effect of changing ℓ_1 from 5.5 to $700^{1/2}$ changes the beam number and height very little. When $\ell_1 = 5.5$, the beam wavenumber is 2.06, whereas for the case $\ell_1 = \infty$, the beam wavenumber is 1.99. This implies that the stratospheric beams of lee wave activity at elevation α given by $k = \ell_1 \cos \alpha$ tends to a more horizontal direction and has disappeared when $\ell_1 = 1.58$. In the case $\ell_1 = 1.58$, there is a trapped tropospheric mode. The effect of decreasing ℓ_1 in this case is to produce leakage into the stratosphere which is not specifically confined to beams. An interesting feature is that the beam height for a particular value of k, is the same as the amplitude in the case $\ell_1 = \ell_2 = 3.16$. The sharp increase in amplitude for larger wavenumbers in the example $\ell_1 = 3.16$ is produced by the real Scorer pole at(3.670,0)which is situated on the lower Ŕiemann sheet. However, the stationary phase approximation is not valid for such small values of α when k is close to ℓ_1.

In figure seven it can be seen that as h increases from 0.2 to 0.4,

the beam moves quickly from k = 3.82 towards k = 0 and disappears. When h = 0 the Gamow pole which produces this beam is a tropospheric Scorer edge wave given by k = (5.573, 0). A second beam appears when h $\approx$ 0.54 at k = ℓ_1. For a range of values of h this beam is very tall, but it decreases quickly from 11.85 when h = 0.65 to 2.73 when h = 0.8. When h equals one, the beam has unit height and is given by k $\approx$ 0.34. Figure eleven is similar except the beam produced when h = 0.65 influences a greater range of wavenumbers. Physically this implies that when ℓ_2 = 3.16, and h = 0 there are two trapped tropospheric modes and no stratospheric beams. As h increases, a beam in which lee wave activity can exist appears at a low elevation in the stratosphere, and one of the trapped modes disappears. This beam increases its elevation and has virtually disappeared when h = 0.4. For higher values of h there is another stratospheric beam whose elevation is nearly horizontal when h = 0.54, and is nearly vertical when h = 1.0.

In figure eight, as ℓ_2 increases from zero the sharp beam monotonically decreases from 4.11 when ℓ_2 = 0.0 to one when $\ell_2 = 55^{1/2}$. The beam wavenumber changes less rapidly from k = 6.393 to k = 6.72. As ℓ_2 increases beyond ℓ_3, the beam monotonically decreases and has disappeared when ℓ_2 = 12.64. This agrees with the theory of section four, which concludes that when $\ell_1 >> \ell_2, \ell_3$, as ℓ_2 increases the first beam monotonically decreases. The second beam is in agreement with the same theory until $\ell_2 \approx$ 12.64. The beam decreases monotonically as ℓ_2 increases from zero to ℓ_3. As ℓ_2 increases beyond ℓ_3, there is one maxima-minima pair until $\ell_2 >$ 12.64.

When ℓ_2 is less than ℓ_3, there is close agreement between the wavenumbers for $\ell_1 = 700^{1/2}$ and those for infinite ℓ_1. When $\ell_2 = 3.16$, the beam wavenumbers for infinite ℓ_1 are 6.428 and 1.682 whereas those for $\ell_1 = 700^{1/2}$ are 6.430 and 1.71. There is less agreement when $\ell_2 > \ell_3$; for the case $\ell_2 = 9.48$ the beams are at 7.30 and 5.22, whereas when ℓ_1 is infinite the wavenumbers are 7.38 and 5.19. As ℓ_2 further increases there is little comparison between this model and the case of infinite ℓ_1. When $\ell_2 = 12.64$ there is only one beam. However, as ℓ_2 increases beyond $\ell_2 = 12.02$ (the value at which the beam attains unit height), the comparison with the model with $\ell_1 \approx \ell_2$ and $\ell_2 \gg \ell_3$ becomes more applicable. The theory (discussed in part five) concludes that a stationary beam is present at k = 5.90, as ℓ_2 varies. The values at which the amplitude factor is one are $\ell_2 = 12.02$ and $\ell_2 = 21.76$. The case of $\ell_2 = 22.12$ is nearly identical with the case $\ell_1 = 700^{1/2}$ and has not been drawn.

Figures ten and twelve enable us to compare and contrast the behaviour of the modes which are internal and external to ℓ_2, as ℓ_1 varies. As ℓ_1 decreases the sharp stratospheric beam in figure ten becomes broader and taller as its elevation decreases, until it becomes a trapped tropospheric mode when $\ell_1 \approx 6.5$. The broad beam when $\ell_1 = 700^{1/2}$ is replaced by an almost uniform amplitude factor when $\ell_1 = 1.58$. We can conclude that stratospheric lee waves are not confined to beams when ℓ_1 is small, but leakage into the stratosphere is substantial at all elevations.

If we naively thought that the modified Scorer modes for $\ell_2 < k < \ell_3$ are the only significant feature we would have anticipated a lyra type

solution for $k < \ell_2$ in the amplitude factor diagrams. This is not the case when $\ell_1 > \ell_2$, but it is the case when $\ell_1 < \ell_2$ provided a Gamow pole is not significantly near to $k = \ell_1$.

In figure 13 we see that introducing a thin layer of thickness 0.1 between the stratosphere and lower troposphere substantially reduces the height of the beams from one to less than 2/3. A similar change occurs when h is large. A thin layer with a smaller Scorer parameter near the ground considerably reduces the magnitude of the beams which radiate into the stratosphere. When h = 0.8 the three beams are each less than $\frac{1}{2}$, whereas for h = 1.0 each beam has unit height. Beams of nearly unit height exist for a range of intermediate values of h and k which nearly satisfy

$$\frac{\tan \nu_2 h}{\nu_2} + \frac{\tan \nu_3 (1-h)}{\nu_3} = 0 \qquad (6.1)$$

together with $\sin \nu_2 h = 0.$ (6.2)

The cases of h = 0.3 and 0.55 are near examples to where the amplitude factor is unity. These occur at h = 0.28 at which k = 5.987 and h = 0.52 at which k = 3.542.

Figure 14 reveals that when $\ell_1 = 700^{1/2}$, the Gamow poles are all complex. These poles are singularities of the amplitude factor, $\frac{1}{|F|}$, in the first quadrant of the k plane. Poles also exist in the third quadrant which are the negative values of those in the first, however, we do not consider these further. The approximation that k^2 is real is least valid for wavenumbers close to zero, at which h = 0.385. By comparison, the locus of the pole for $\ell_1 = 1000$ is much closer to the axes as h varies.

It can be seen from the amplitude factor diagrams that a pole close to the real axis produces a sharp peak, whereas a complex wavenumber which has a larger imaginary part generates one which is considerably broader. This is most particularly noticeable for poles as they pass near the origin. It may be conjectured from figures 14 and five that the tall amplitude factor beam has its tallest peak when the corresponding pole is closest to the real axis. This, however, does not occur. The pole is closest to the real axis when h = 0.49, whereas the peak is tallest for h = 0.57.

An interesting feature of the Gamow poles of figures 14, 15 and 16 is the existence of loops as h varies. The number of these is one less than the index of the pole. When $\ell_2 = 12.64$, the second pole becomes considerably more trapped for values of h close to 0.28 where k = (6.003, .165) and when h = 0.51 where k = (3.690, .731). In this case the poles have their least imaginary part very close to the values of h for which the amplitude factor has its highest beams (0.28 and 0.52). We may conjecture that provided the imaginary part of the complex pole does not vary slowly (as in the case $\ell_2 = 4.74$) the amplitude factor beam maxima occur close to where the Gamow pole has its smallest imaginary part.

A remarkable result from figure seventeen is that as h tends to zero, and the model becomes the lyra model, the Gamow poles remain finite for a remarkable time. When h = 0.1 the leading pole is at (7.249, .395), while when $h = 10^{-4}$ it has become (8.252, .852). There is fairly close agreement with the poles of figure eighteen for small values

of h. When $\ell_2 = 3.16$, the leading pole is at (7.604, .616) while for $h = 1 \times 10^{-4}$, the Gamow pole is at (8.162, .827).

As h varies between zero and one, the model of figure 19 changes from a Scorer type two layer model in which the leading poles are both real, to a Berkshire type two layer model in which all the poles are complex. When h = .04 one of the Scorer poles disappears, and reappears as a Gamow pole in the complex plane. The second pole becomes a complex Gamow pole for h = 0.59. This produces high beams in the amplitude factor diagram, figure eleven, for a range of values of h near h = 0.65.

We observe from figure 21 that for a small range of values of h there is a Gamow pole close to the real axis. For the particular case h = 0.3, a broad beam occurs near the branch point ℓ_1 in the amplitude factor diagram figure ten. The Scorer pole which remains real longest, as h increases, falls through the branch point and remains a real pole on the lower Riemann sheet disappearing to infinity when h = 1. No beams are produced by this pole, only a disturbance for wavenumbers near $k = \ell_1$ for a discrete range of h. Compare with figure 6 for the case $\ell_1 = \ell_2 = 3.16$, h = 0.8.

An interesting observation from figures 23, 24, 25 is that as the interface disappears between the stratosphere and upper troposphere, poles disappear to infinity while others remain finite. These poles are clearly a consequence of this interface. Figure twenty-five enables us to compare the model with large ℓ_1, with that for infinite ℓ_1. When $\ell_1 = 700^{1/2}$, the Gamow pole for the first beam is at (6.482, .014)

and is close to its position for infinite ℓ_1. However, the second pole is situated at (2.423, .293) and has not reached its terminal position. When $\ell_1 = 100.0$, the Gamow pole is situated at (2.383, .079) and is changing less rapidly as ℓ_1 varies.

An examination of figure 24 reveals that the beam close to k = 5.90 is associated with the second pole, as ℓ_2 increases from 12.64 to ℓ_1. The real part of this pole varies between 5.82 and 6.20. When ℓ_2 approaches ℓ_1, the first and third complex poles disappear to infinity through the branch cut at k = ℓ_1, onto the lower Riemann sheet. The value at which the real part of the second and third complex poles are equal is approximately 17.0.

The conclusion to be drawn for the model in which $\ell_1 > \ell_2 > \ell_3$ is that the theory for infinite ℓ_1 can be extended to cases where ℓ_2 is nearly as large as ℓ_1, provided the tropospheric depth h is large. When h is small, the theory of a rigid lid at the mid troposphere can be extended to values of ℓ_2 which are considerably smaller than ℓ_1.

In figure 26 the maximal wave amplitude for a non zero ℓ_2 upper troposphere is presented for the first downstream wave at approximately z = 10. The position of this maximum was found to vary between x = 1.0 and x = 2.04. A large resonance occurs at h = 0.365, which is close to 0.388 the value at which the eigenvalue for infinite ℓ_1, is at k = 0. The smaller resonance at h = 0.72 is fairly close to where the amplitude factor beam crosses k = ℓ_2 at h = 0.68. A comparison should be made with $\ell_2 = 0$, which was plotted in Berkshire 1970, as a maximal wave amplitude in the vicinity of x = 2, z = 10.

Contours of G(x, z) are presented for this model for both resonances, and h = 0. 15 which is fairly close to where one wavelength is a simple multiple of the other. The high level stratospheric waves have an amplitude which has not decreased substantially from its value just above the tropopause. In the upper stratosphere the contours are tilted at about the same angle as they are just above the tropopause. The troposphere-stratosphere interface is clearly defined on the low level contours, since their direction changes there, from being nearly vertical in the troposphere. Tropospheric wave amplitudes are considerably greater than those in the stratosphere. In figure 35 the maximal wave amplitude for the first tropospheric wave is 10. 61, while the value at x = 0. 82, z = 0. 14 is 2. 24.

For small values of z, the residue theory of Berkshire 1975 is valid, and the low level contours could have been obtained directly from a calculation of pole residues. However, these contours for G(x, z) were obtained by direct computer evaluation of the integrals concerned.

7. The Quasi Wave Drag Integral

The wave-drag integral (see e.g. Sawyer 1959) is represented by

$$I = - \int_{-\infty}^{\infty} \rho \, u \, w \, dx \tag{7.1}$$

This can be rewritten in terms of the modified displacement $\bar{\zeta}$ as

$$I = \rho(-1)\, U(-1)^2 \int_{-\infty}^{\infty} \frac{\partial \bar{\zeta}}{\partial x} \frac{\partial \bar{\zeta}}{\partial z} \, dx \tag{7.2}$$

where

$$\bar{\zeta} = \zeta \frac{\rho^{1/2} \, U(z)}{\rho^{1/2}(-1)\, U(-1)} \tag{7.3}$$

The modified displacement $\bar{\zeta}$ is related to the influence function by

$$\bar{\zeta} = \frac{1}{\pi} \int_{-\infty}^{\infty} d\xi \, f(\xi) \, G(x, z, \xi) \tag{7.4}$$

where

$$G = \mathrm{Re} \int_{0}^{\infty} dk \, \frac{F(k, z)}{F(k, -1)} \, e^{ik(x-\xi)} \tag{7.5}$$

On using Parseval's theorem, and the properties of Fourier transforms, we obtain the formula

$$I = -\rho(-1)\, U(-1)^2 \, 2\pi i \int_{-\infty}^{\infty} dk \, \frac{|\bar{f}(k)|^2 \, k \, \overline{F(k, z)}}{|F(k, -1)|^2} \, \frac{\partial F}{\partial z}(k, z) \tag{7.6}$$

where a bar denotes the complex conjugate.

Equation (7.6) can be readily evaluated when there are no real zeros of $|F(k, -1)|$ as

$$I = 4\pi\rho(-1)\, U(-1)^2 \, \mathrm{Im} \int_{0}^{\ell_1} dk \, \frac{|\bar{f}(k)|^2}{|F(k, -1)|^2} \, k \, \overline{F(k, z)} \, \frac{\partial F}{\partial z}(k, z) \tag{7.7}$$

which can be written as

$$I = \frac{\rho(-1)\, U(-1)^2}{\pi}\, Q \tag{7.8}$$

Here Q is termed the quasi wave drag. For the three layer model of this chapter for flow over a delta function mountain, so that $f(x) = \delta(x)$, and $\overline{f(k)} = \frac{1}{2\pi}$,

$$Q = \int_0^{\ell_1} dk\, \frac{k\,\nu_1}{|F(k,-1)|^2} \tag{7.9}$$

where $|F(k,-1)|^2 = (\ell_1^2 - \ell_2^2)\left[\frac{\sin \nu_2 h}{\nu_2} \cos \nu_3(1-h) + \cos \nu_2 h\, \frac{\sin \nu_3(1-h)}{\nu_3}\right]^2 + 1 - \frac{(\ell_3^2 - \ell_2^2)}{\nu_3^2} \sin^2 \nu_3(1-h)$ (7.10)

It is clear from the numerical evaluation of $\frac{1}{|F(k,-1)|}$, the amplitude factor, that a complex pole near the real axis greatly increases the value of the quasi drag integral. In figures 41 - 50, Q has been computed and plotted against h for various values of ℓ_1, ℓ_2 and ℓ_3. Some cases of ℓ_1 less than ℓ_3 are included. In these examples, for certain values of h, real poles of (7.10) exist and equation (7.8) is modified by a pole residue contribution. This contribution will not be discussed in this thesis.

In figure 41 when $\ell_2 > \ell_3$ maxima occur for certain values of h. For the case $\ell_2 = 9.48$ and $\ell_2 = 12.64$, these values are close to where a loop occurs in a complex pole whose imaginary part is small. This also occurs when a beam of near unit height exists for the amplitude factor. When $\ell_2 = 9.48$, an amplitude factor beam has unit height for h = 0.40. The maxima in the wave drag integral occur for h = 0.44.

The drag also has maxima for values of h close to zero and at h = 1, at which beams of unit height occur for the amplitude factor.

In figure 41, for values of ℓ_2 smaller than ℓ_3, the maxima in the wave drag integral curves occur close to where they exist when $\ell_2 = 1.58$. As ℓ_2 increases, the maxima become less resonant, until when $\ell_2 = 6.32$, the maxima have become very much less pronounced. It was discussed in Berkshire thesis 1970 that the maxima in the quasi wave drag curves for $\ell_2 = 0$ occur when (2.11) is satisfied for k close to zero. This condition becomes

$$\frac{\tan \ell_3(1-h)}{\ell_3} + h = 0 \qquad (7.11)$$

When $\ell_3 = 55^{1/2}$, the values of h satisfying (7.11) are h = 0.745 and h = 0.309.

It is possible to conjecture that for ℓ_2 non zero and less than ℓ_3, that the maxima in the quasi wave drag curves occur near to where they would occur for $\ell_2 = 0$, however, the resonances become blunter for increasing ℓ_2. For the case $\ell_2 = 4.74$, the maximal wave amplitude peaks do not coincide with the quasi-wave drag peaks. Hence it is reasonable to assume a difference in form between them.

A comparison between figure 41 and 43 reveals that if the values of ℓ_2 and ℓ_3 are interchanged for constant ℓ_1, the drag is larger for ℓ_3 greater than ℓ_2, provided h and 1-h are interchanged. This holds true for all values of h, except those close to h = 0 and h = 1.

In figures 49 and 50, we see that the position of the maxima are not altered very much by reducing ℓ_1 from $700^{1/2}$ to $55^{1/2}$. When ℓ_1

is smaller than ℓ_3, the sharp increase in the quasi wave drag is caused by a Scorer pole dropping through the branch point at k = ℓ_1. The actual drag for these cases is modified by pole residues. However, for h greater than 0.77, no Scorer poles exist, and a direct comparison can be made, as ℓ_1 varies, in the quasi wave drag curves. It was not possible to evaluate the sharp drag maxima as accurately as the blunt maxima for an interval of .001 between successive values of h. Consequently in table two, three of the drag maxima have no decimal values.

We can conclude that the parameter ℓ_3 is the important quantity in determining the maxima in the quasi wave drag curves, when ℓ_1 is greater than ℓ_3. Equation (7.11) determines where these occur for large ℓ_1 and zero ℓ_2. The effect of changing the value of ℓ_2 (provided it is less than ℓ_3), and the effect of varying ℓ_1 (provided it is not less than ℓ_3) only sharpen or blunt these characteristics, but do not substantially alter their position.

Lastly, if we consider the parameter ℓ_1 to be infinite, the model has real eigenvalue wavenumber solutions given by (2.11). The drag integral (7.9) can be evaluated in terms of pole residues to give

$$Q = \pi \sum_{k>0} \nu_3^2 \Big/ \left[1 + \frac{\$^2}{\nu_2^2} \left(\frac{\sin \nu_3(1-h)}{\nu_3} \cos \nu_3(1-h) + h \cos^2 \nu_3(1-h) \right) \right] \tag{7.12}$$

where the summation for wavenumbers k, is for real wavenumbers satisfying (2.11). For $\ell_2 = 0$ equation (7.12) is modified by putting $\nu_2^2 = -k^2$ and $\$^2 = \ell_3^2$.

Figures 44 to 47 represent a comparison between the quasi wave drag as determined by (7.12) and that evaluated for $\ell_1 = 700^{1/2}$ from

equation (7.9). As no error function to (7.12) was readily evaluable, when an eigenvalue wavenumber solution k changed from real to imaginary it was discounted from (7.12). In these regions where there is a discontinuity in the drag, there is a discrepancy from the actual quasi wave drag for $\ell_1 = 700^{1/2}$. However, when no pole is close to the origin, there is good agreement with the computed curves, for $\ell_2 = 1.58$ and $\ell_2 = 3.16$. There is less agreement for $\ell_2 = 6.32$, and it may be supposed that $\ell_1 = 700^{1/2}$ was not a sufficiently large value for the approximation of real poles to be made.

At h = 1, equation (7.12) reduces to

$$\Omega = \pi^3 \sum_{n=1}^{N} n^2 \qquad (7.13)$$

where N is the number of zeros of $\frac{\sin \nu_2}{\nu_2}$ in $0 < k < \ell_2$. For the four values of ℓ_2 which were used in figures 44 to 47 this gives Ω the value 0, 31.03, 31.03 and 155.15 at h = 1.

TABLE 1

POSITION OF IMPORTANT GAMOW POLES IN RELATION TO AMPLITUDE FACTOR BEAMS FOR FIGURES 3 TO 13

Fig. 3 $\ell_1 = 700^{1/2}$ $\ell_3 = 55^{1/2}$ h = 0.8

ℓ_2	k_1	k_2	k_3	Beam wavenumbers			Amplitude factors		
3.16	(1.997, 0.104)	-	-	1.99	-	-	2.71	-	-
4.74	(3.867, .069)	-	-	3.86	-	-	1.96	-	-
9.48	(8.878, .053)	(6.805, .266)	(1.348, 2.819)	8.87	6.78	-	0.59	0.67	-
18.96	Closest wavenumber to k (1.430, 13.909)			18.60	17.49	15.45	0.06	0.08	0.10
				12.05	5.25	-	0.16	0.32	-
$700^{1/2}$	k (3.246, 13.387)			No Beams					

Fig. 5 $\ell_1 = 700^{1/2}$ $\ell_2 = 4.74$ $\ell_3 = 55^{1/2}$

h	k_1	k_2	Beam wavenumbers		Amplitude factors	
0.2	(6.634, .024)	(3.413, .235)	6.633	3.39	1.67	1.46
0.3	(6.482, .014)	(2.423, .293)	6.482	2.395	2.50	1.65
0.4	(6.244, .009)	(.794, 1.115)	6.244	-	3.61	-
0.8	(3.867, .069)	-	3.86	-	1.96	-

Fig. 6 $\ell_2 = 3.16$ $\ell_3 = 55^{1/2}$ h = 0.8

ℓ_1	k_1	k_2	Beam wavenumbers		Amplitude factors	
$700^{1/2}$	(1.997, .104)	-	1.99	-	2.71	-
$55^{1/2}$	(2.100, .366)	-	2.02	-	2.72	-
5.5	(2.201, .490)	-	2.06	-	2.73	-
3.16	(3.670, 0.0)	-	At branch point 3.16	-	4.41	-
Lower Riemann sheet						
1.58	-	(1.450, 2.123)	-	No beams	-	-

Fig. 7 $\ell_1 = 5.5 \quad \ell_2 = 3.16 \quad \ell_3 = 55^{1/2}$

h	k_1	k_2	Beam wavenumbers		Amplitude factors	
0.2	-	(3.892, .524)	-	3.82	-	2.35
0.3	-	(2.477, .835)	-	2.26	-	2.32
0.4	-	(1.196, 2.431)	-	No beams	-	-
0.65	(4.491, .027)	-	4.490	-	11.85	-
0.8	(2.201, .490)	-	2.06	-	2.73	-

Fig. 8 $\ell_1 = 700^{1/2}$ $\ell_3 = 55^{1/2}$ h = 0.3

ℓ_2	k_1	k_2	k_3	Beam wavenumbers		Amplitude factors	
0.0	(6.396, .006)	(1.062, .341)	-	6.393	1.00	4.11	2.48
3.16	(6.430, .009)	(1.738, .283)	-	6.430	1.71	3.33	2.07
4.74	(6.482, .014)	(2.423, .293)	-	6.482	2.40	2.50	1.65
9.48	(7.383, .244)	(5.249, .342)	-	7.30	5.22	0.26	0.86
12.64	(10.138, .543)	(5.992, .171)	(1.148, 3.737)	-	5.98	-	0.99
15.80	-	(6.205, .367)	(3.846, 3.219)	-	6.10	-	0.64
18.96	-	(5.832, .299)	(9.593, 3.171)	-	5.79	-	0.84
22.12	-	(5.931, .187)	-	-	5.91	-	1.0
25.28	-	(5.934, .202)	-	-	5.91	-	0.96
$700^{1/2}$	-	(5.922, .189)	-	-	5.90	-	1.0

Case not drawn

Fig. 9 $\ell_1 = 55^{1/2}$ $\ell_2 = 4.74$ $\ell_3 = 55^{1/2}$

h	k_1	k_2	Beam wavenumbers		Amplitude factors	
0.2	(6.726, .062)	(3.886, .725)	6.722	3.75	2.77	1.59
0.3	(6.531, .038)	(2.895, .934)	6.530	2.63	3.95	1.69
0.8	(3.941, .285)	-	3.88	-	1.96	-

Fig. 10 $\ell_2 = 4.74$ $\ell_3 = 55^{1/2}$ h = 0.3

ℓ_1	k_1	k_2	k_3	Beam wavenumbers		Amplitude factors	
1.58	-	-	(1.955, 3.561)	No beam			
3.0	-	(3.599, 0)	(2.583, 3.617)	value at branch point	3.00	2.01	
4.74	-	(4.041, 1.235)	-	-	3.72	-	2.01
5.5	-	(3.368, 1.177)	-	-	3.02	-	1.77
$55^{1/2}$	(6.531, .038)	(2.895, .934)	-	6.530	2.63	3.95	1.69
$700^{1/2}$	(6.482, .014)	(2.423, .293)	-	6.482	2.40	2.50	1.65

Fig. 11 $\ell_1 = 5.5 \quad \ell_2 = 4.74 \quad \ell_3 = 55^{1/2}$

h	k_1	k_2	Beam wavenumbers		Amplitude factors	
0.2	-	(4.420, .727)	-	4.30	-	2.00
0.3	-	(3.386, 1.177)	-	3.02	-	1.77
0.4	-	(2.631, 2.219)	-	No beam	-	-
0.65	(5.082, .080)	-	5.077	-	6.63	-
0.8	(4.095 , .475)	-	3.92	-	1.97	-

Fig. 12 $\ell_2 = 4.74 \quad \ell_3 = 55^{1/2} \quad h = 0.4$

ℓ_1	k_1	k_2	k_3	Beam wavenumbers		Amplitude factors	
1.58	-	-	(1.434, 4.036)	No beam			
3.0	-	(3.251, 0)	(1.822, 4.008)	-	At branch point 3.0	-	2.71
4.74	-	(3.317, 3.017)	-	No beam			
5.5	-	(2.631, 2.219)	-	No beam			
$55^{1/2}$	(6.274, .028)	(1.961, 1.811)	-	6.273	-	5.177	-
$700^{1/2}$	(6.244, .009)	(.794, 1.115)	-	6.244	-	3.61	-

Fig. 13 $\ell_1 = 700^{1/2}$ $\ell_2 = 12.64$ $\ell_3 = 55^{1/2}$

h	k_1	k_2	k_3	k_4	Beam wavenumbers				Amplitude factors			
0.1	(6.737, .147)	(4.228, .902)	(1.383, 5.528)	(1.141, 9.680)	6.71	3.99	-	-	0.63	0.65	-	-
0.3	(10.138, .543)	(5.992, .171)	(1.148, 3.737)	(1.110, 8.749)	-	5.98	-	-	-	0.99	-	-
0.4	(11.039, .282)	(6.223, .478)	(3.199, 1.969)	(.759, 7.884)	10.94	6.04	2.44	-	.012	.54	.61	-
0.55	(11.697, .128)	(8.547, .565)	(3.659, .801)	(1.220, 7.023)	11.68	8.30	3.48	-	.03	.13	.95	-
0.8	(12.148, .049)	(10.556, .213)	(7.306, .645)	(1.454, 5.076)	12.14	10.54	7.20	-	.27	.33	.45	-

TABLE 2

DETAILS OF QUASI WAVE DRAG CURVES AGAINST h

Fig. 41 and 42 $\ell_1 = 700^{1/2}$ $\ell_3 = 55^{1/2}$ as ℓ_2 varies

ℓ_2	Drag Maxima		h	
1.58	207.44	231.58	0.283	.722
3.16	201.97	192.25	0.293	.709
4.74	190.52	142.16	0.311	.683
6.32	169.45	185.19	0.329	.713
9.48	126.04		0.439	
11.06	162.24		0.530	
12.64	190.95		0.509	

Fig. 43 $\ell_1 = 700^{1/2}$ $\ell_2 = 55^{1/2}$ $\ell_3 = 9.48$

Drag Maxima			h		
298.76	258.51	317.41	.045	.418	.770

Fig. 48 $\ell_1 = 55^{1/2}$ $\ell_3 = 55^{1/2}$ as ℓ_2 varies

ℓ_2	Drag Maxima		h	
1.58	182.71	229.30	.271	.717
3.16	175.12	195.30	.274	.707
4.74	162.17	163.46	.277	.693
6.32	146.02	153.04	.274	.697

Fig. 49 $\ell_2 = 3.16$ $\ell_3 = 55^{1/2}$ as ℓ_1 varies

ℓ_1	Drag Maxima		h	
3.16	115.	146.	.298	.766
5.5	127.63	196.06	.253	.706
$55^{1/2}$	175.12	195.30	.274	.707
$700^{1/2}$	201.97	192.25	.293	.709

Fig. 50 $\ell_2 = 4.74$ $\ell_3 = 55^{1/2}$ as ℓ_1 varies

ℓ_1	Drag Maxima		h	
4.74	114.87	169.	.239	.725
5.5	118.37	169.47	.240	.697
$55^{1/2}$	162.17	163.46	.277	.693
$700^{1/2}$	190.52	142.16	.311	.683

Fig. 1 The three layer model in which each stratum is characterised by a Scorer parameter ℓ.

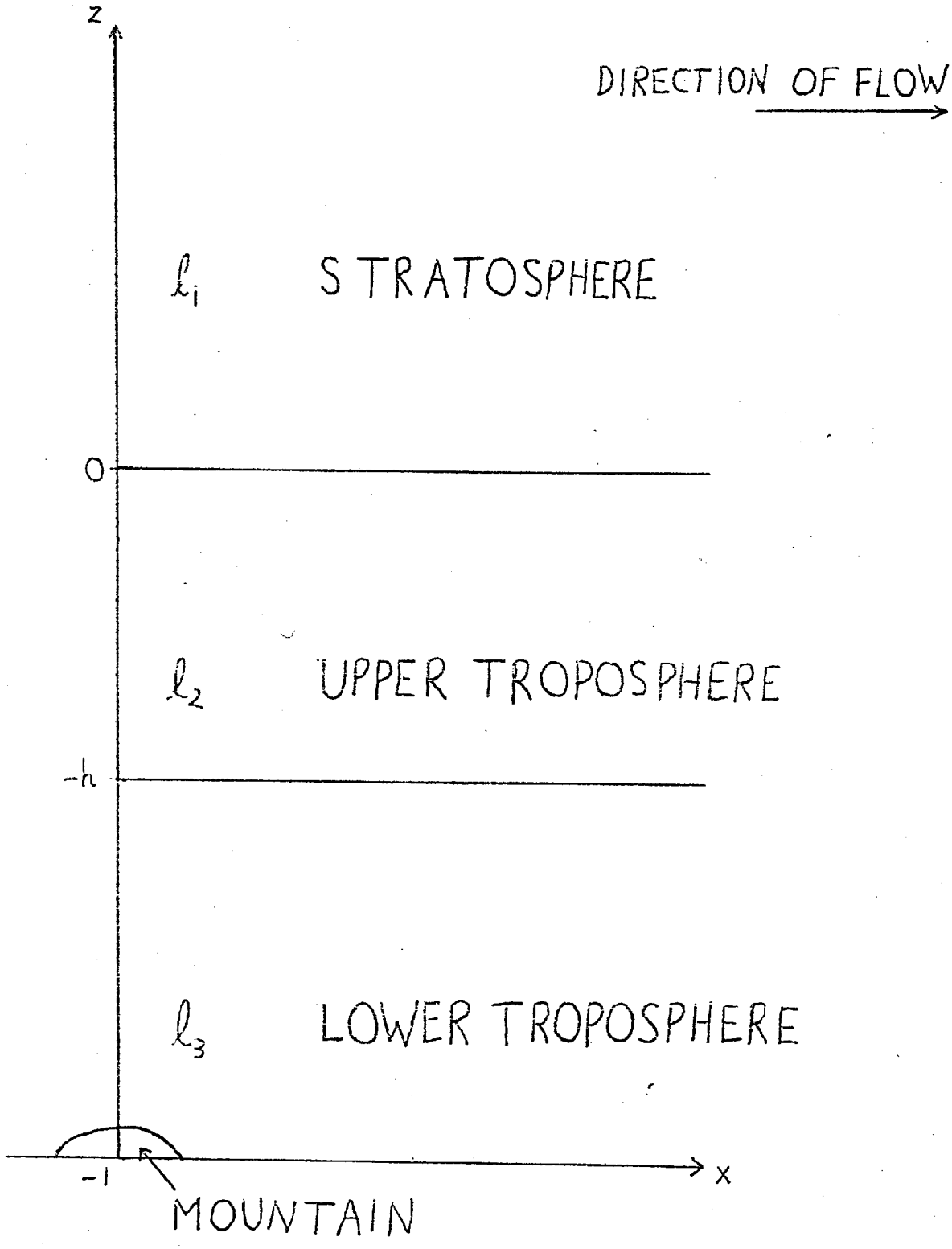

Fig. 2 The path of integration of G in the complex θ plane for the method of stationary phase. There is a branch point at $\theta = \frac{\pi}{2}$ and a saddle point at $\theta = \frac{\pi}{2} - \alpha$.

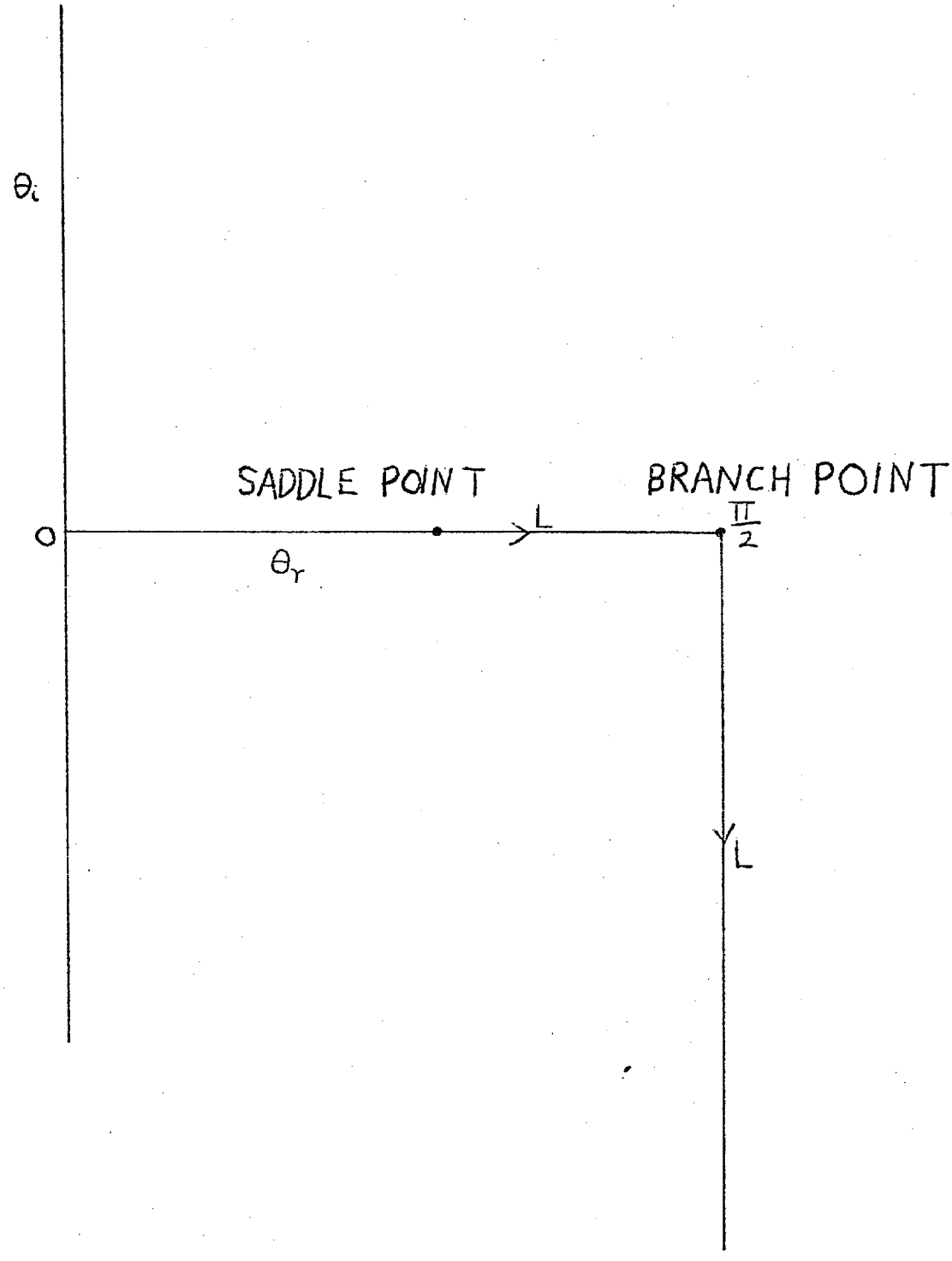

Fig. 3 Plot of $\frac{1}{|F|}$ against wavenumber for $\ell_1 = 700^{1/2}$, $\ell_3 = 55^{1/2}$, h = 0.8 as ℓ_2 varies.

As ℓ_2 increases, beams appear, for real values of k, at the origin, and increase in wavenumber and decrease in height. When ℓ_2 has increased to ℓ_1, all the beams present in the three layer model have disappeared. See Table 1 for details.

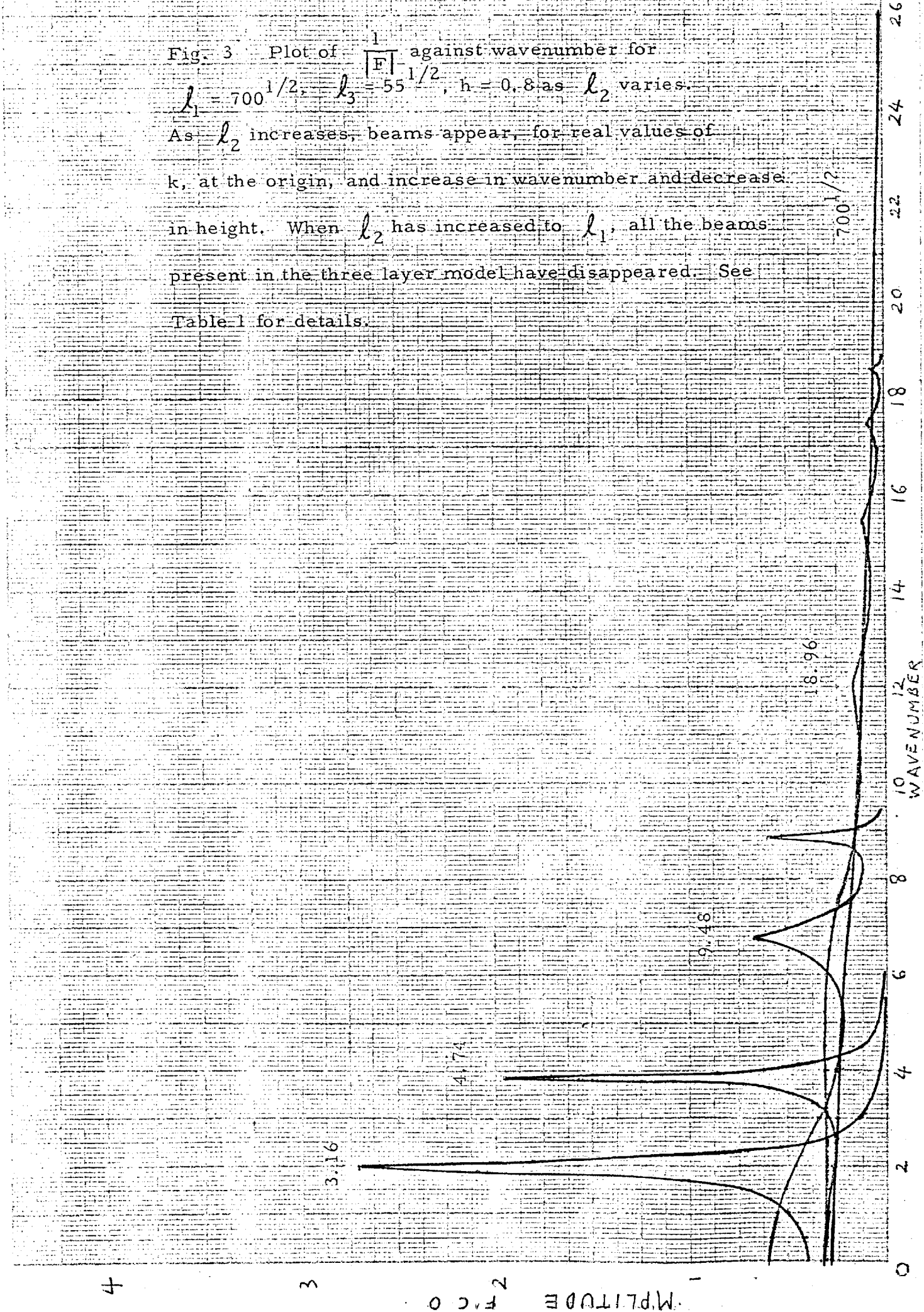

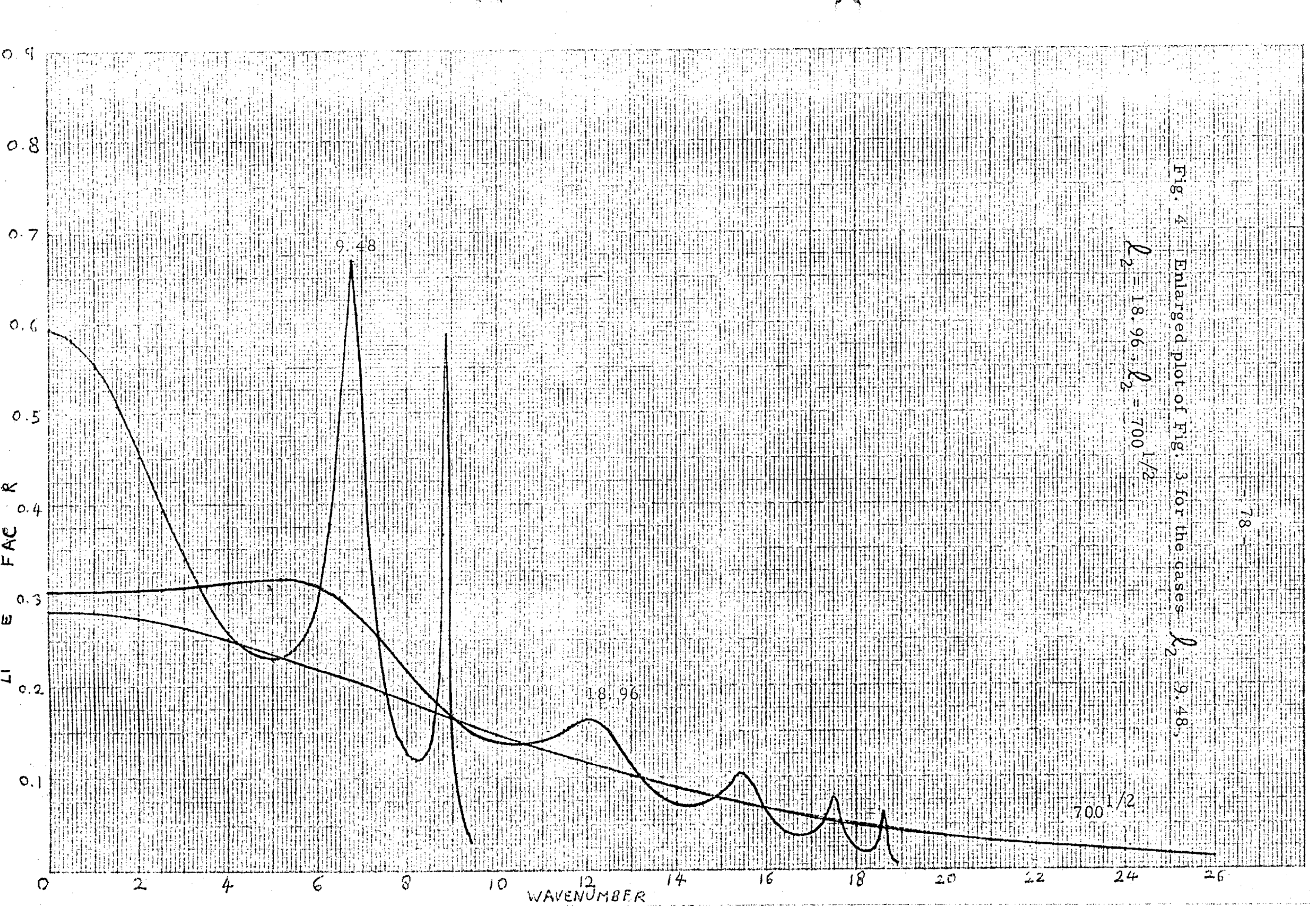

Fig. 4' Enlarged plot of Fig. 3 for the cases $\ell_2 = 9.48$, $\ell_2 = 18.96$, $\ell_2 = 700^{1/2}$

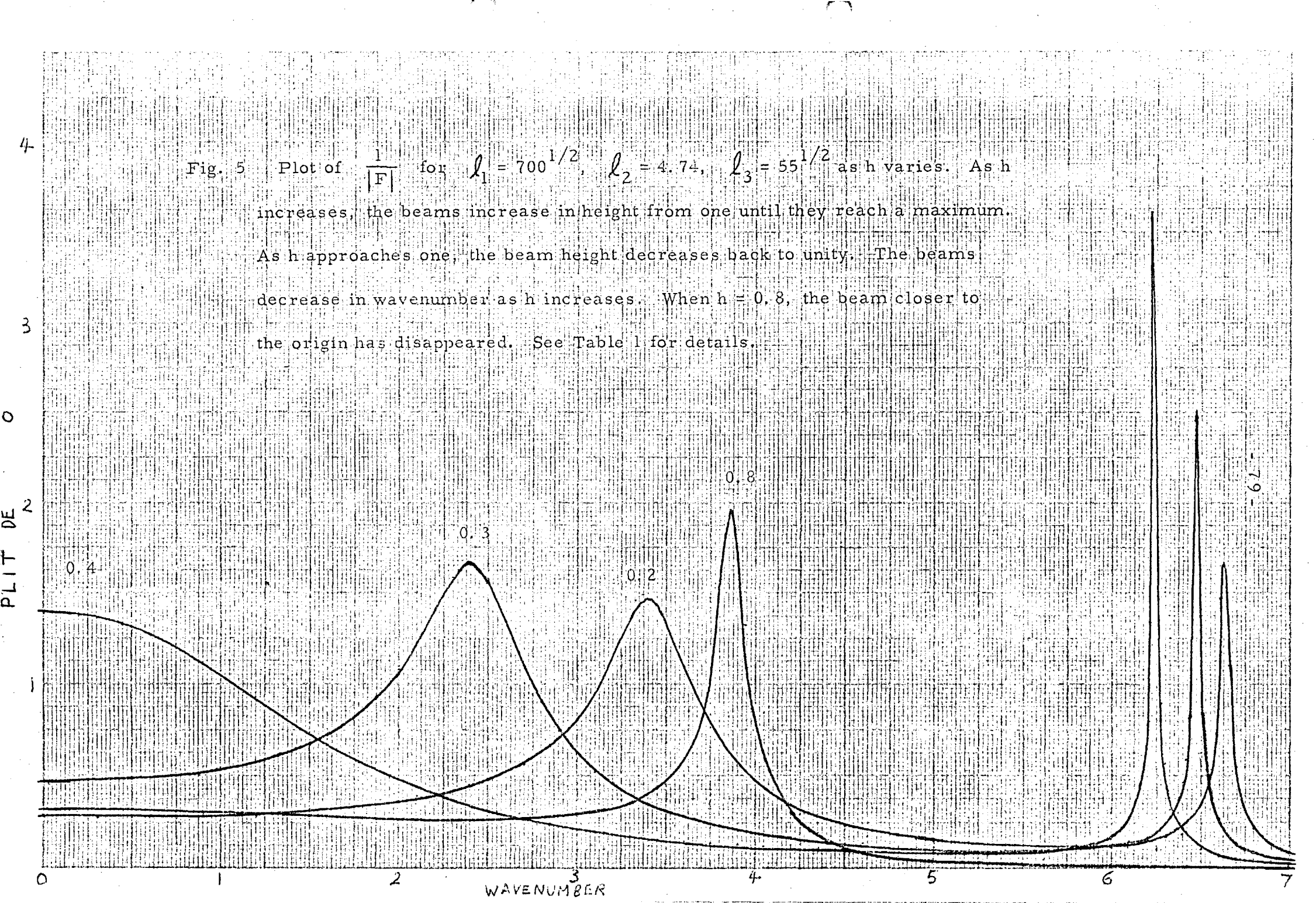

Fig. 5 Plot of $\frac{1}{|F|}$ for $\ell_1 = 700^{1/2}$, $\ell_2 = 4.74$, $\ell_3 = 55^{1/2}$ as h varies. As h increases, the beams increase in height from one until they reach a maximum. As h approaches one, the beam height decreases back to unity. The beams decrease in wavenumber as h increases. When h = 0.8, the beam closer to the origin has disappeared. See Table 1 for details.

Fig. 6 Plot of $\frac{1}{|F|}$ for $\ell_2 = 3.16$, $\ell_3 = 55^{1/2}$, $h = 0.8$, as ℓ_1 varies. The effect of increasing ℓ_1 is to produce a sharper beam. The value of the amplitude factor for each beam is the same for that wavenumber, as when $\ell_1 = \ell_2 = 3.16$. There is no beam for ℓ_1 less than ℓ_2. See Table 1 for details.

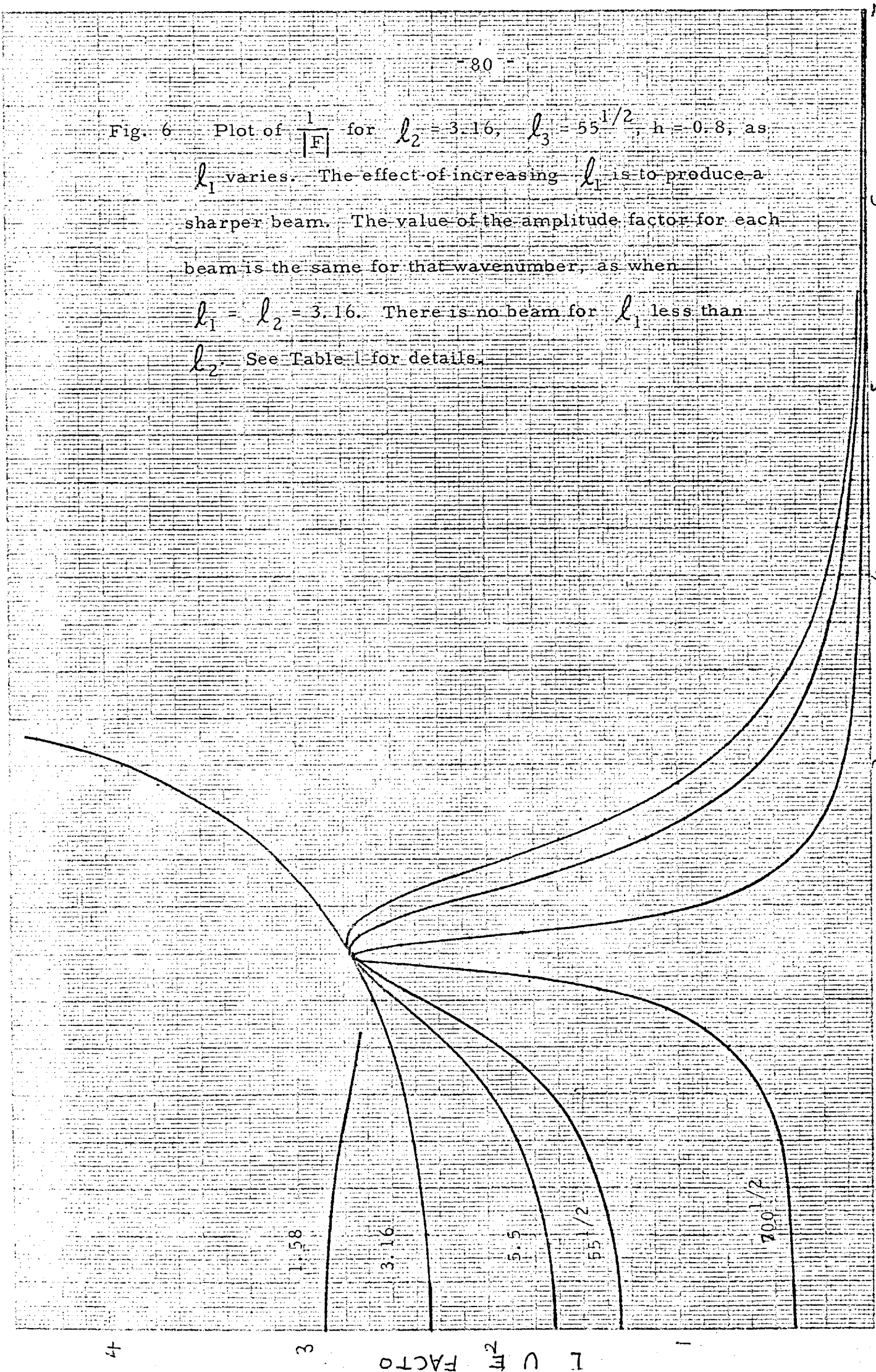

Fig. 7 Plot of $\frac{1}{|F|}$ for $\ell_1 = 5.5$, $\ell_2 = 3.16$ $\ell_3 = 55^{1/2}$ as h varies. The beam for h = 0.2 disappears at k = 0, as h increases. A taller, sharper beam appears at k = 5.5, and moves towards k = 0 as h increases. See Table 1 for details.

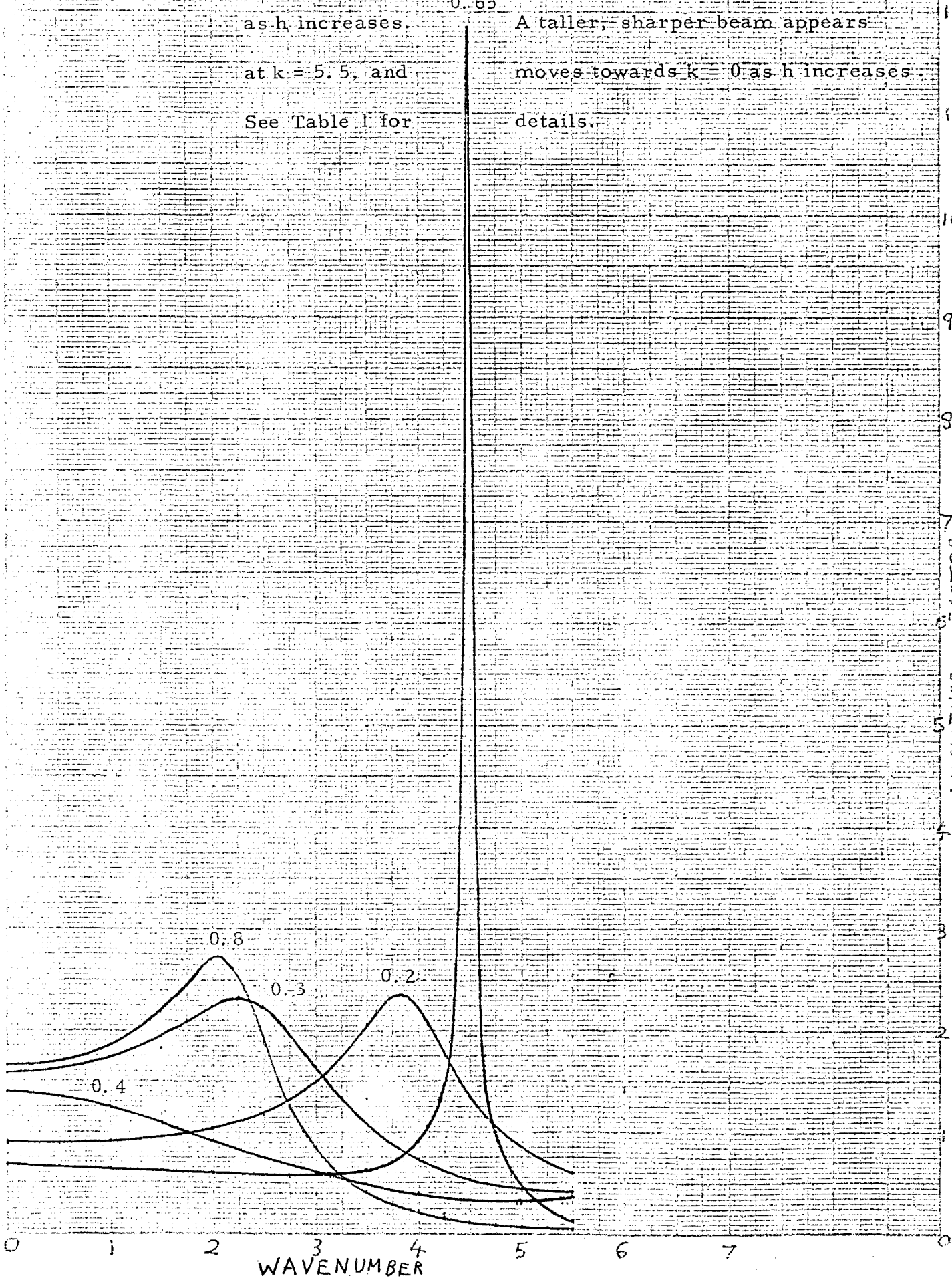

Fig. 8 Plot of $\frac{1}{|F|}$ for $\ell_1 = 700^{1/2}$, $\ell_3 = 55^{1/2}$, $h = 0.3$ as ℓ_2 varies. As ℓ_2 increases the beam for longer wavenumbers decreases in height and the beam wavenumber increases. When $\ell_2 = 12.64$, this beam has disappeared. The beam for smaller wavenumbers decreases from its value at $\ell_2 = 0$, reaches a minimum, and increases to one for a value of ℓ_2 close to 12.64 (12.02). As ℓ_2 further increases, the wavenumber changes little. See Table 1.

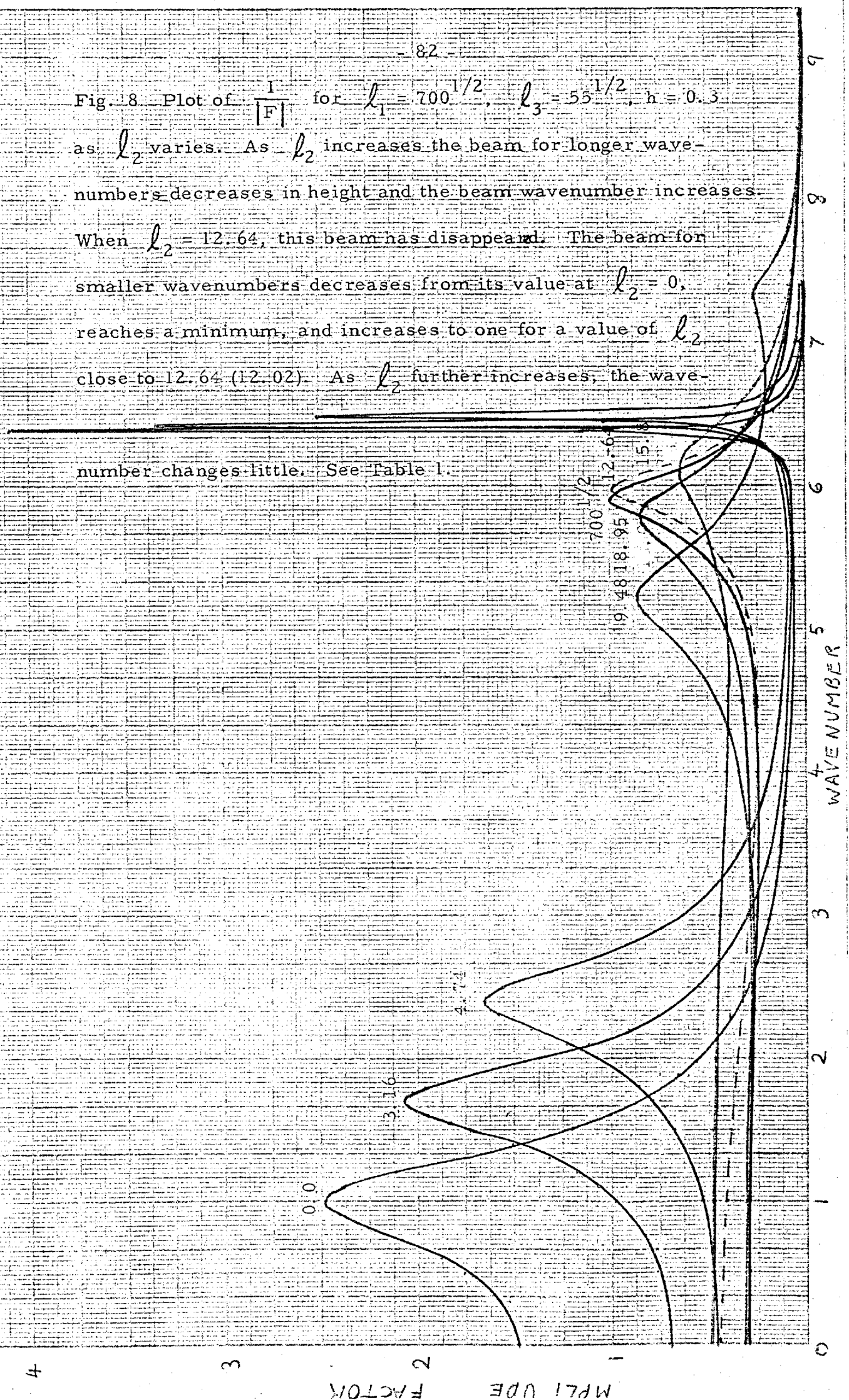

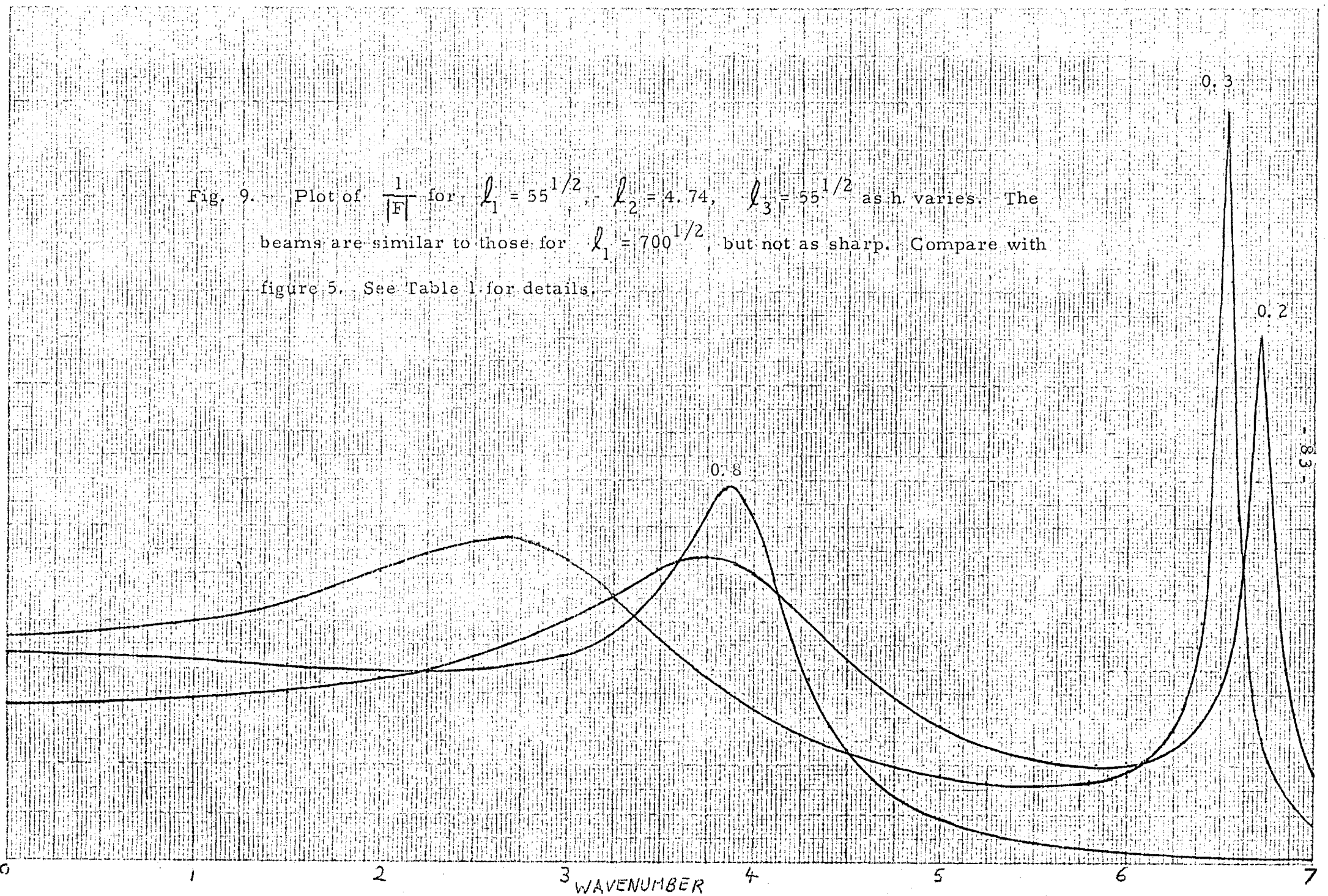

Fig. 9. Plot of $\frac{1}{|F|}$ for $\ell_1 = 55^{1/2}$, $\ell_2 = 4.74$, $\ell_3 = 55^{1/2}$ as h varies. The beams are similar to those for $\ell_1 = 700^{1/2}$, but not as sharp. Compare with figure 5. See Table 1 for details.

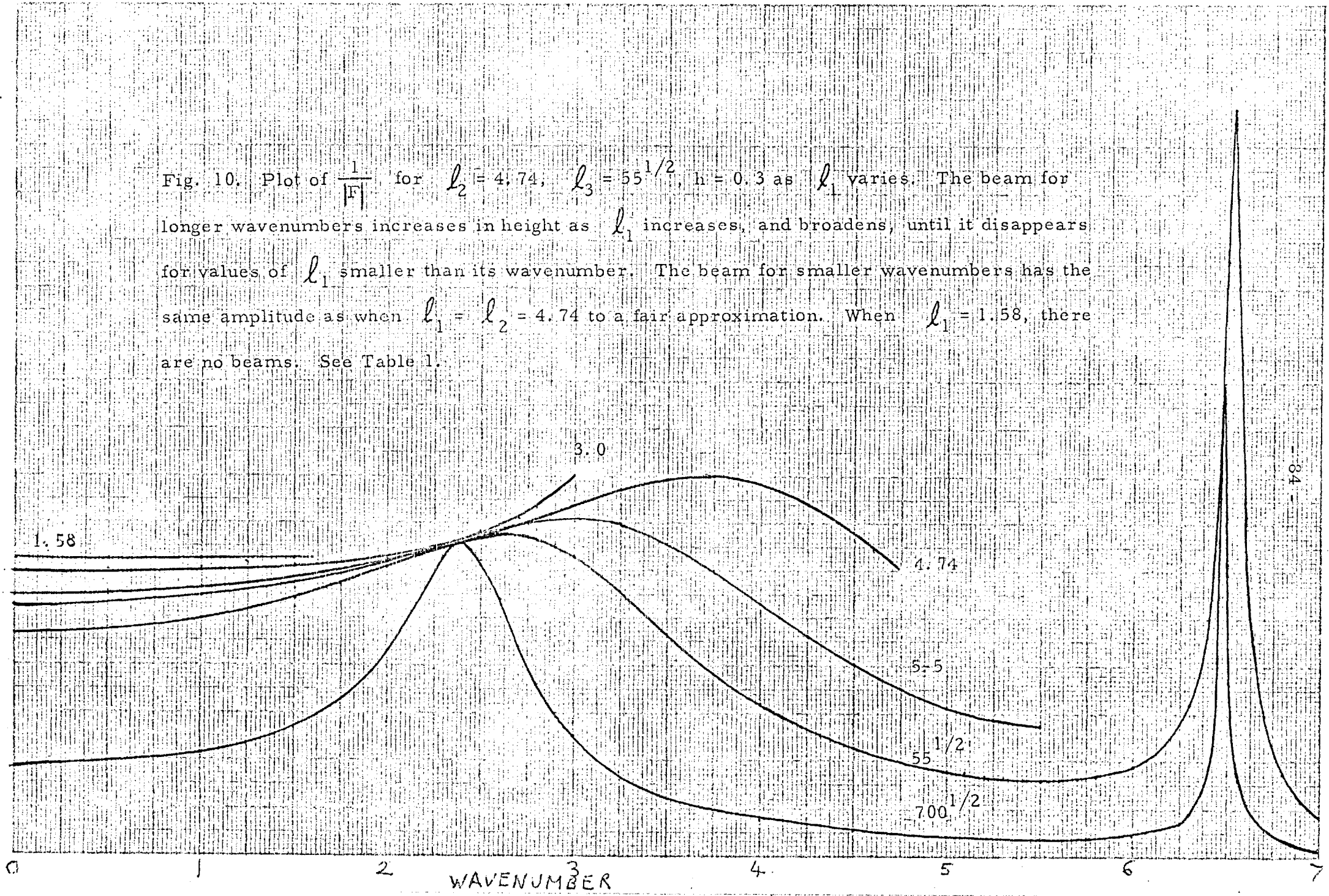

Fig. 10. Plot of $\frac{1}{|F|}$ for $\ell_2 = 4.74$, $\ell_3 = 55^{1/2}$, $h = 0.3$ as ℓ_1 varies. The beam for longer wavenumbers increases in height as ℓ_1 increases, and broadens, until it disappears for values of ℓ_1 smaller than its wavenumber. The beam for smaller wavenumbers has the same amplitude as when $\ell_1 = \ell_2 = 4.74$ to a fair approximation. When $\ell_1 = 1.58$, there are no beams. See Table 1.

Fig. 11 Plot of $\frac{1}{|F|}$ against wavenumber for $\ell_1 = 5.5$, $\ell_2 = 4.74$, $\ell_3 = 55^{1/2}$ as h varies. There is a comparison with fig. 7. See Table 1 for details.

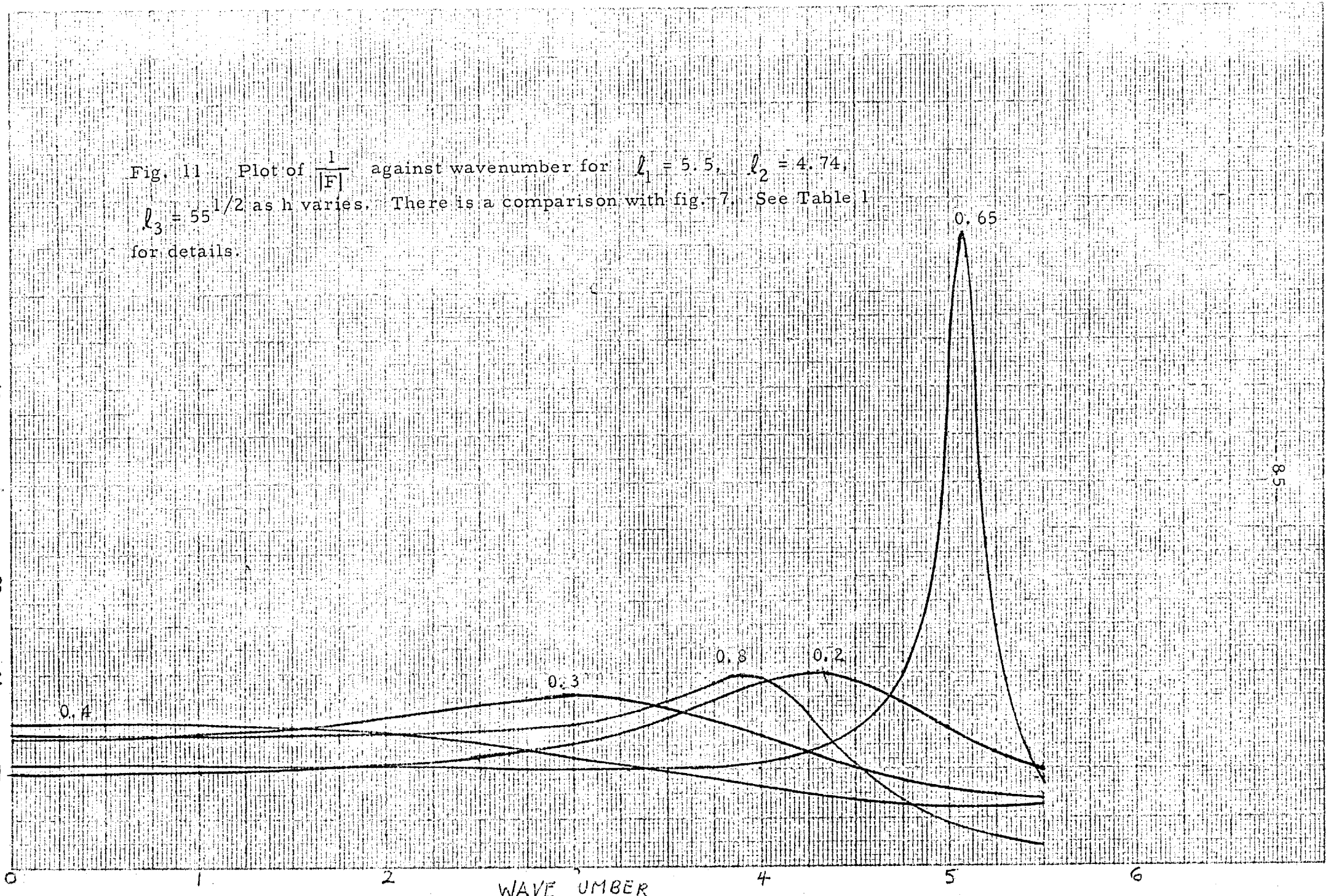

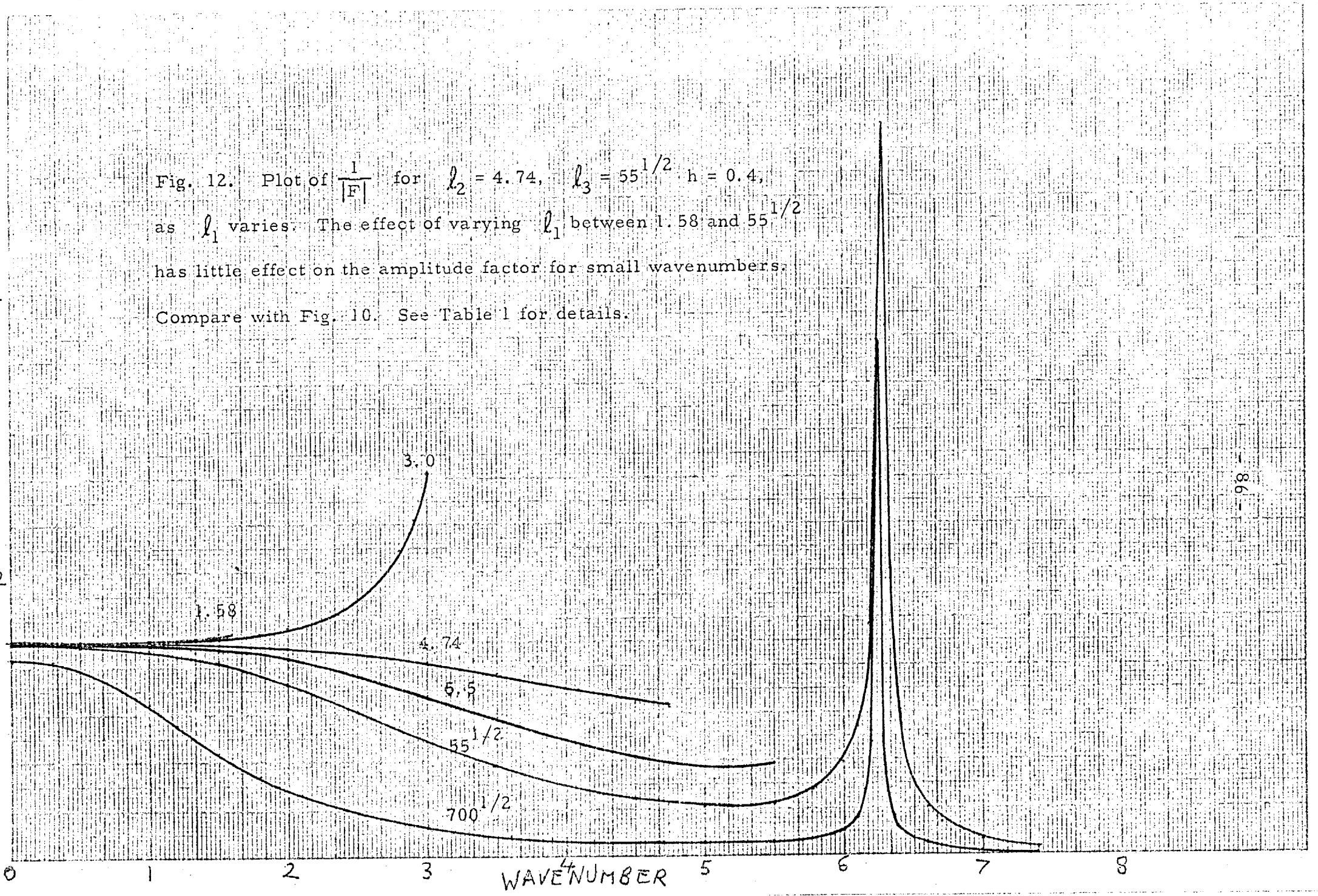

Fig. 12. Plot of $\frac{1}{|F|}$ for $\ell_2 = 4.74$, $\ell_3 = 55^{1/2}$ $h = 0.4$, as ℓ_1 varies. The effect of varying ℓ_1 between 1.58 and $55^{1/2}$ has little effect on the amplitude factor for small wavenumbers. Compare with Fig. 10. See Table 1 for details.

Fig. 13 Plot of $\frac{1}{|F|}$ against wavenumber for $\ell_1 = 700^{1/2}$, $\ell_2 = 12.64$, $\ell_3 = 55^{1/2}$ as h varies. When h = 0, the beams have amplitude one, a small change in h to 0.1 considerably reduces the beam amplitude. Large beam amplitudes near unity are produced for certain intermediate values of h. As h tends to one the beam amplitudes increase sharply back to one. See Table 1 for details

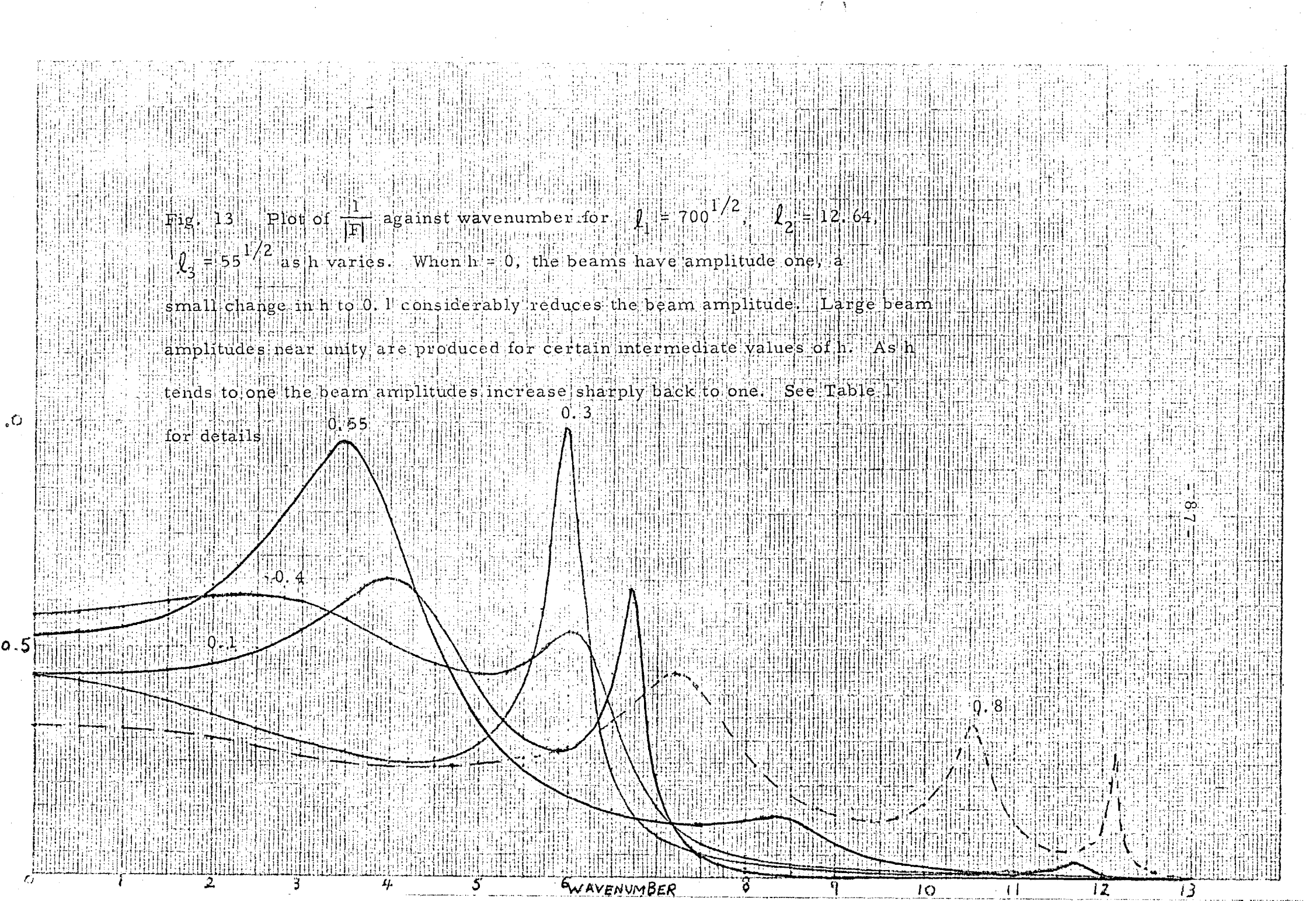

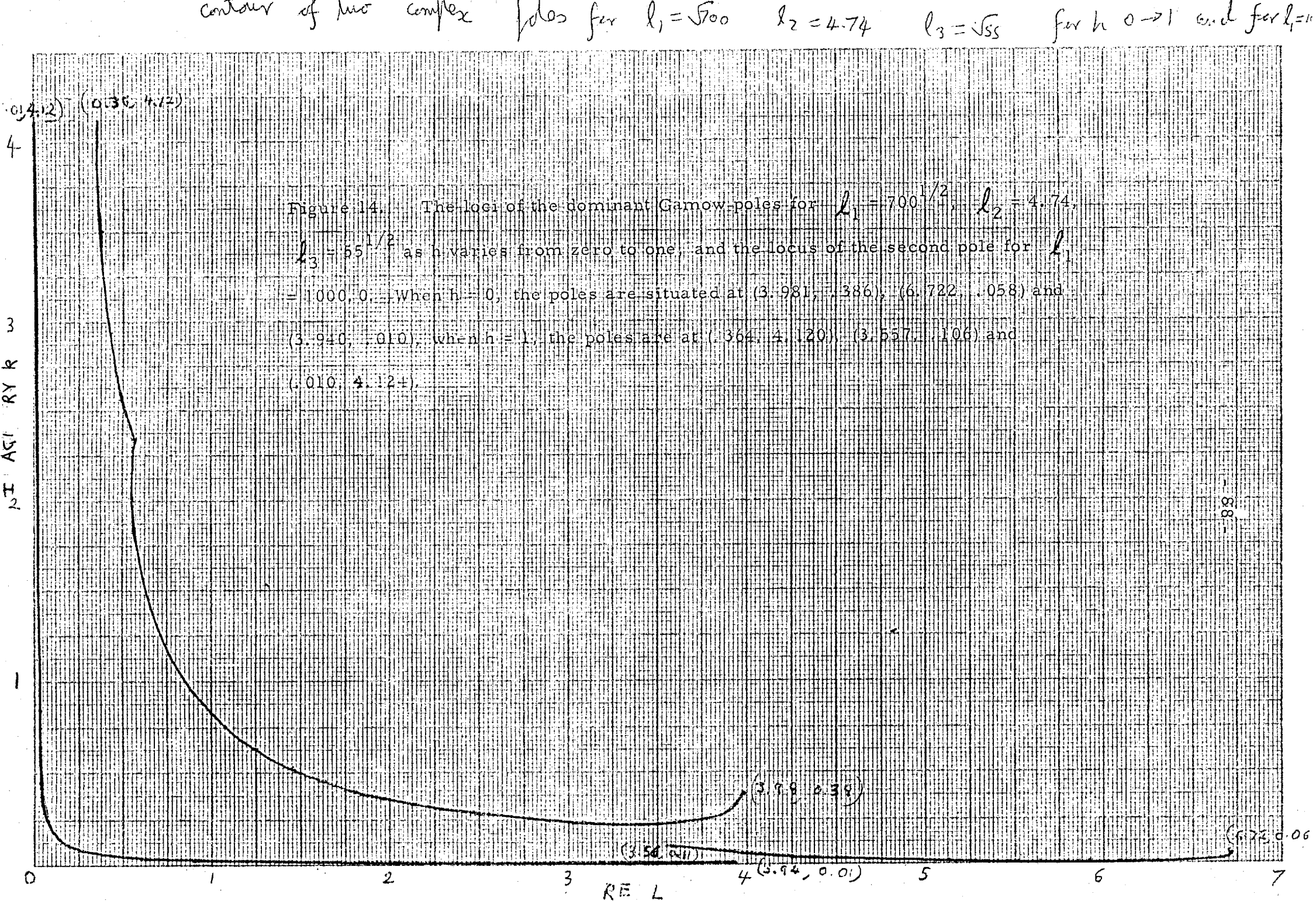

Figure 14. The loci of the dominant Gamow-poles for $\ell_1 = 700^{1/2}$, $\ell_2 = 4.74$, $\ell_3 = 55^{1/2}$ as h varies from zero to one, and the locus of the second pole for $\ell_1 = 1000.0$. When h = 0, the poles are situated at (3.981, .386), (6.722, .058) and (3.940, .010). When h = 1, the poles are at (.364, 4.120), (3.557, .106) and (.010, 4.12+).

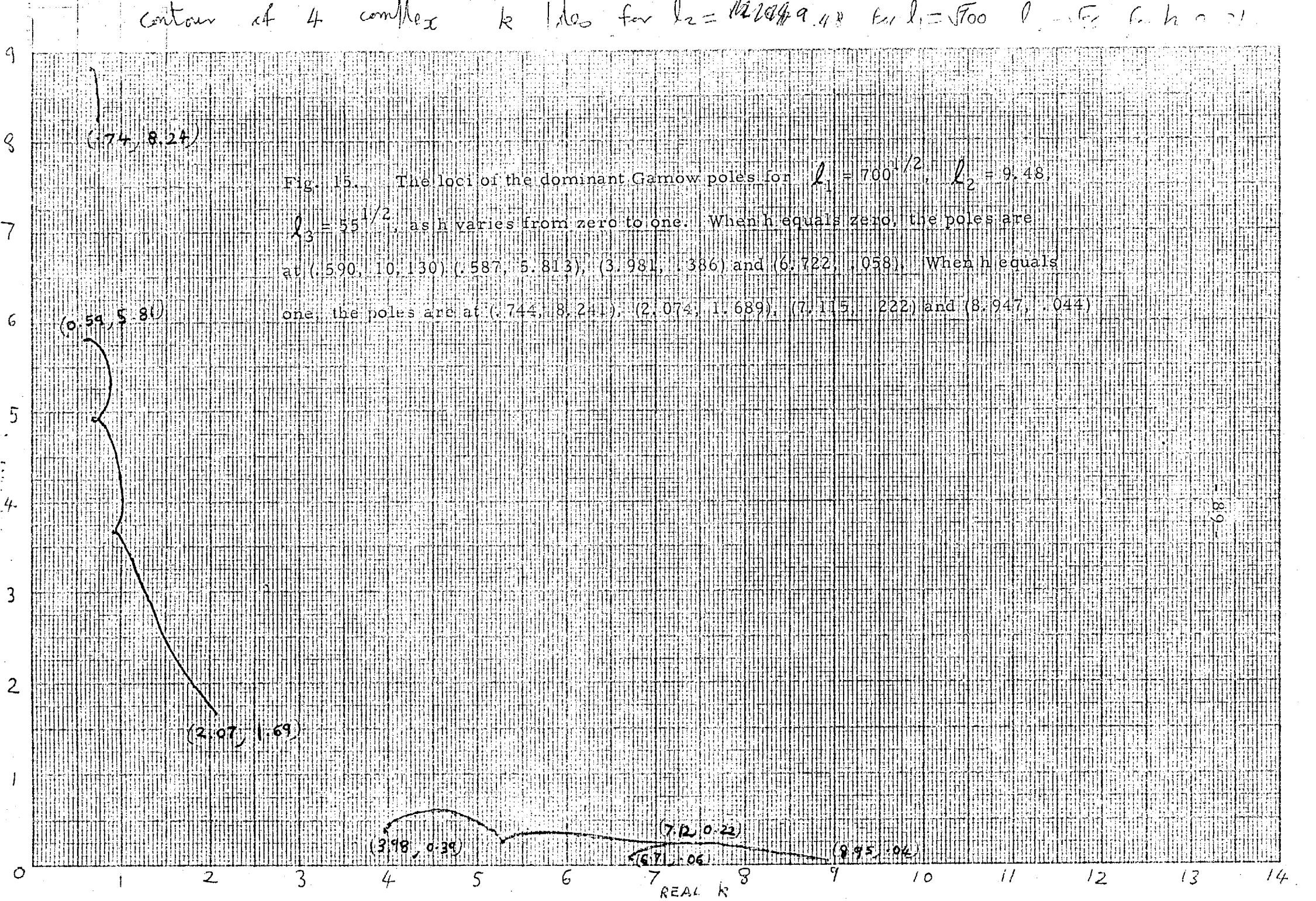

Fig. 15. The loci of the dominant Gamow poles for $\ell_1 = 700^{1/2}$, $\ell_2 = 9.48$, $\ell_3 = 55^{1/2}$, as h varies from zero to one. When h equals zero, the poles are at (.590, 10.130), (.587, 5.813), (3.981, .386) and (6.722, .058). When h equals one, the poles are at (.744, 8.244), (2.074, 1.689), (7.115, .222) and (8.947, .044)

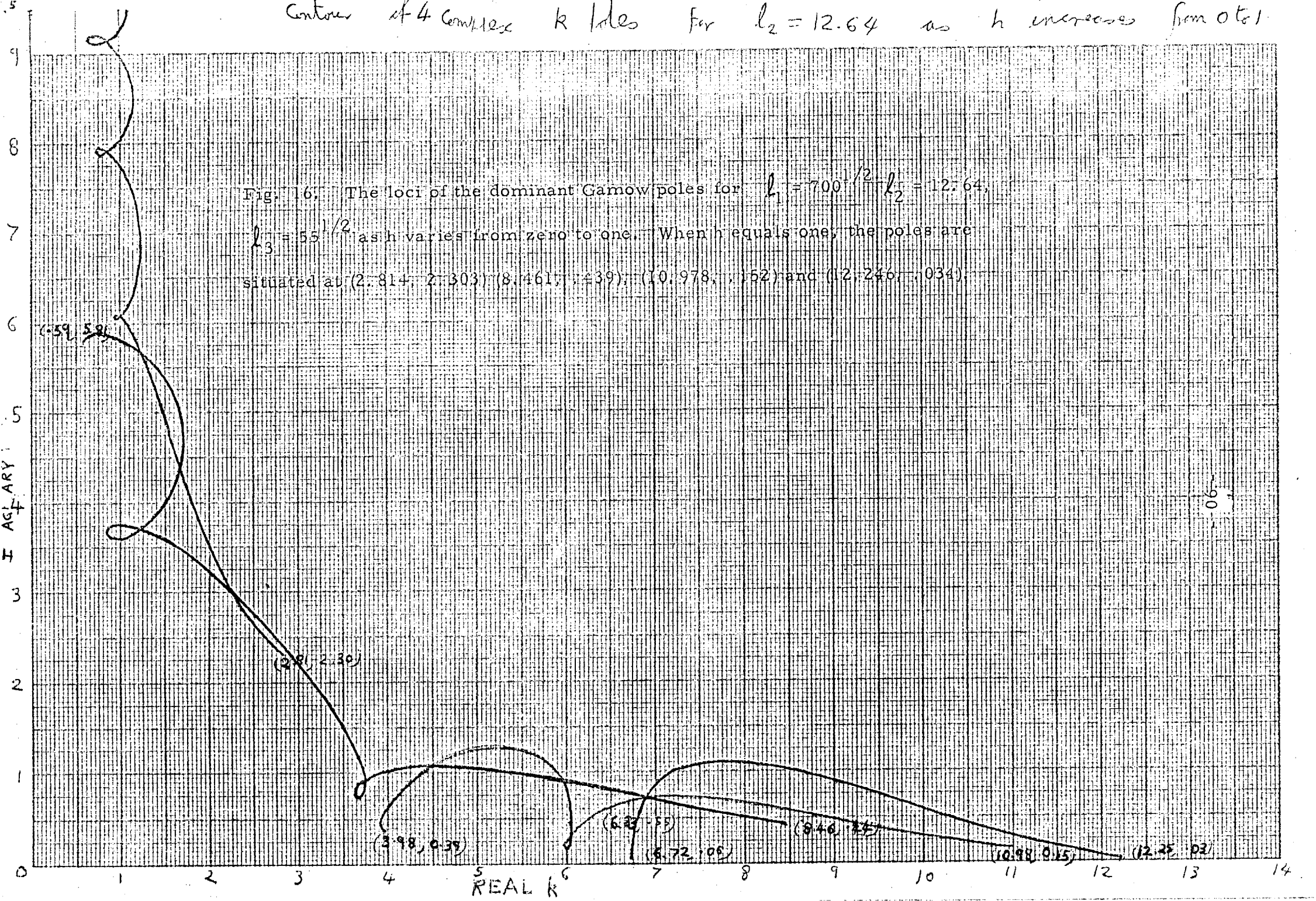

Fig. 16. The loci of the dominant Gamow poles for $l_1 = 700^{1/2}$ $l_2 = 12.64$, $l_3 = 55^{1/2}$ as h varies from zero to one. When h equals one, the poles are situated at (2.814, 2.303) (8.461, .039), (10.978, .152) and (12.246, .034).

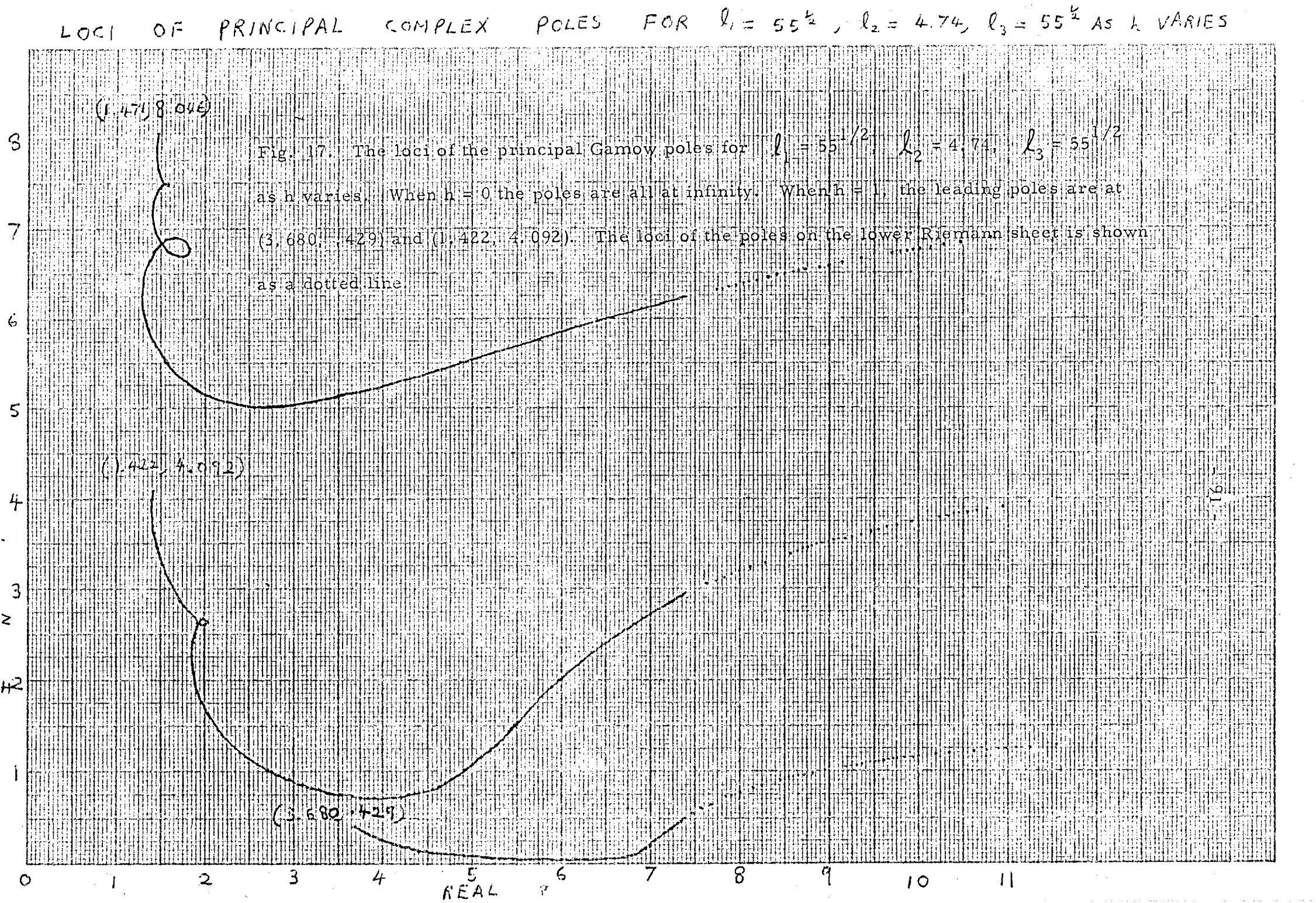

Fig. 17. The loci of the principal Gamow poles for $l_1 = 55^{1/2}$, $l_2 = 4.74$, $l_3 = 55^{1/2}$ as h varies. When h = 0 the poles are all at infinity. When h = 1, the leading poles are at (3.680, .429) and (1.422, 4.092). The loci of the poles on the lower Riemann sheet is shown as a dotted line.

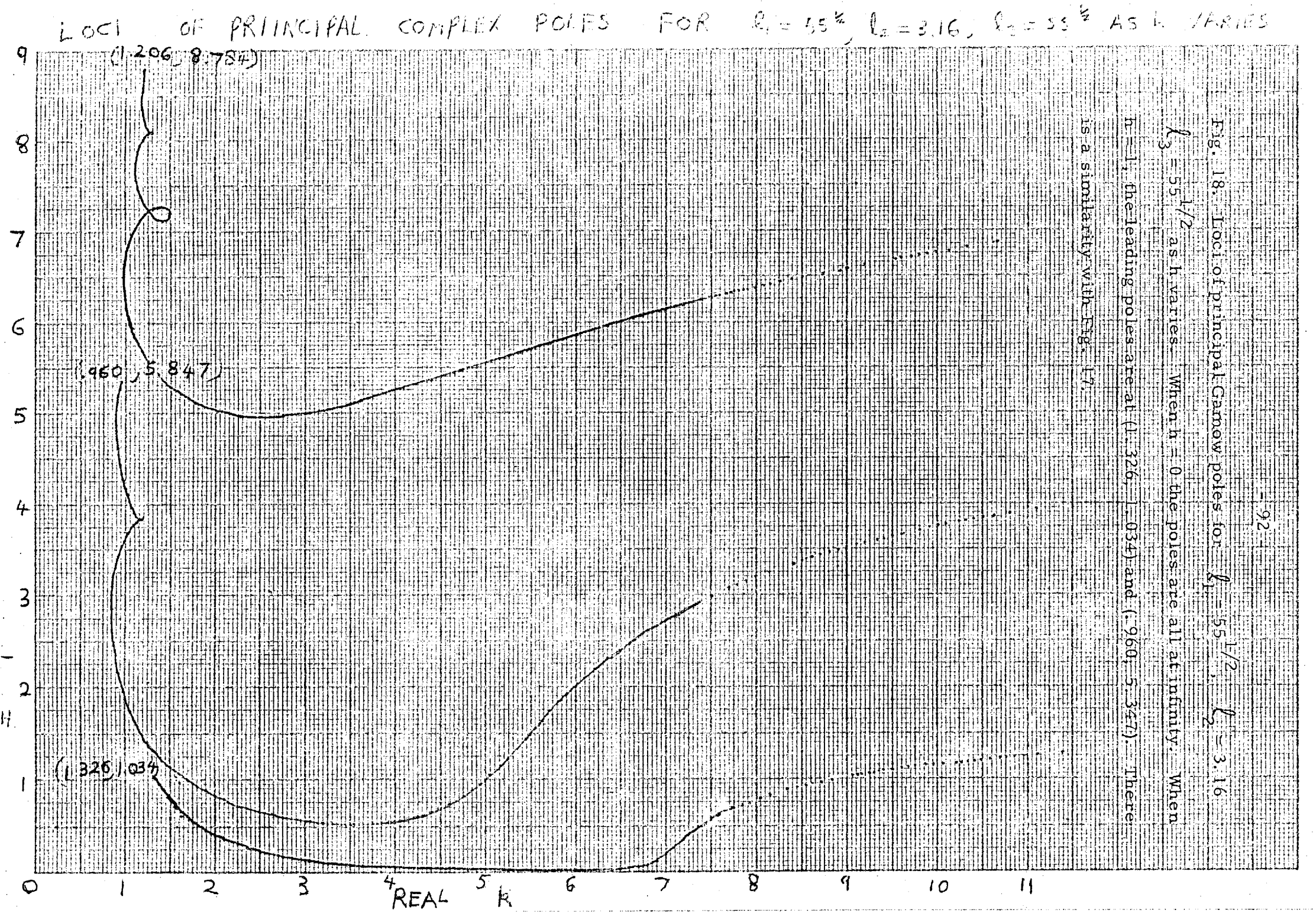

Fig. 18. Loci of principal Gamow poles for $R_1 = 55^{1/2}$, $R_2 = 3.16$, $R_3 = 55^{1/2}$ as h varies. When h = 0 the poles are all at infinity. When h = 1, the leading poles are at (1.326, .034) and (.960, 5.847). There is a similarity with Fig. 17.

LOCI OF PRINCIPAL COMPLEX POLES FOR $\ell_1 = 5.5$, $\ell_2 = 4.74$, $\ell_3 = 55^{1/2}$

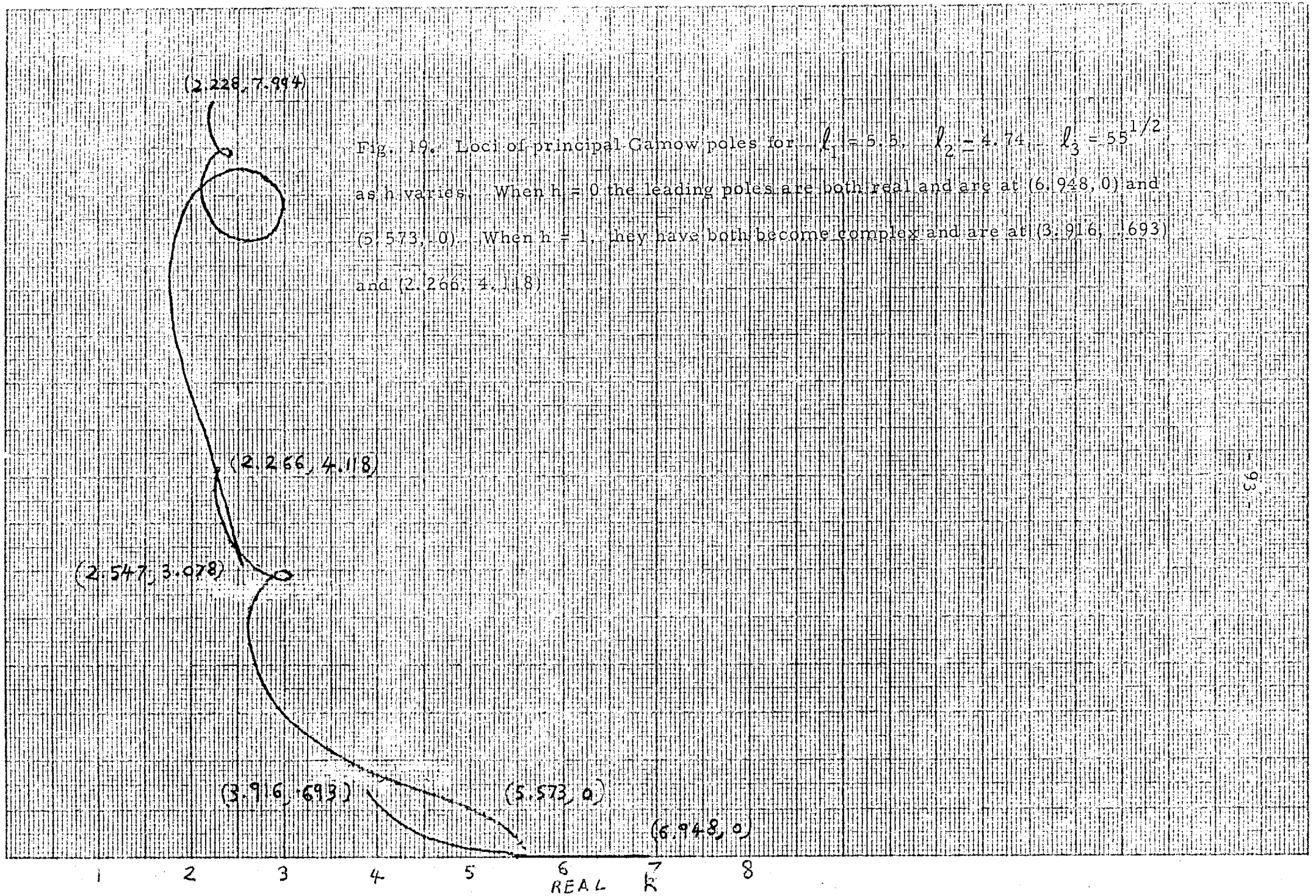

Fig. 19. Loci of principal Gamow poles for $\ell_1 = 5.5$, $\ell_2 = 4.74$, $\ell_3 = 55^{1/2}$ as h varies. When h = 0 the leading poles are both real and are at (6.948, 0) and (5.573, 0). When h = 1, they have both become complex and are at (3.916, .693) and (2.266, 4.118).

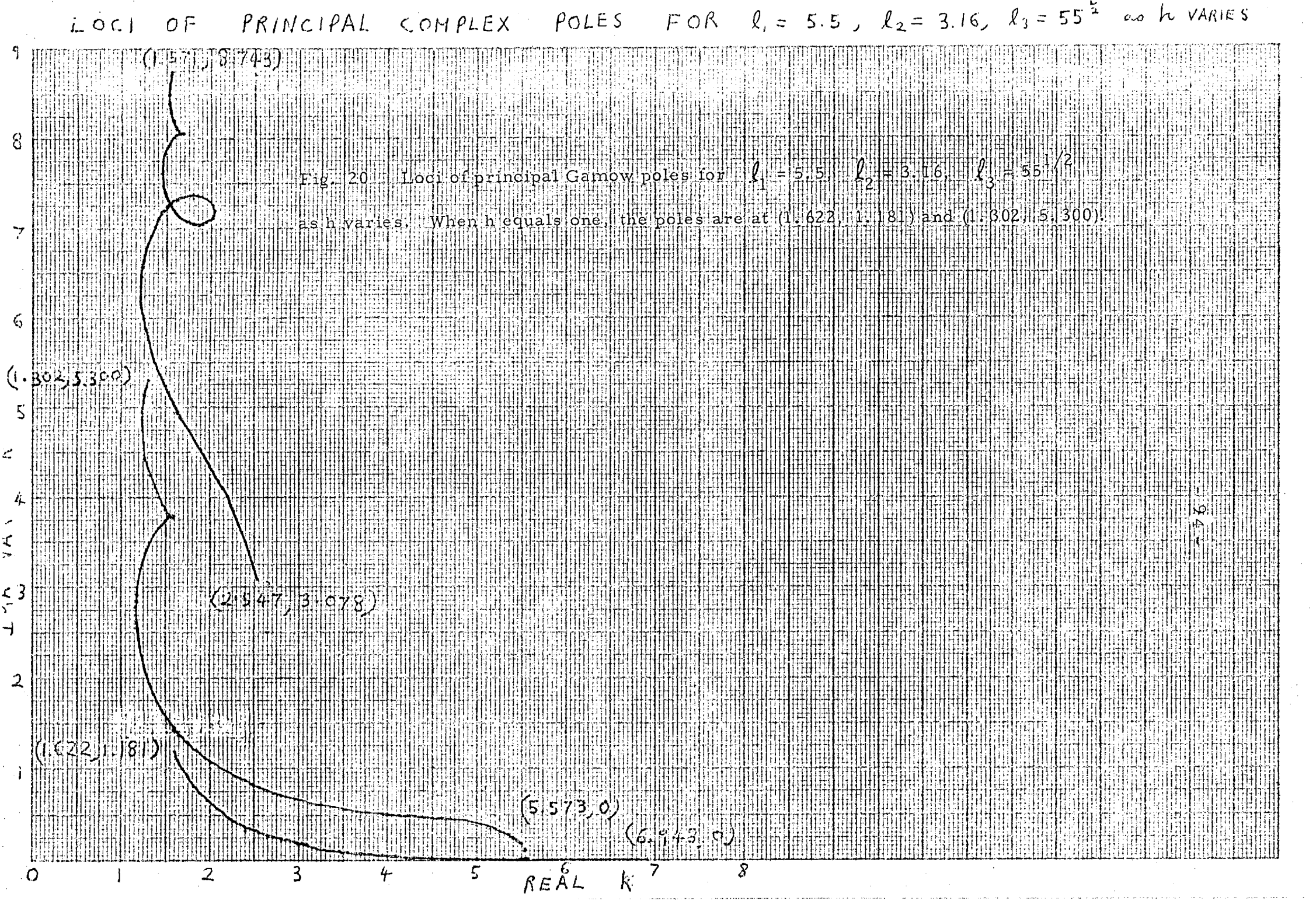

Fig. 20 Loci of principal Gamow poles for $\ell_1 = 5.5$, $\ell_2 = 3.16$, $\ell_3 = 55^{1/2}$ as h varies. When h equals one, the poles are at (1.622, 1.181) and (1.302, 5.300).

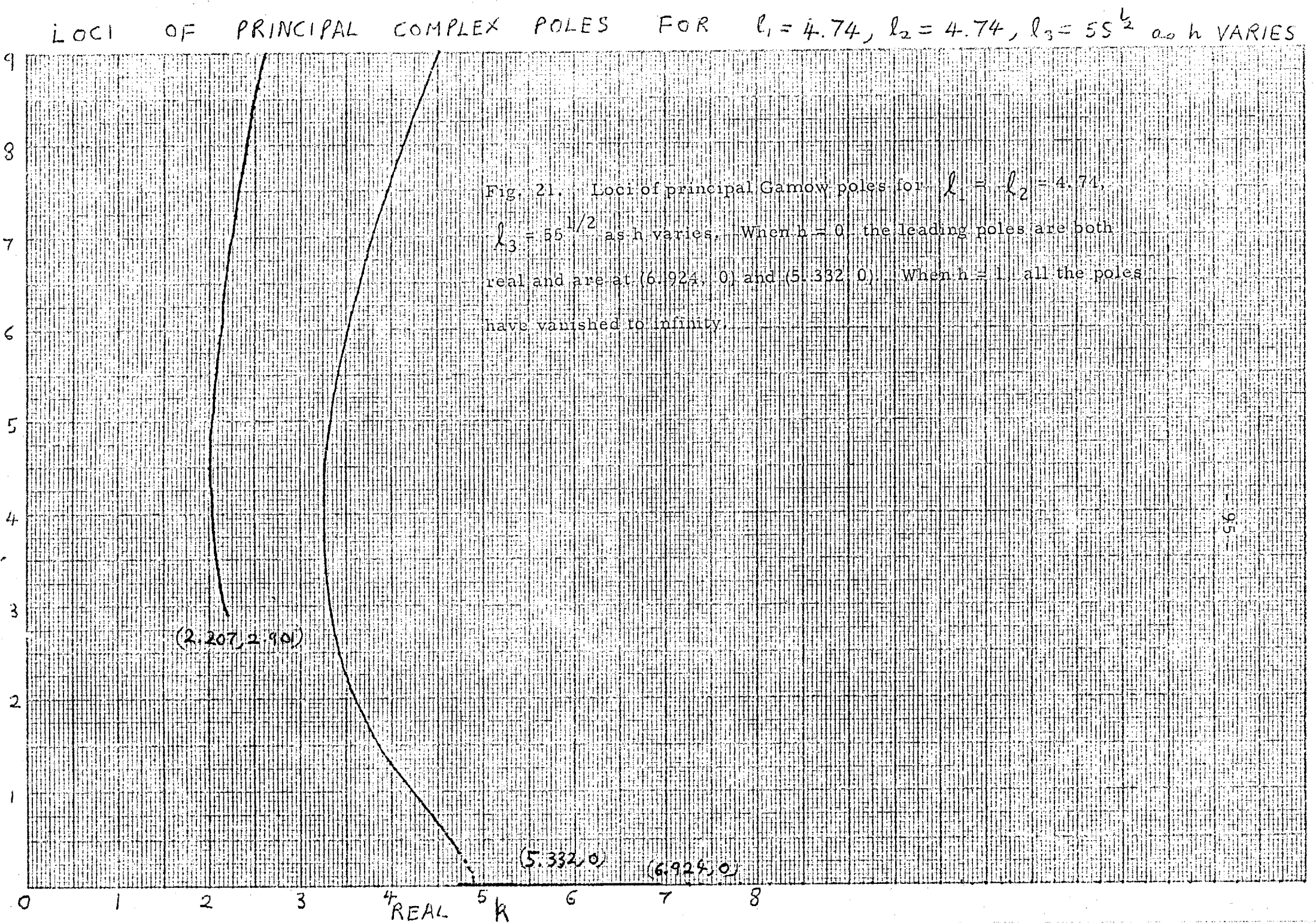

Fig. 21. Loci of principal Gamow poles for $\ell_1 = \ell_2 = 4.74$, $\ell_3 = 55^{1/2}$ as h varies. When h = 0 the leading poles are both real and are at (6.924, 0) and (5.332, 0). When h = 1, all the poles have vanished to infinity.

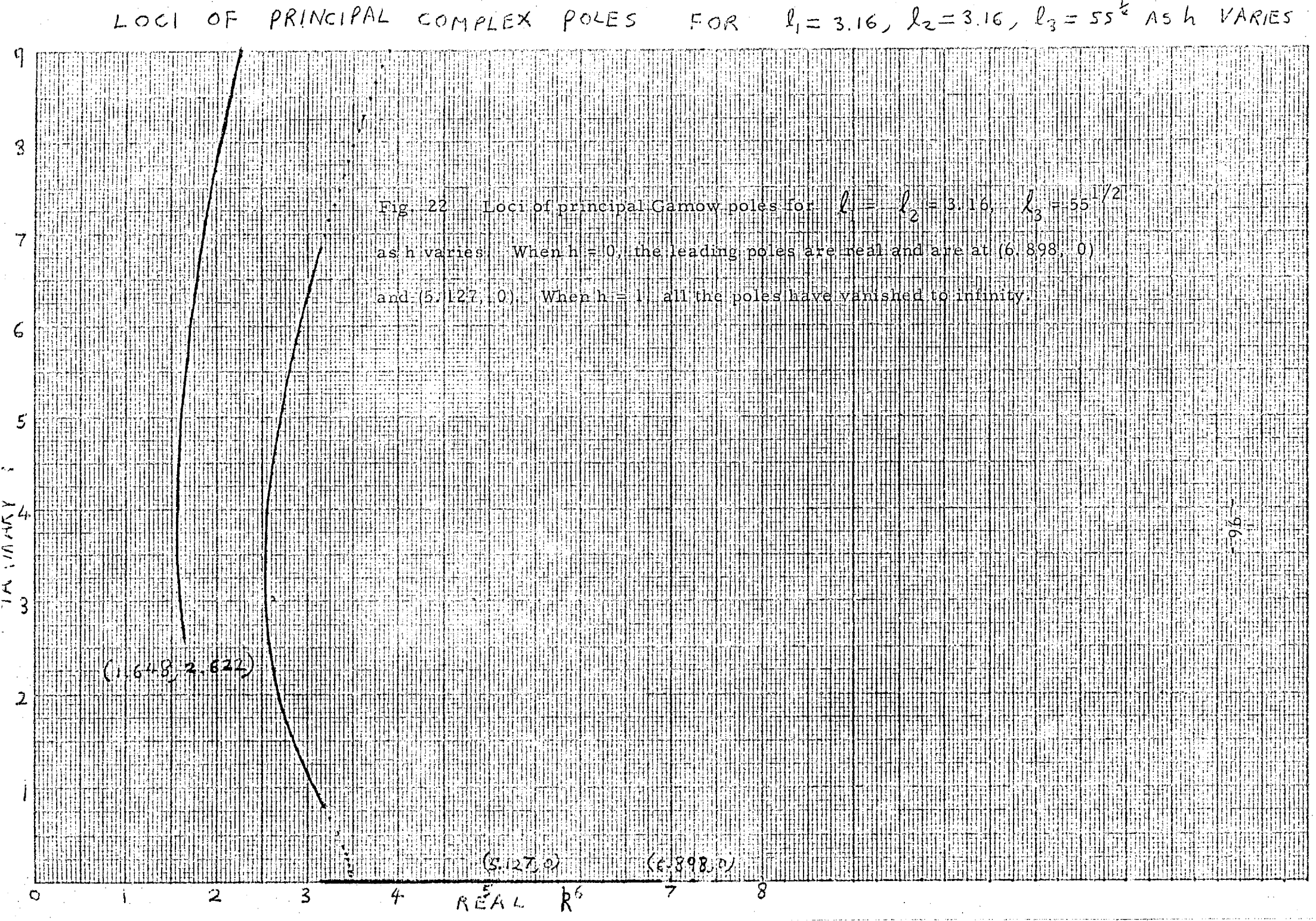

Fig. 22 Loci of principal Gamow poles for $\ell_1 = \ell_2 = 3.16$, $\ell_3 = 55^{1/2}$ as h varies. When h = 0, the leading poles are real and are at (6.898, 0) and (5.127, 0). When h = 1, all the poles have vanished to infinity.

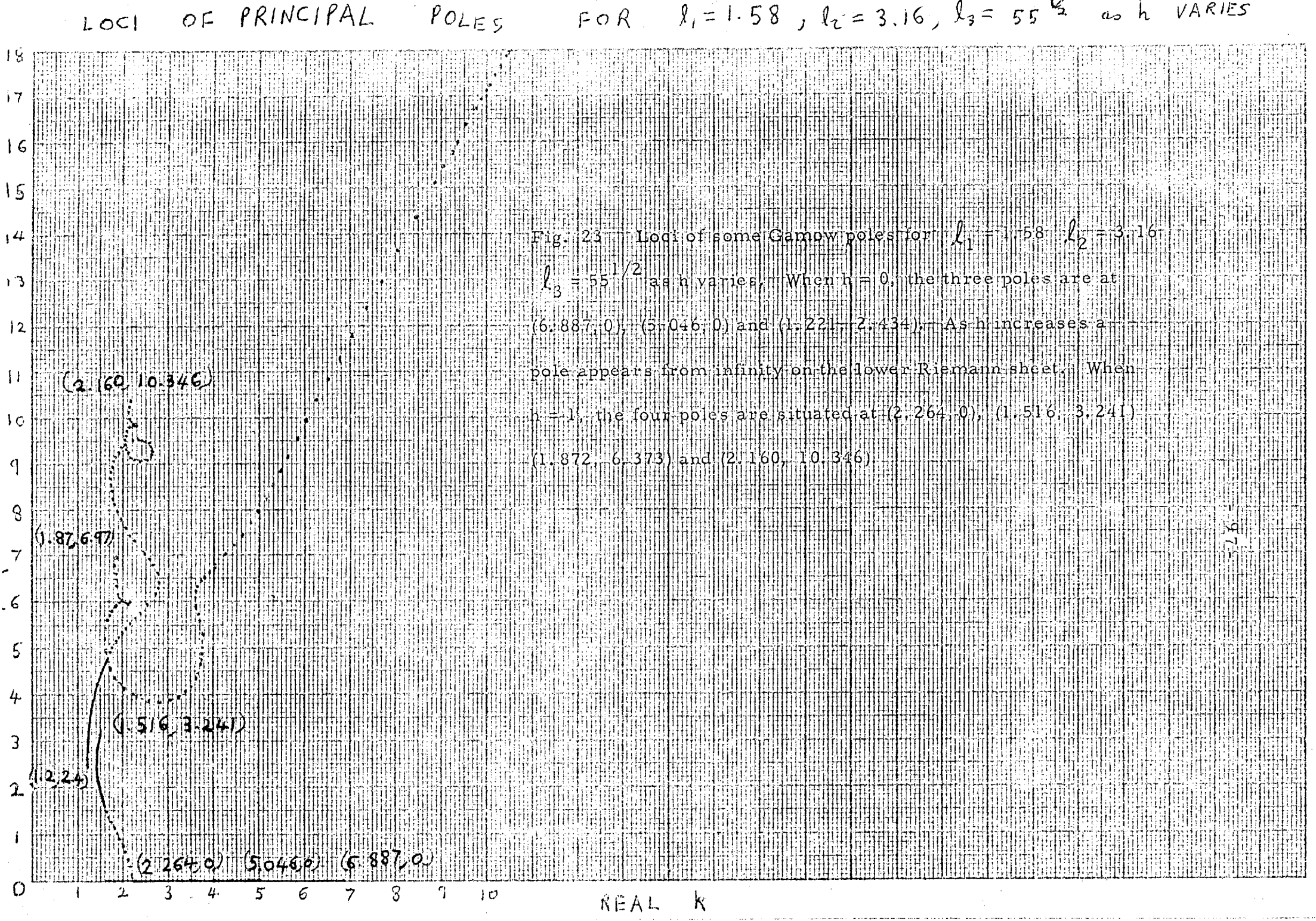

Fig. 23 Loci of some Gamow poles for $l_1 = 1.58$, $l_2 = 3.16$, $l_3 = 55^{1/2}$ as h varies. When h = 0, the three poles are at (6.887, 0), (5.046, 0) and (1.221, 2.434). As h increases a pole appears from infinity on the lower Riemann sheet. When h = 1, the four poles are situated at (2.264, 0), (1.516, 3.241), (1.872, 6.373) and (2.160, 10.346).

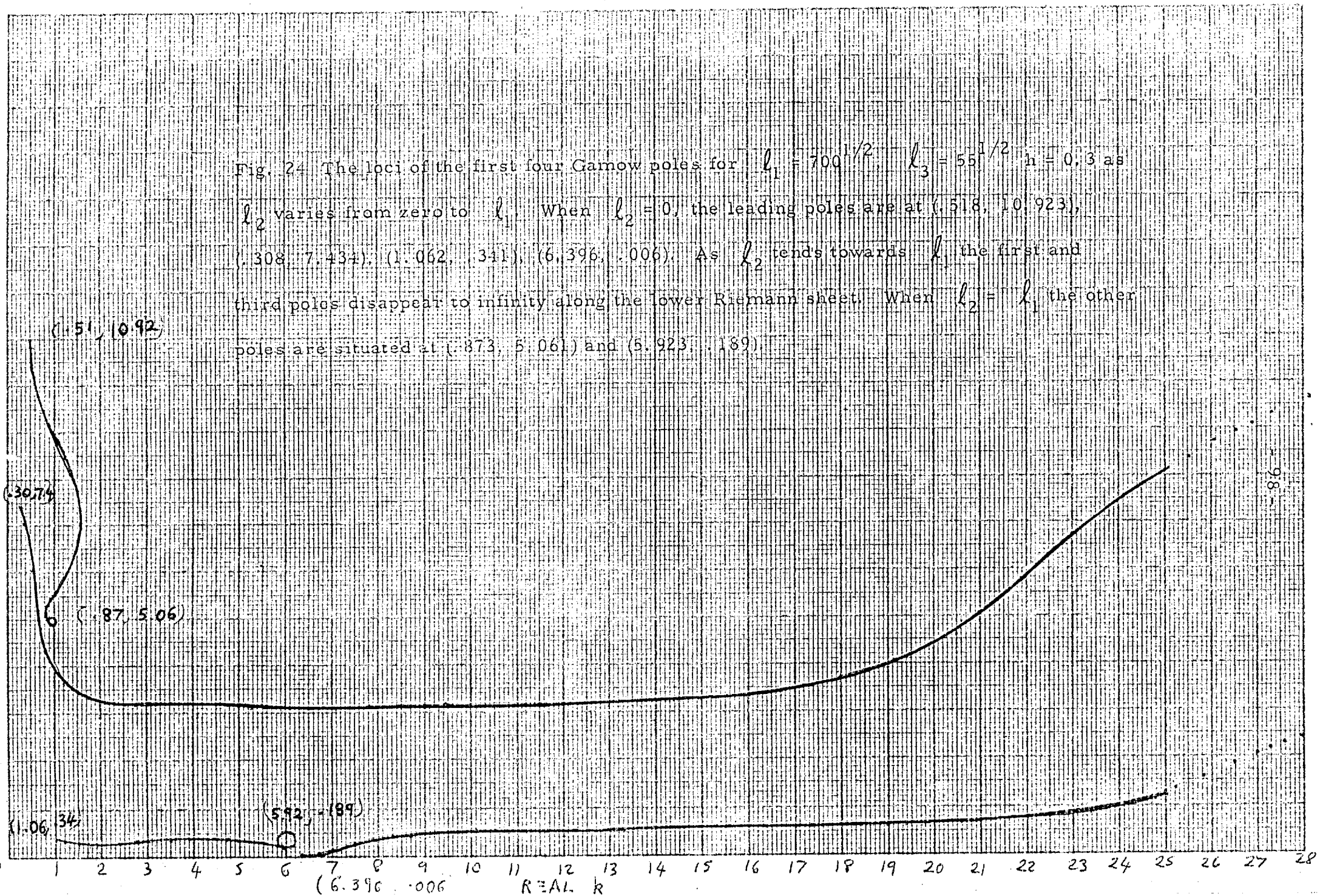
Locus of first four Gamow poles for h = 0.3 $\ell_1 = \sqrt{700}$ ℓ_2 varies from 0 to ℓ_1 $\ell_3 = \sqrt{55}$
Fig. 24 The loci of the first four Gamow poles for $\ell_1 = 700^{1/2}$ $\ell_3 = 55^{1/2}$ h = 0.3 as ℓ_2 varies from zero to ℓ_1. When $\ell_2 = 0$, the leading poles are at (.518, 10.923), (.308, 7.434), (1.062, .341), (6.396, .006). As ℓ_2 tends towards ℓ_1 the first and third poles disappear to infinity along the lower Riemann sheet. When $\ell_2 = \ell_1$ the other poles are situated at (.873, 5.061) and (5.923, .189).
(.51, 10.92)
(.30, 7.4)
(.87, 5.06)
(1.06, .34)
(5.92, .189)
(6.396, .006)
REAL k
IMAG k

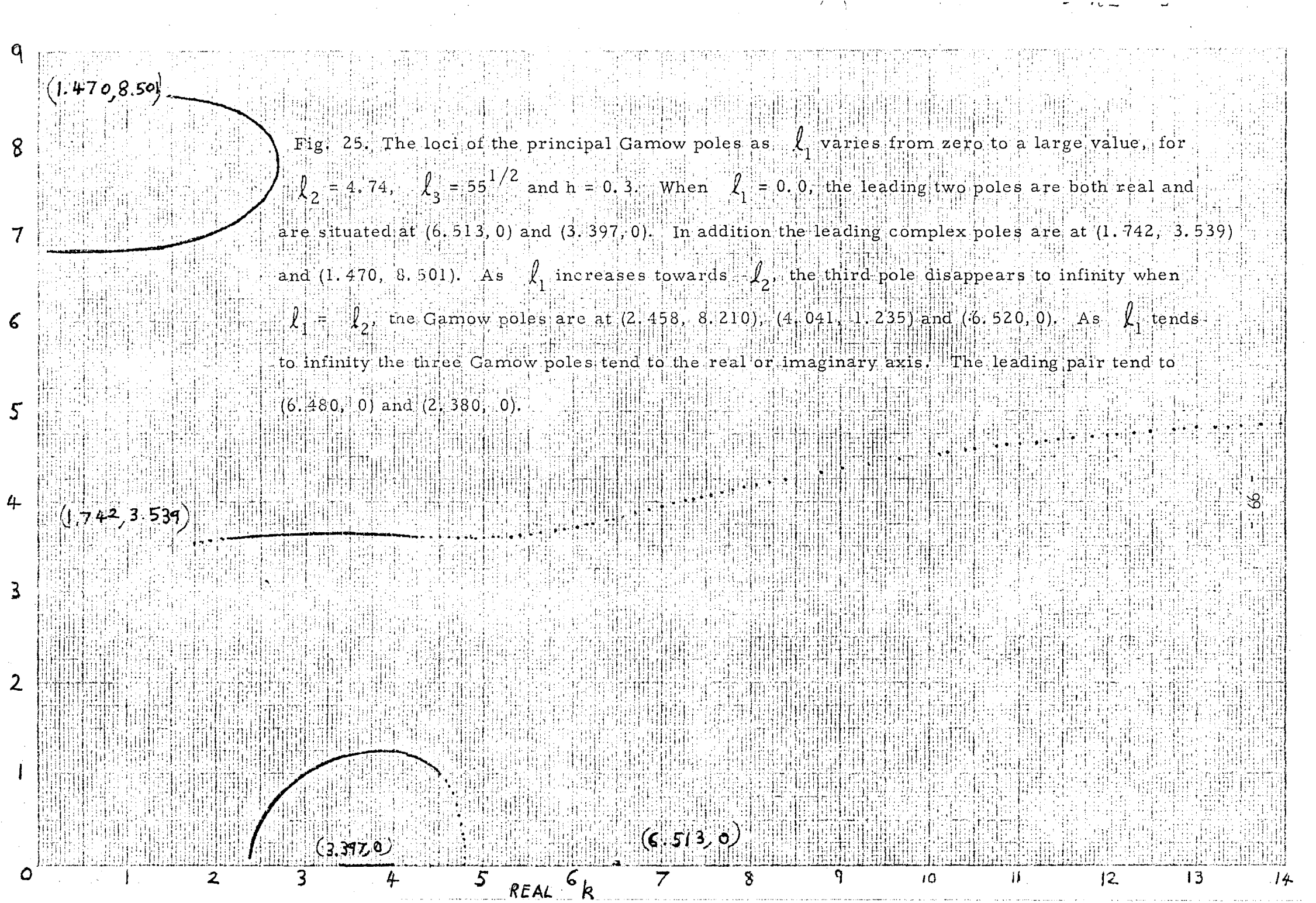

Fig. 25. The loci of the principal Gamow poles as ℓ_1 varies from zero to a large value, for $\ell_2 = 4.74$, $\ell_3 = 55^{1/2}$ and h = 0.3. When $\ell_1 = 0.0$, the leading two poles are both real and are situated at (6.513, 0) and (3.397, 0). In addition the leading complex poles are at (1.742, 3.539) and (1.470, 8.501). As ℓ_1 increases towards ℓ_2, the third pole disappears to infinity when $\ell_1 = \ell_2$, the Gamow poles are at (2.458, 8.210), (4.041, 1.235) and (6.520, 0). As ℓ_1 tends to infinity the three Gamow poles tend to the real or imaginary axis. The leading pair tend to (6.480, 0) and (2.380, 0).

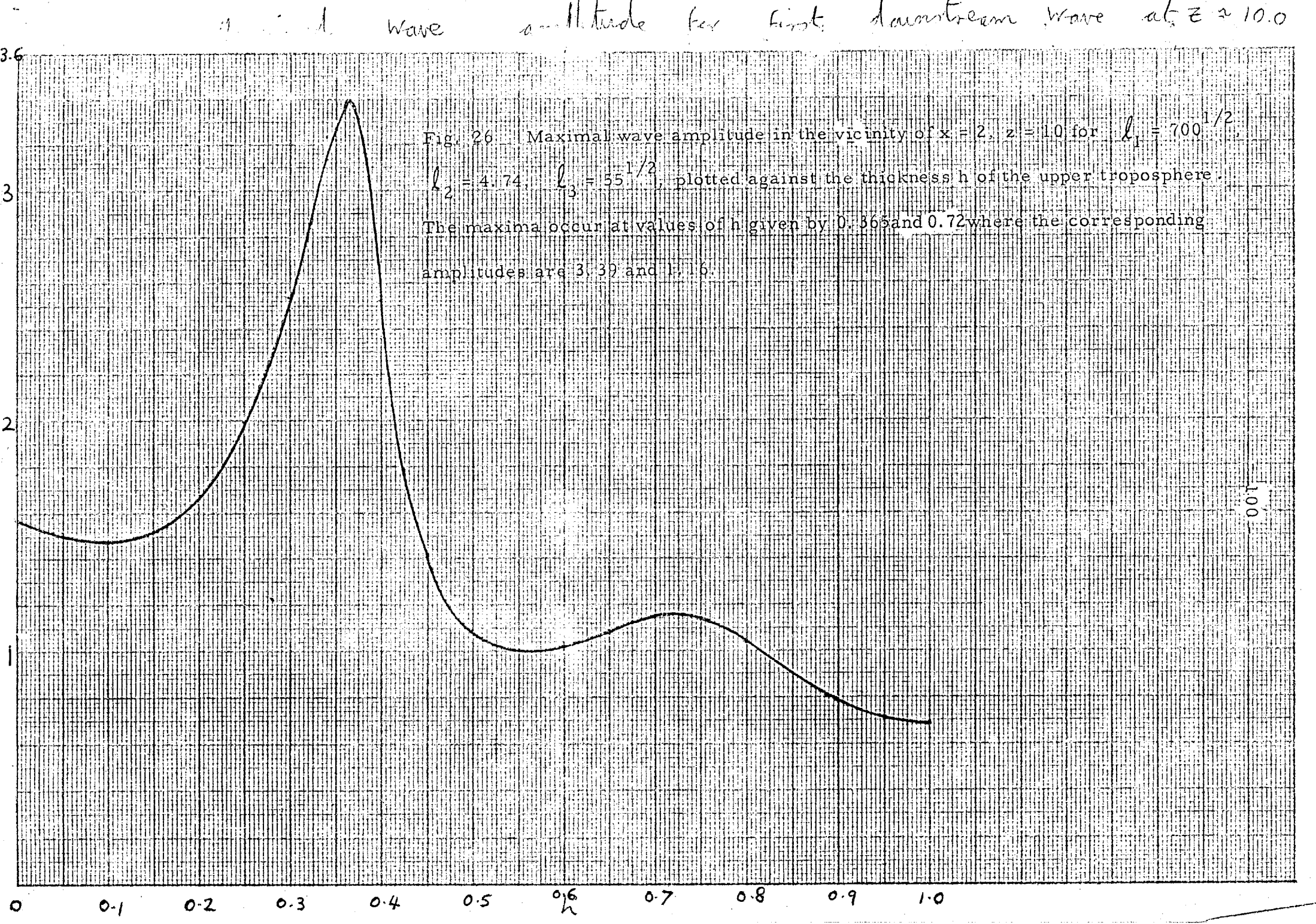

Fig. 26 Maximal wave amplitude in the vicinity of x = 2, z = 1.0 for $\ell_1 = 700^{1/2}$, $\ell_2 = 4.74$, $\ell_3 = 55^{1/2}$, plotted against the thickness h of the upper troposphere. The maxima occur at values of h given by 0.365 and 0.72 where the corresponding amplitudes are 3.39 and 1.16.

Fig. 27

Some high level contours of G(x, z) for $\ell_1 = 700^{1/2}$, $\ell_2 = 4.74$, $\ell_3 = 55^{1/2}$, h = 0.15. There are nine contours, the lowest is at -1.6 and the interval is 0.4. The dominant Gamow poles are at (3.712, .256) and (6.681, .033)

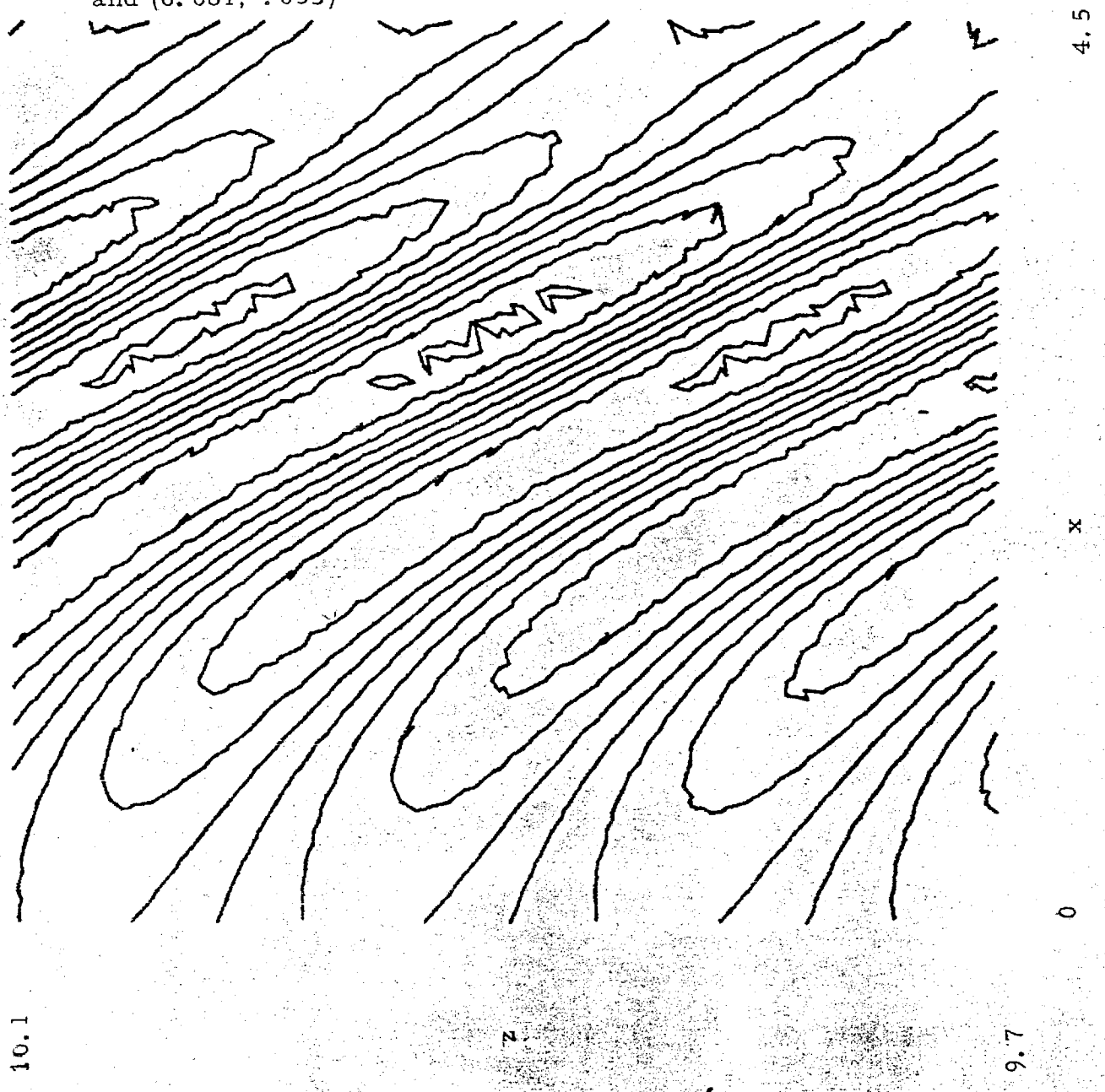

Fig. 28 A three dimensional representation of the contours of G(x, z) for Fig. 27.

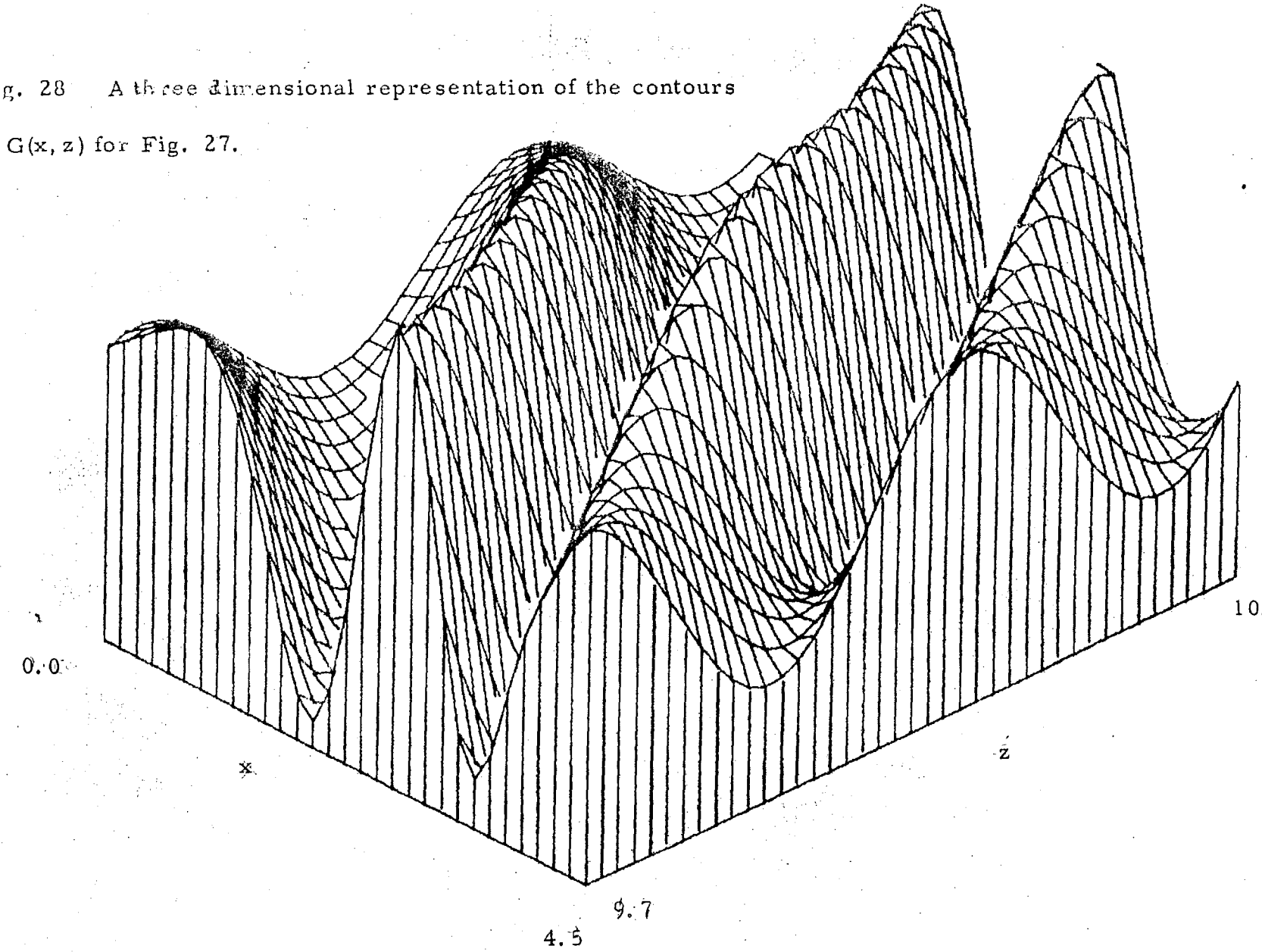

Fig. 29. Some high level contours of G(x, z) for $\ell_1 = 700^{1/2}$, $\ell_2 = 4.74$, $\ell_3 = 55^{1/2}$, h = 0.365. Eleven contours are drawn, the lowest is -3.0 with an interval of 0.6. The dominant complex poles are at (6.339, .011) and (1.365, .581).

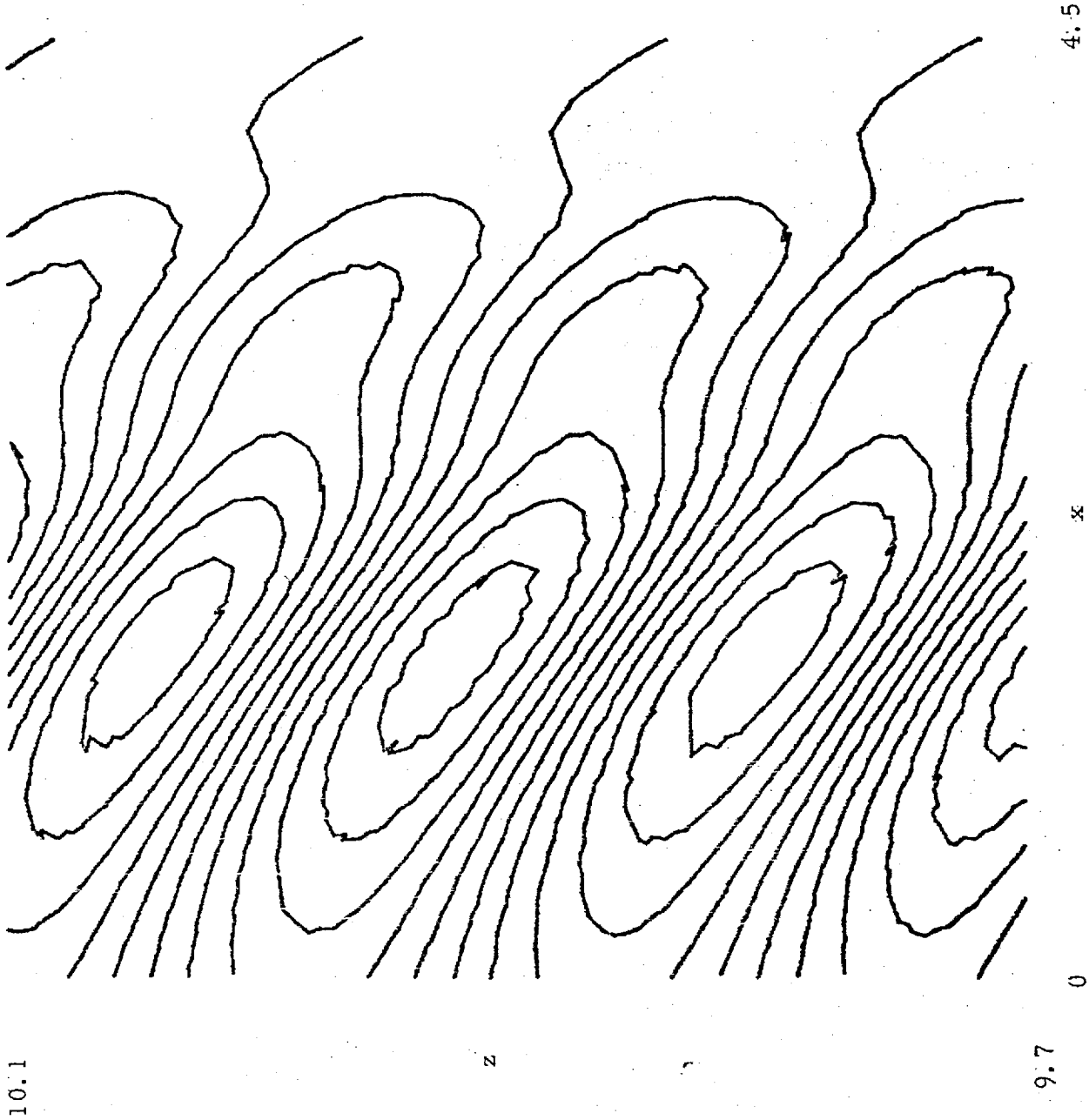

Fig. 30. A three dimensional representation of the contours of G(x, z) for figure 29.

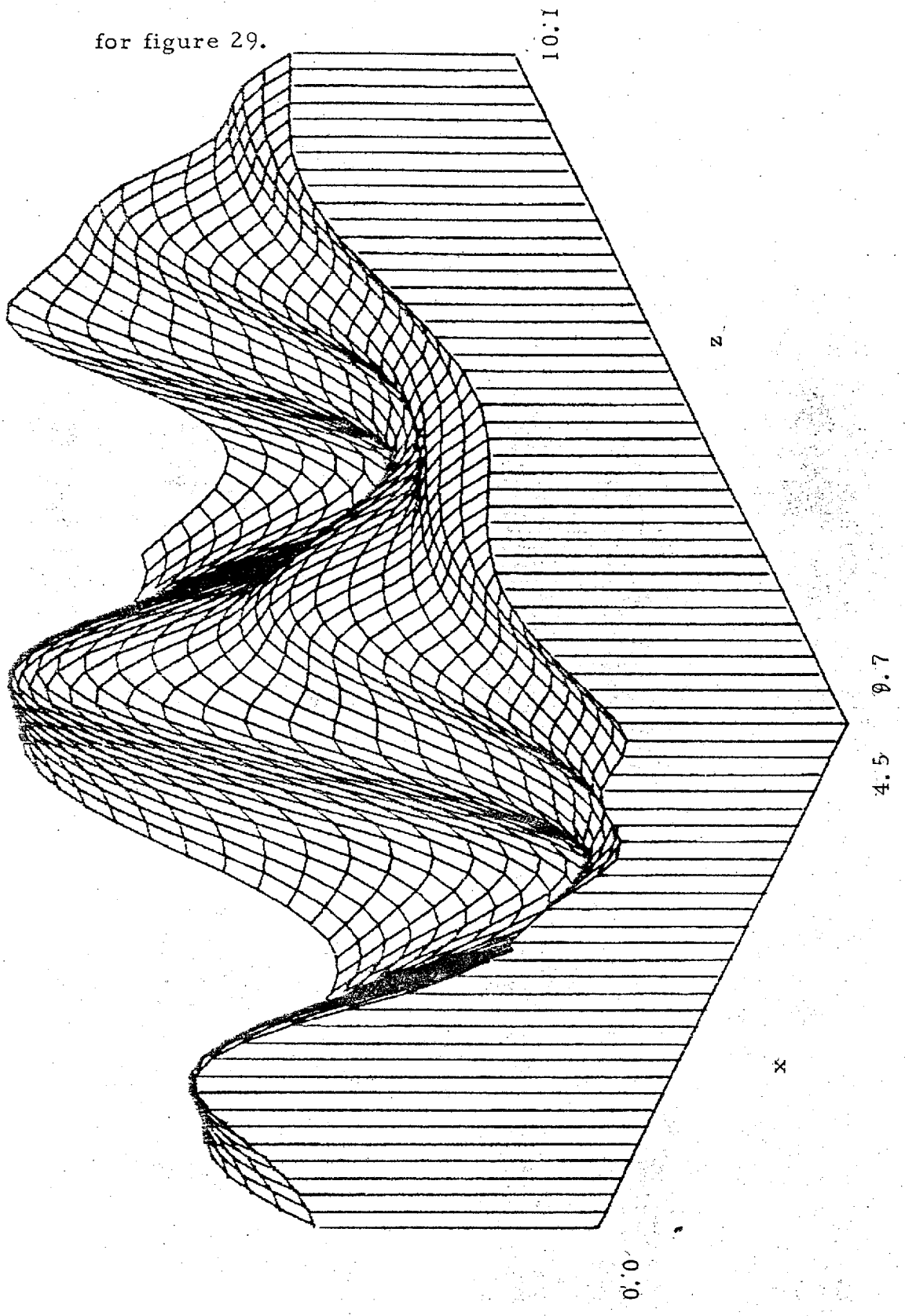

Fig. 31. Some high level contours of G(x, z) for $\ell_1 = 700^{1/2}$, $\ell_2 = 4.74$, $\ell_3 = 55^{1/2}$, h = 0.45. Nine contours are drawn, the lowest is -1.2, with an interval between contours of 0.3. The dominant Gamow poles are at (.572, 1.848) and (6.083, .008).

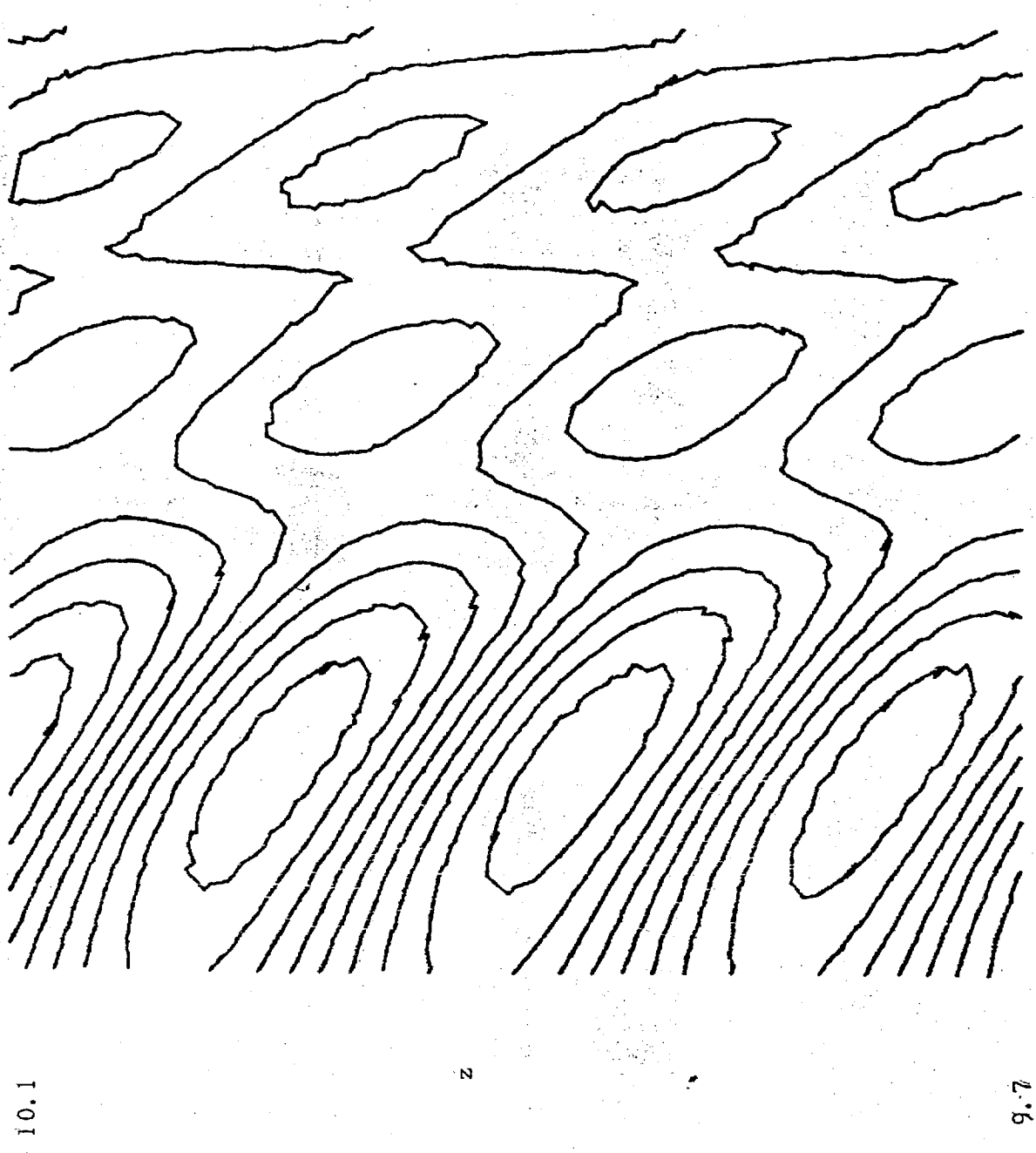

Fig. 32. A three dimensional representation of the contours of G(x, z) for figure 31.

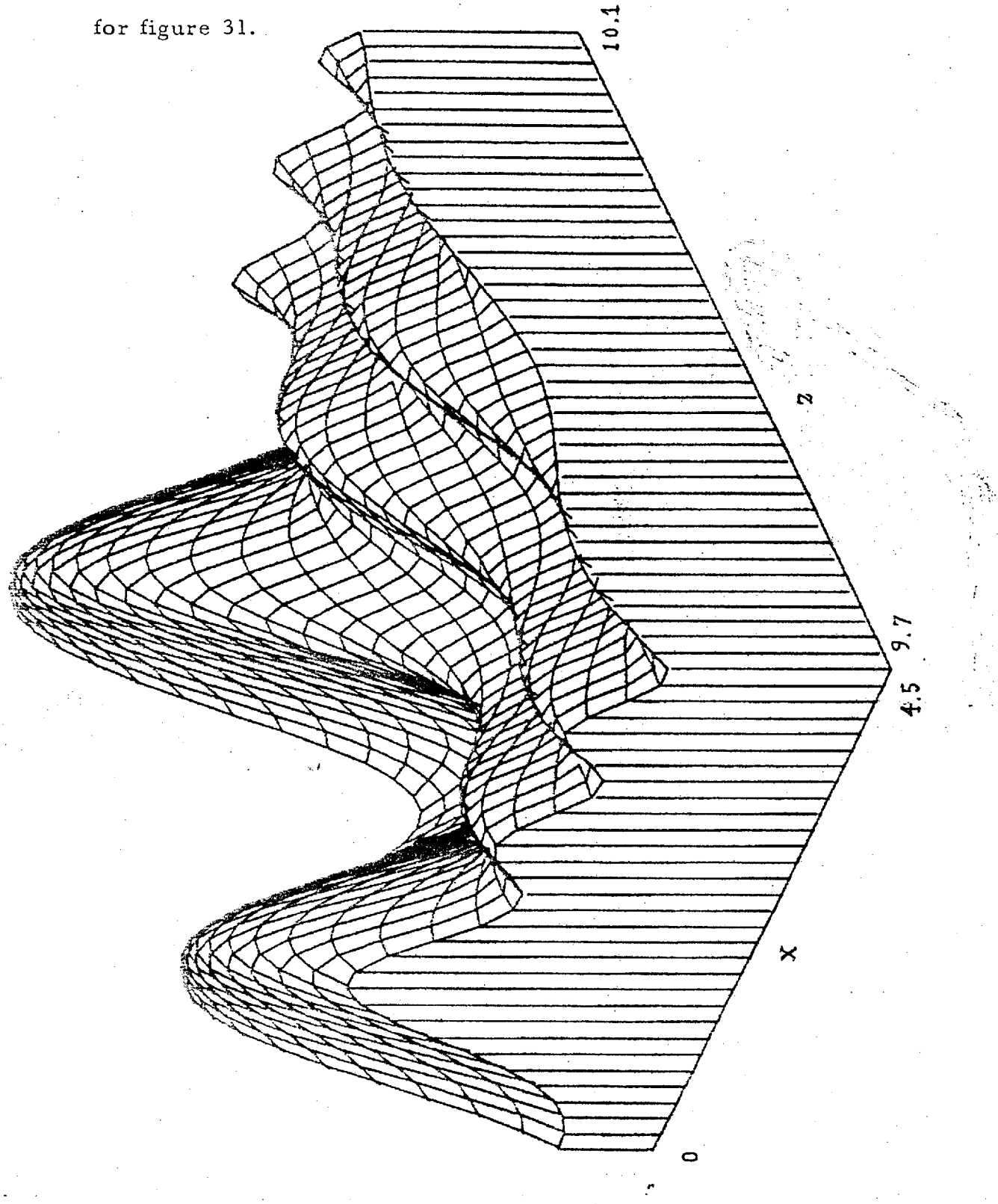

Fig. 33. Some high level contours for G(x, z) for $\ell_1 = 700^{1/2}$, $\ell_2 = 4.74$, $\ell_3 = 55^{1/2}$, $h = 0.72$. Seven contours are drawn, the lowest is at -0.9. There is an interval of 0.3 between contours. The important Gamow poles are at (.485, 2.628) and (4.416, .032).

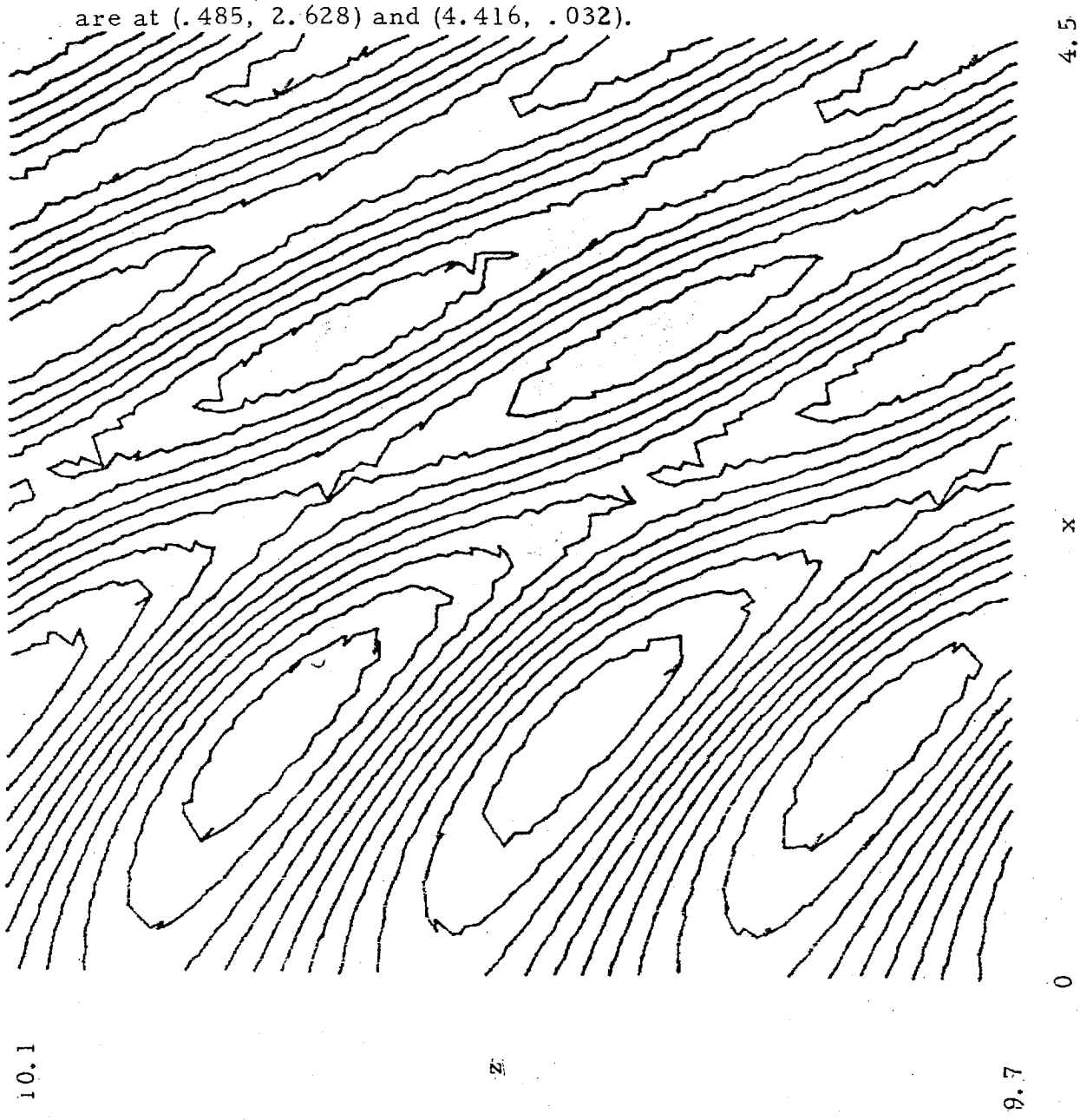

Fig. 34. A three dimensional representation of the contours of G(x, z) for figure 33.

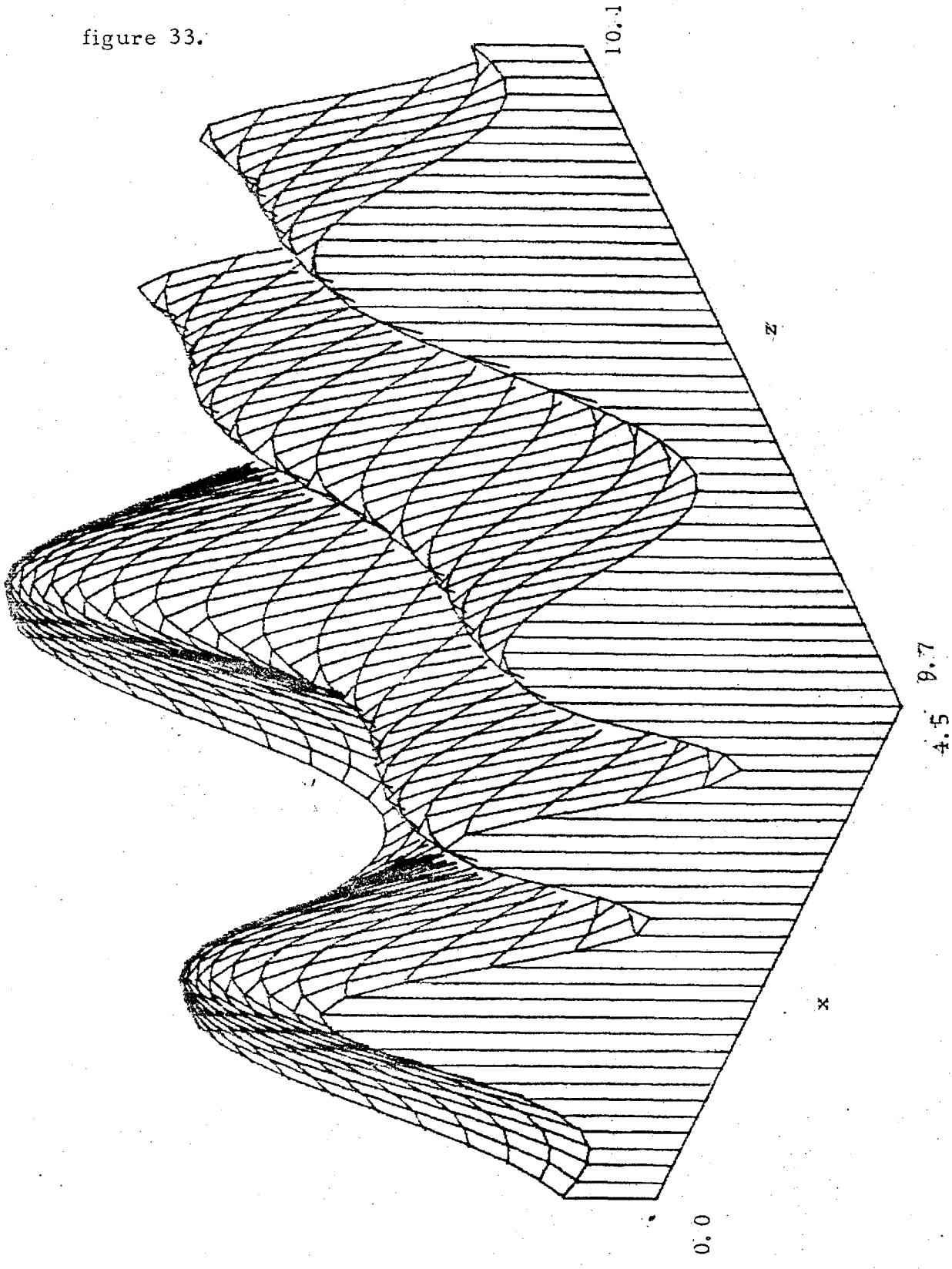

Fig. 35. Some low level stratosphere and troposphere contours for G(x, z for $\ell_1 = 700^{1/2}$, $\ell_2 = 4.74$, $\ell_3 = 55^{1/2}$, h = 0.15. The tilt in the direction of the contours in the lower stratosphere is about the same as that in the upper stratosphere. Note the difference in the scale of the axes exaggerates the tilt. In the troposphere the direction is nearly vertical. There are twenty contours, the lowest is at -9.0, with an interval between contours of 1.0. Note the highest contour is 10.0.

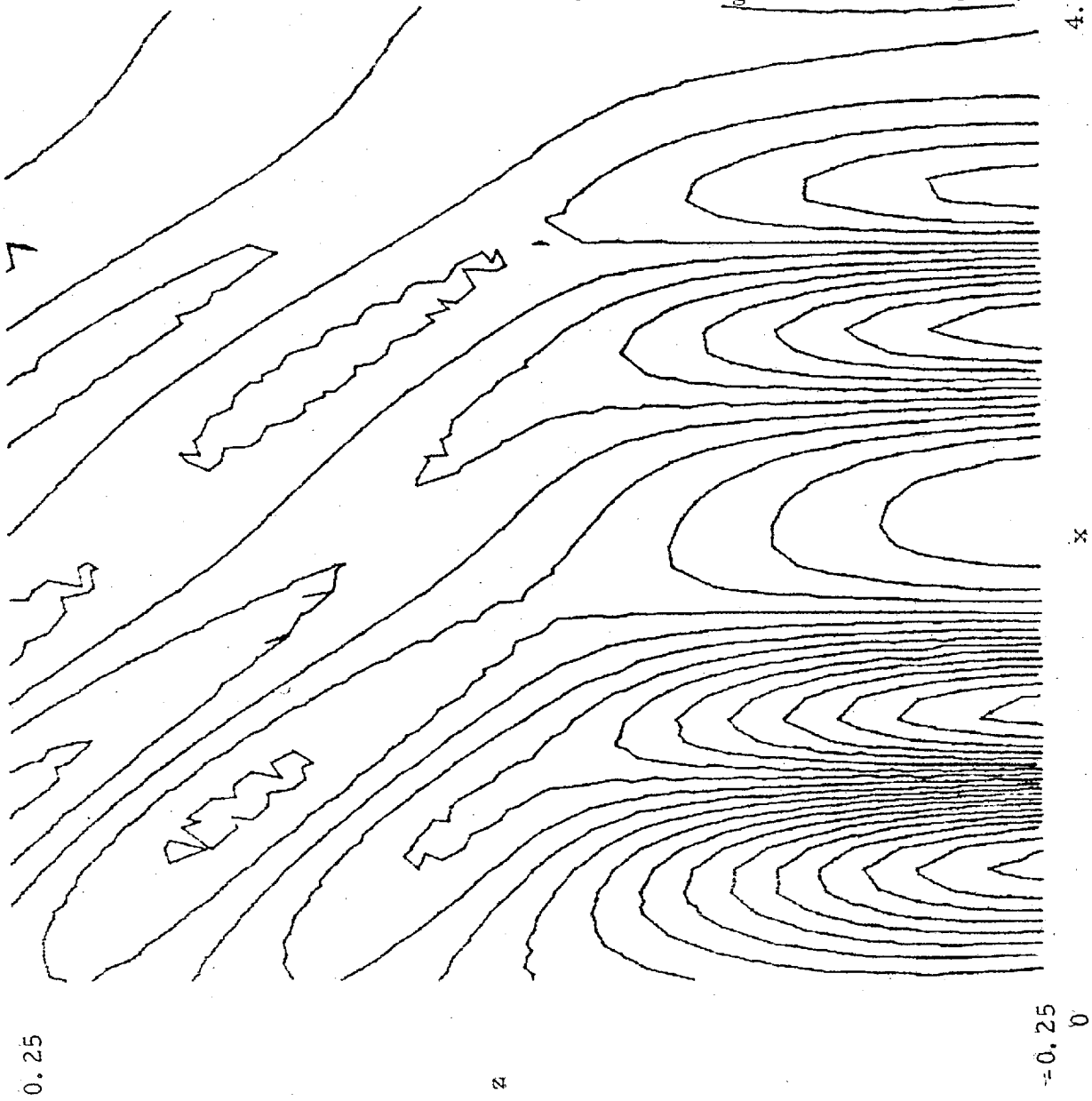

Fig. 36. A three dimensional representation of the contours of G(x, z) for figure 35.

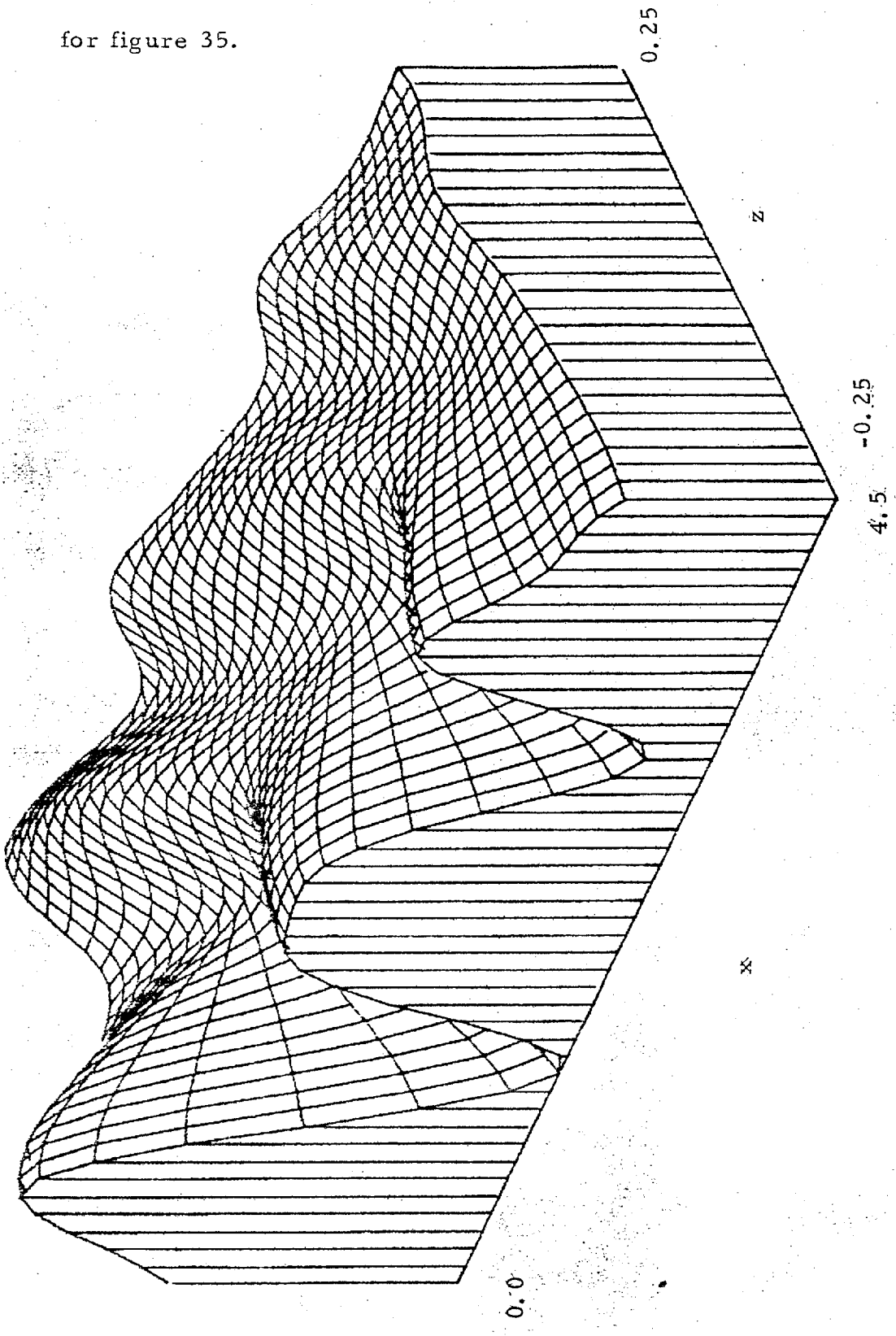

Fig. 37. Some low level contours for G(x, z) for $\ell_1 = 700^{1/2}$, $\ell_2 = 4.74$, $\ell_3 = 55^{1/2}$, h = 0.365. There are twenty five contours, the lowest is at -19.5, with an interval of 1.5 between contours.

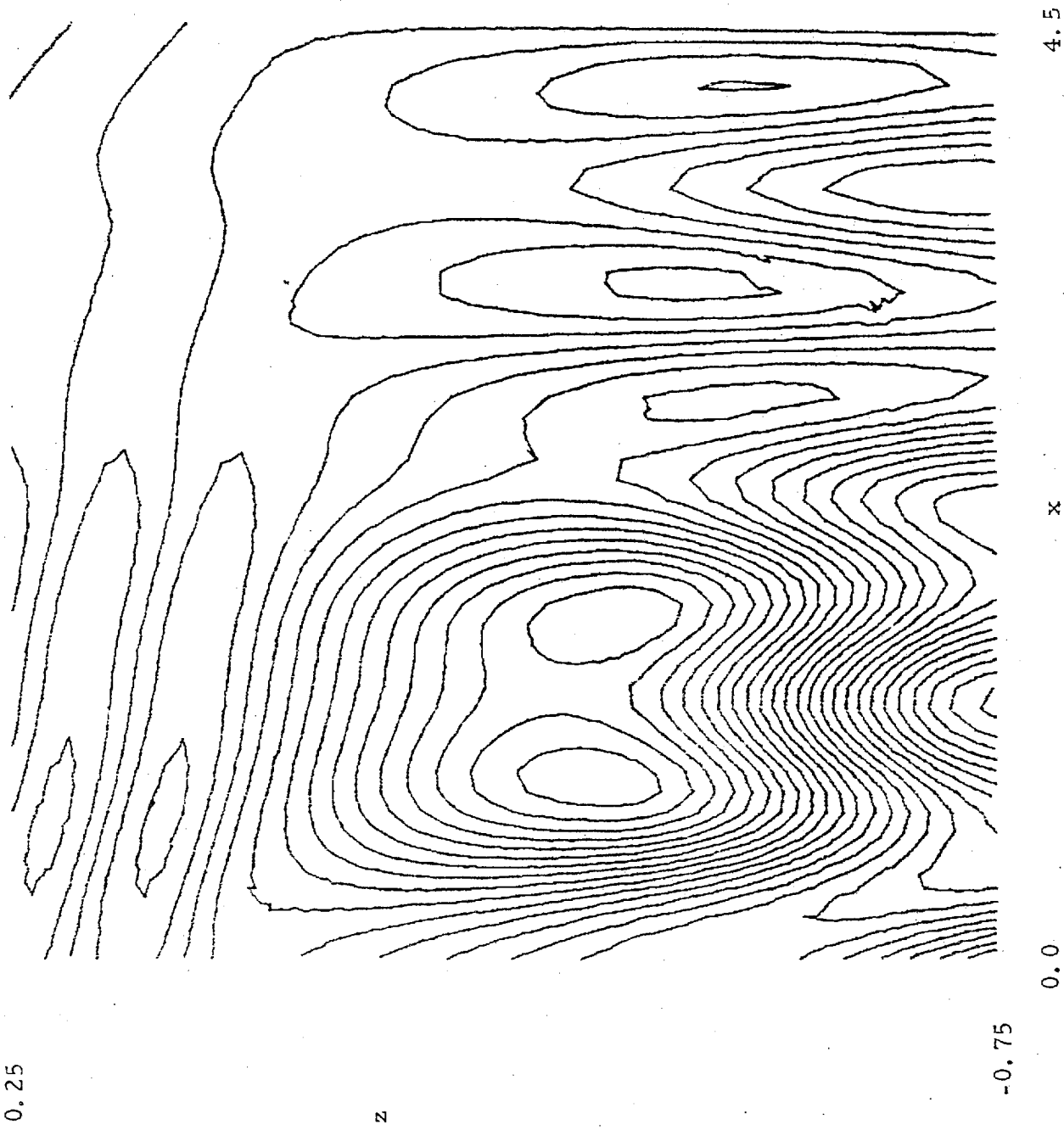

Fig. 38. A three dimensional representation of the contours of G(x, z) for figure 37.

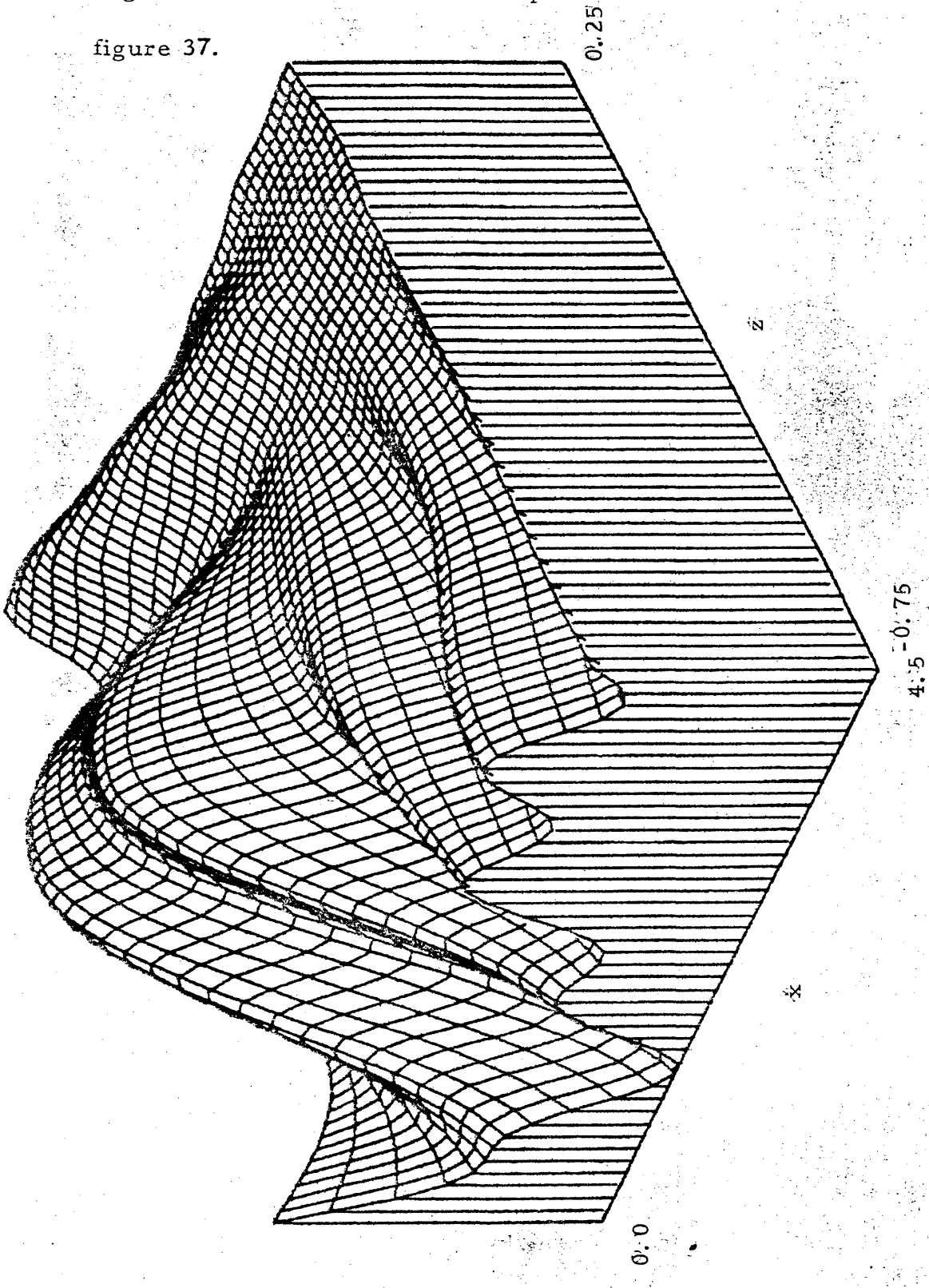

Fig. 39. Some low level contours for G(x, z) for $\ell_1 = 700^{1/2}$, $\ell_2 = 4.74$, $\ell_3 = 55^{1/2}$, h = 0.72. There are twelve contours, the lowest is at -9.0, with an interval of 1.5.

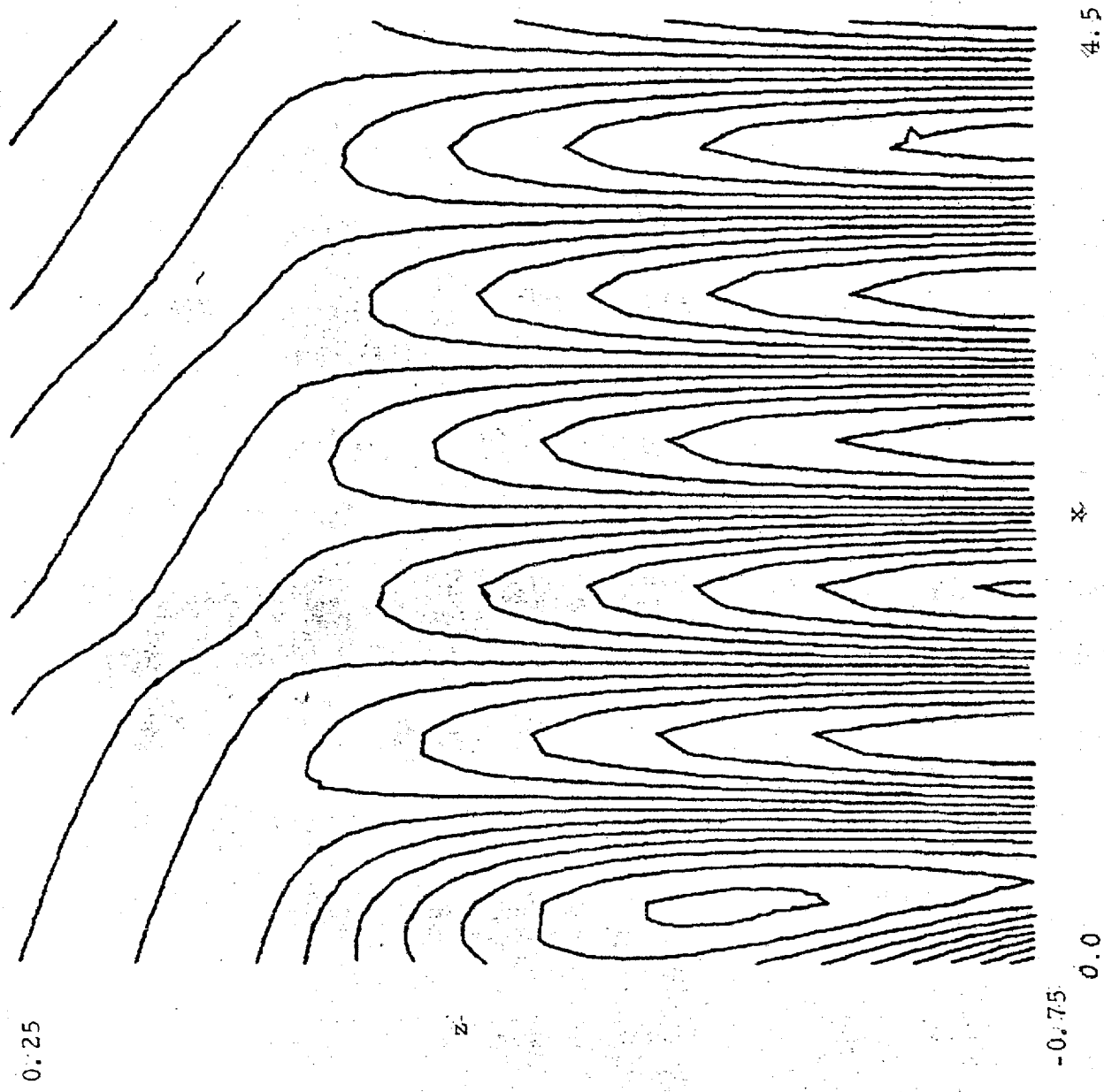

Fig. 40. A three dimensional representation of the contours of G(x, z) for figure 39.

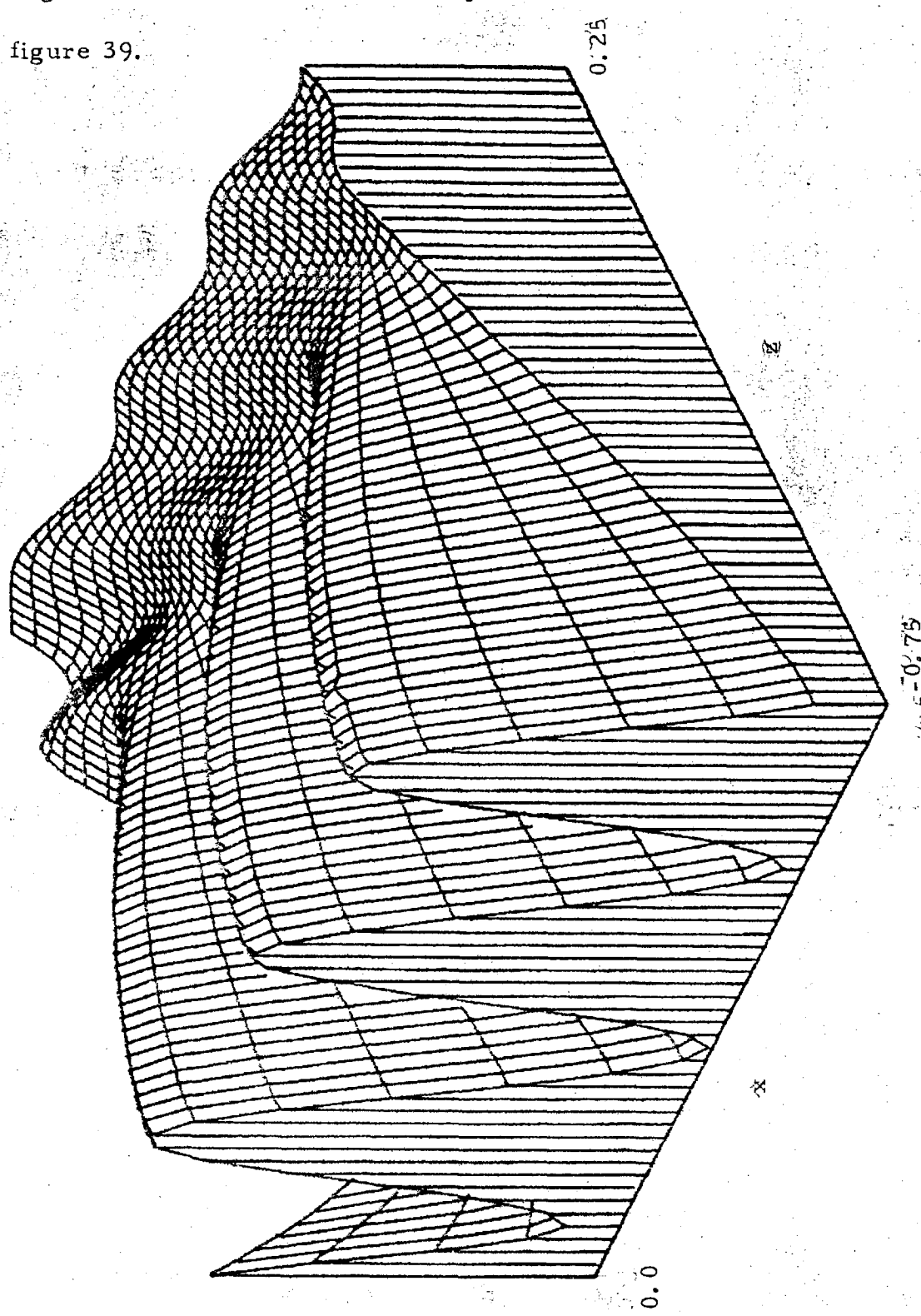

Fig. 41. Quasi-wave drag against h for $\ell_1 = 700^{1/2}$, $\ell_3 = 55^{1/2}$, as ℓ_2 varies between 1.58 and 11.06. See table 2 for details of all wave drag plots.

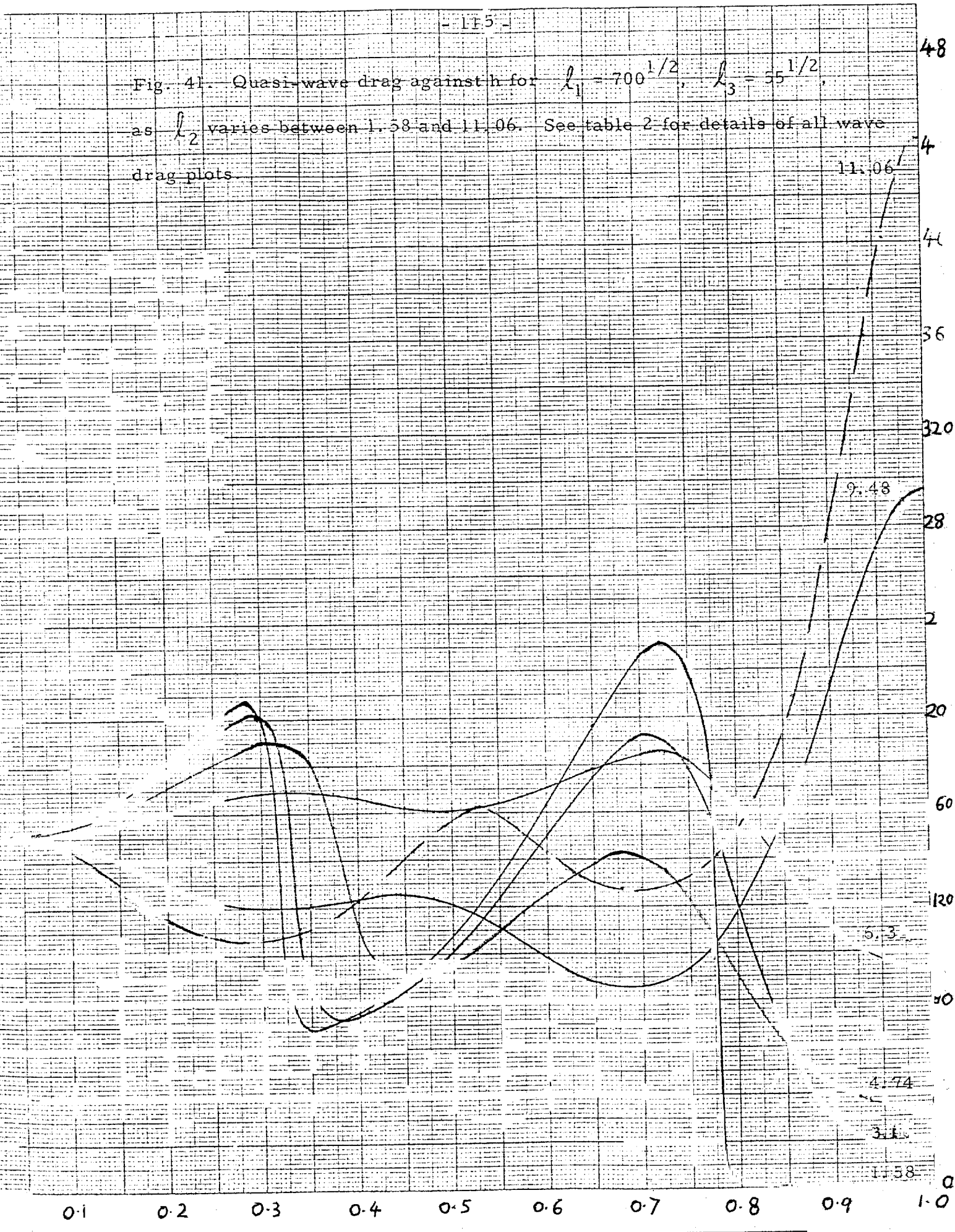

Fig. 42. Quasi-wave drag against h for $\ell_1 = 700^{1/2}$, $\ell_3 = 55^{1/2}$, $\ell_2 = 12.64$. Note the difference in the vertical scale from that used on all other drag plots.

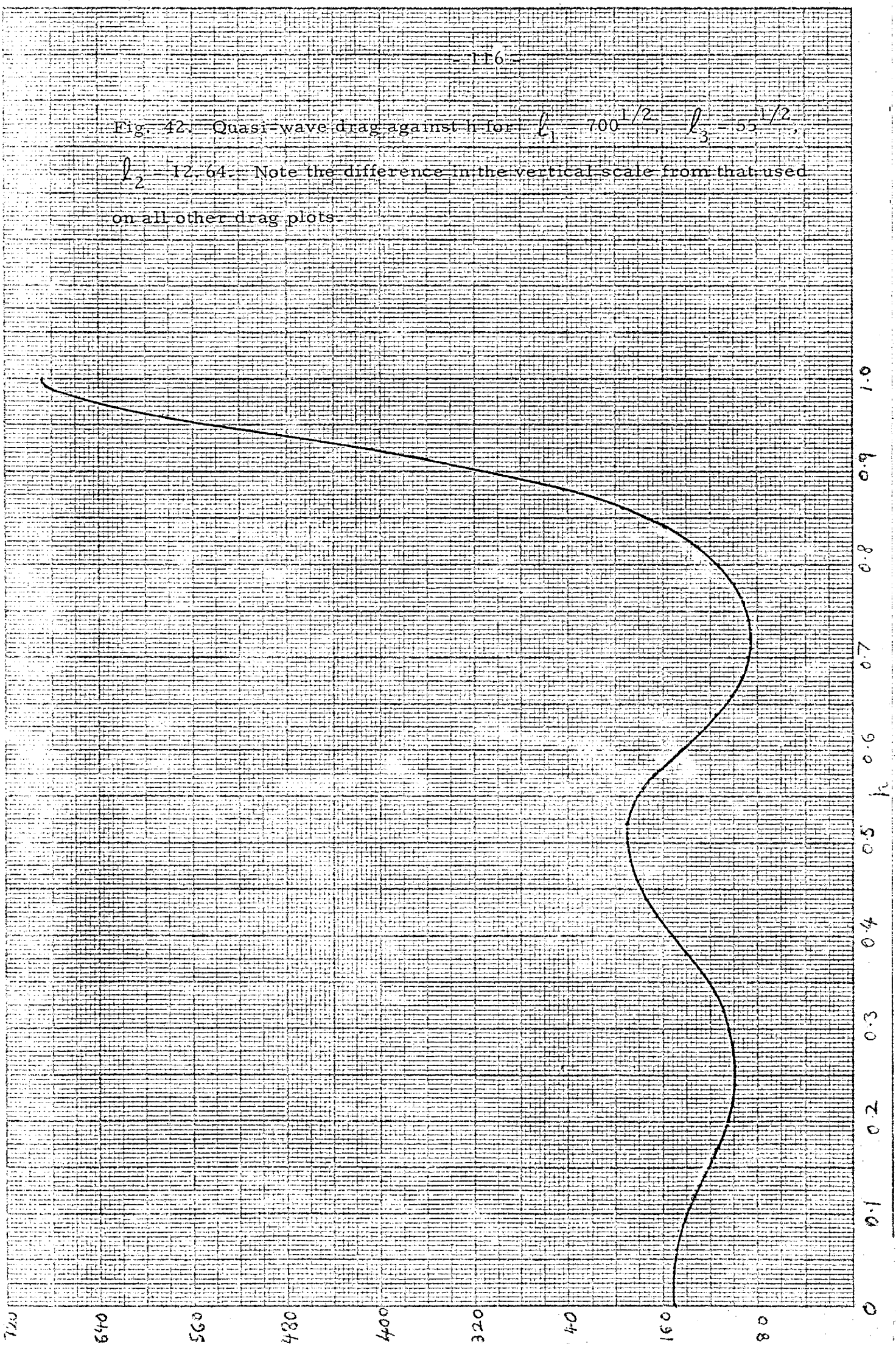

Fig. 43. Quasi-wave drag against h for $\ell_1 = 700^{1/2}$, $\ell_2 = 55^{1/2}$, $\ell_3 = 9.48$.

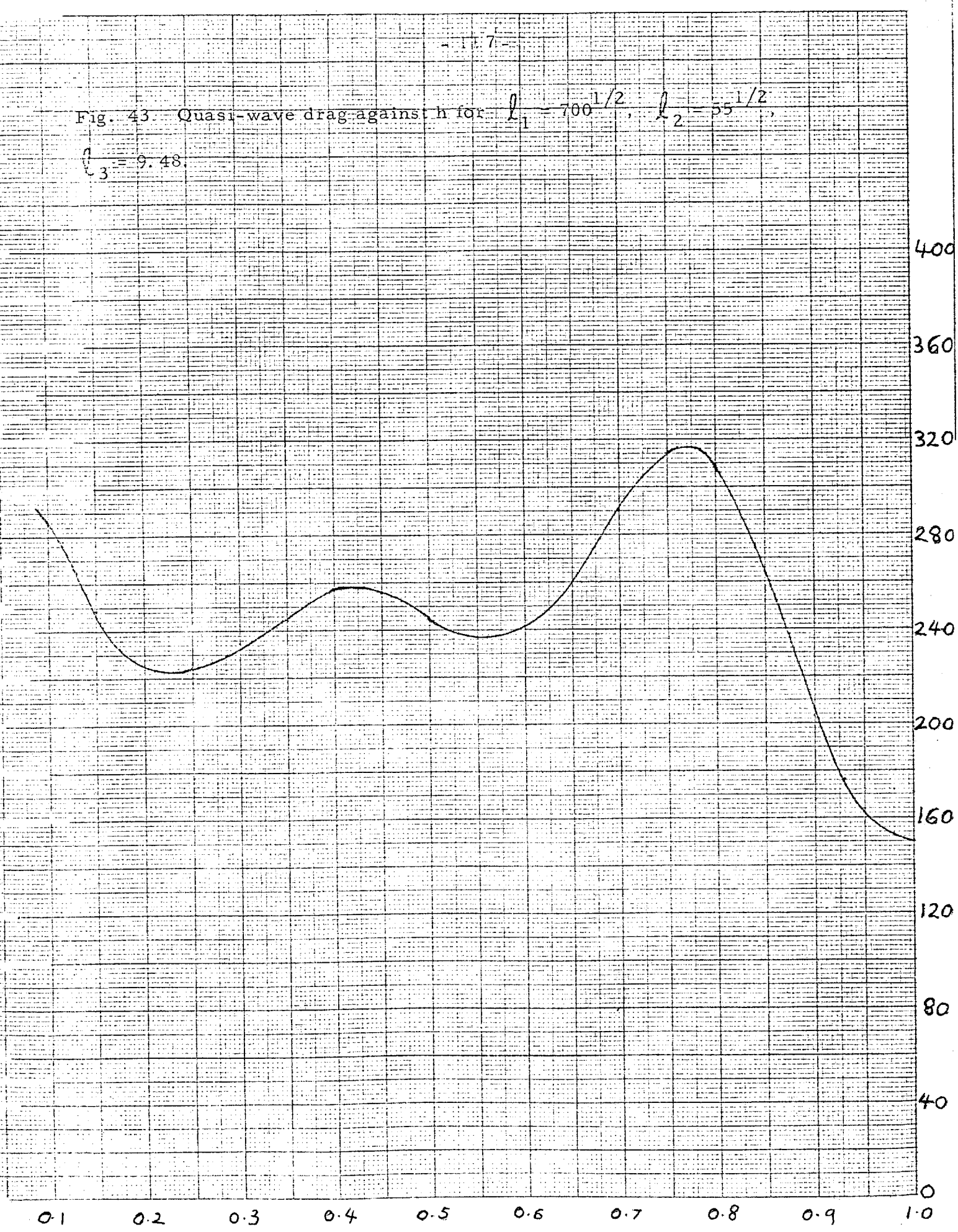

Fig. 44. Quasi-wave-drag against h for $\ell_1 = 700^{1/2}$, $\ell_2 = 1.58$, $\ell_3 = 55^{1/2}$. The dots represent the drag for infinite ℓ_1. There are discontinuities as a pole passes close to the origin, and is excluded from the calculation.

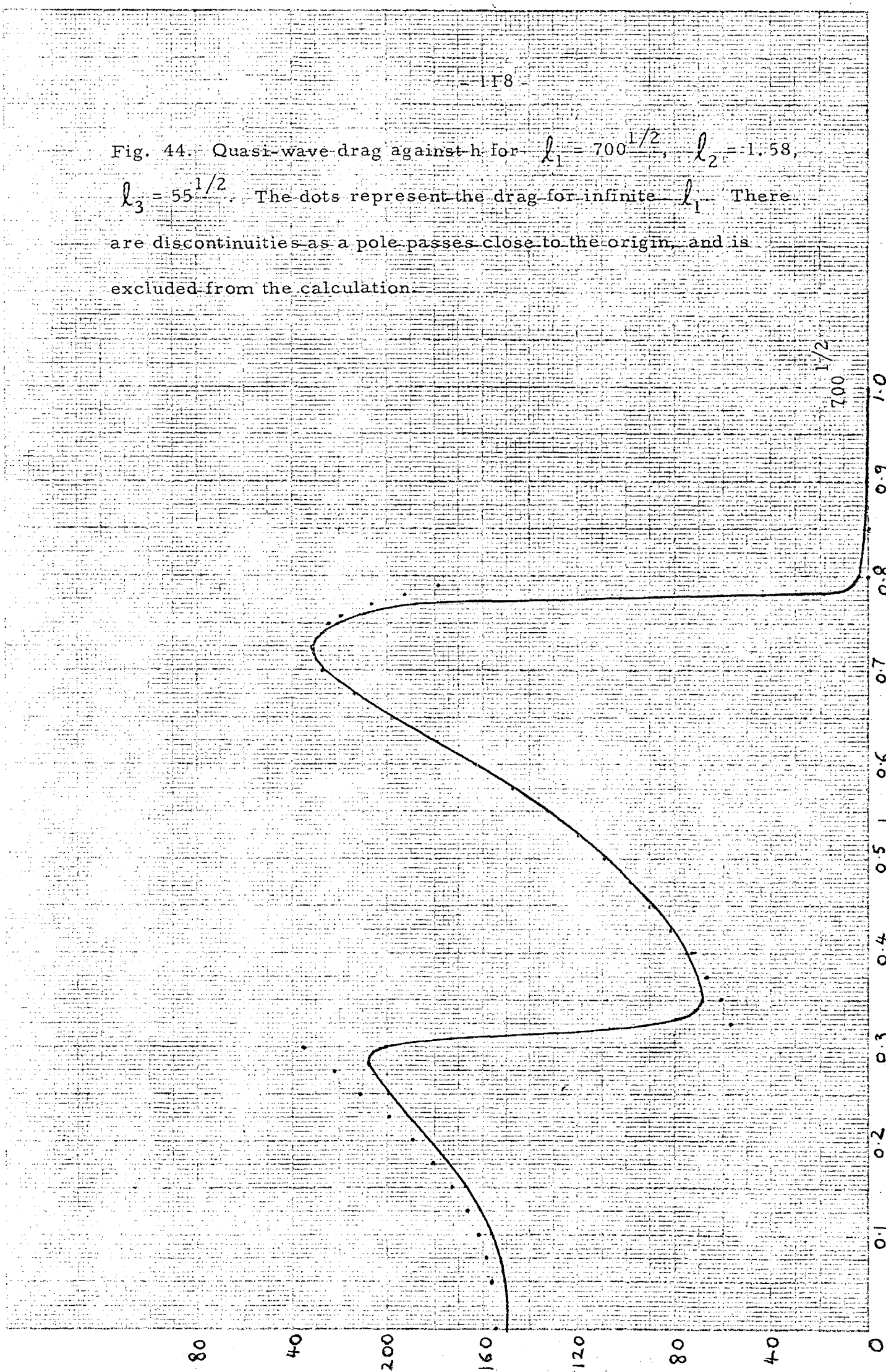

Fig. 45. Quasi-wave drag against h for $\ell_1 = 700^{1/2}$, $\ell_2 = 3.16$; $\ell_3 = 55^{1/2}$. The dots represent the drag for infinite ℓ_1.

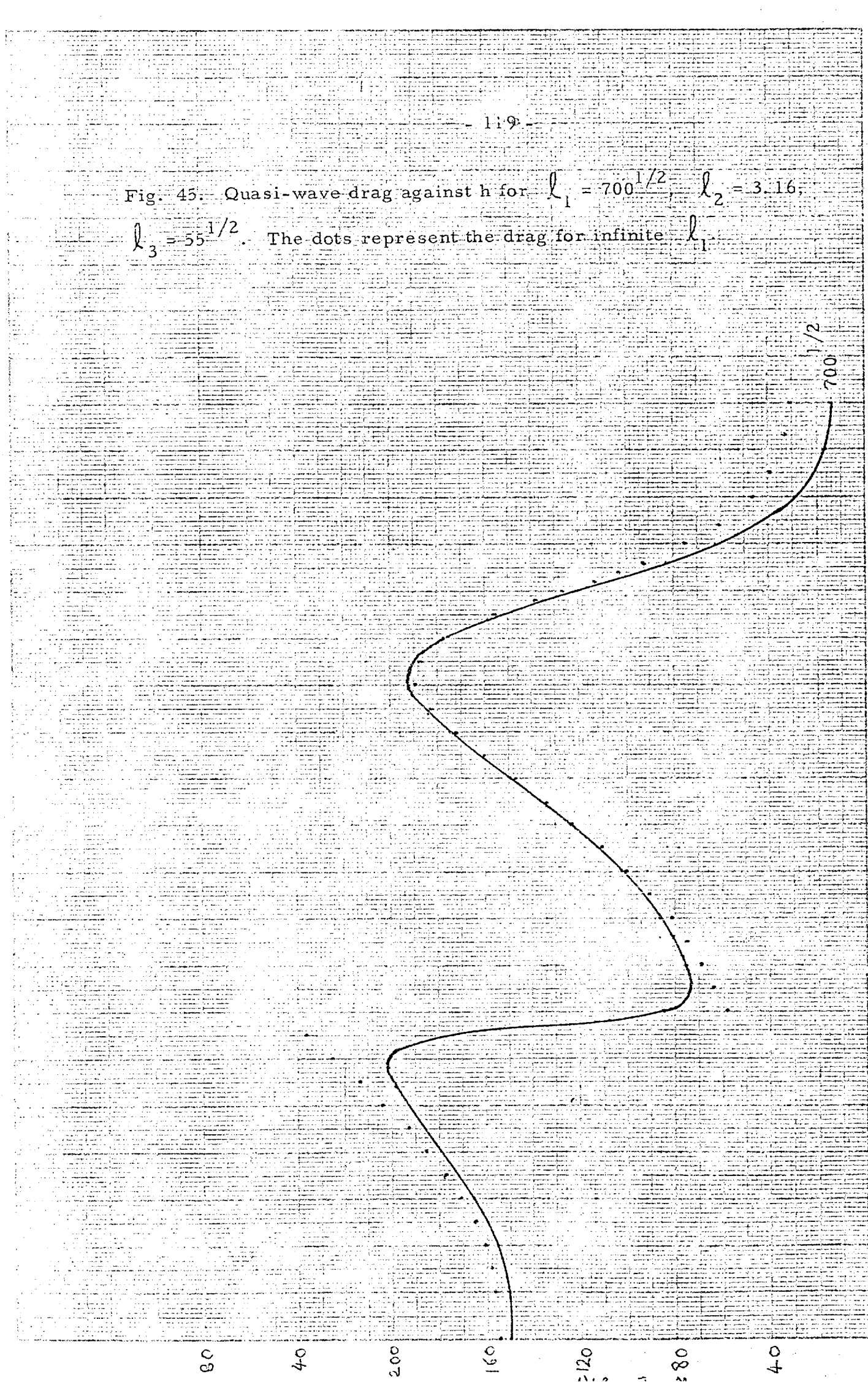

Fig. 46. Quasi-wave drag against h for $\ell_2 = 4.74$, $\ell_3 = 55^{1/2}$, for $\ell_1 = 700^{1/2}$ and for infinite ℓ_1.

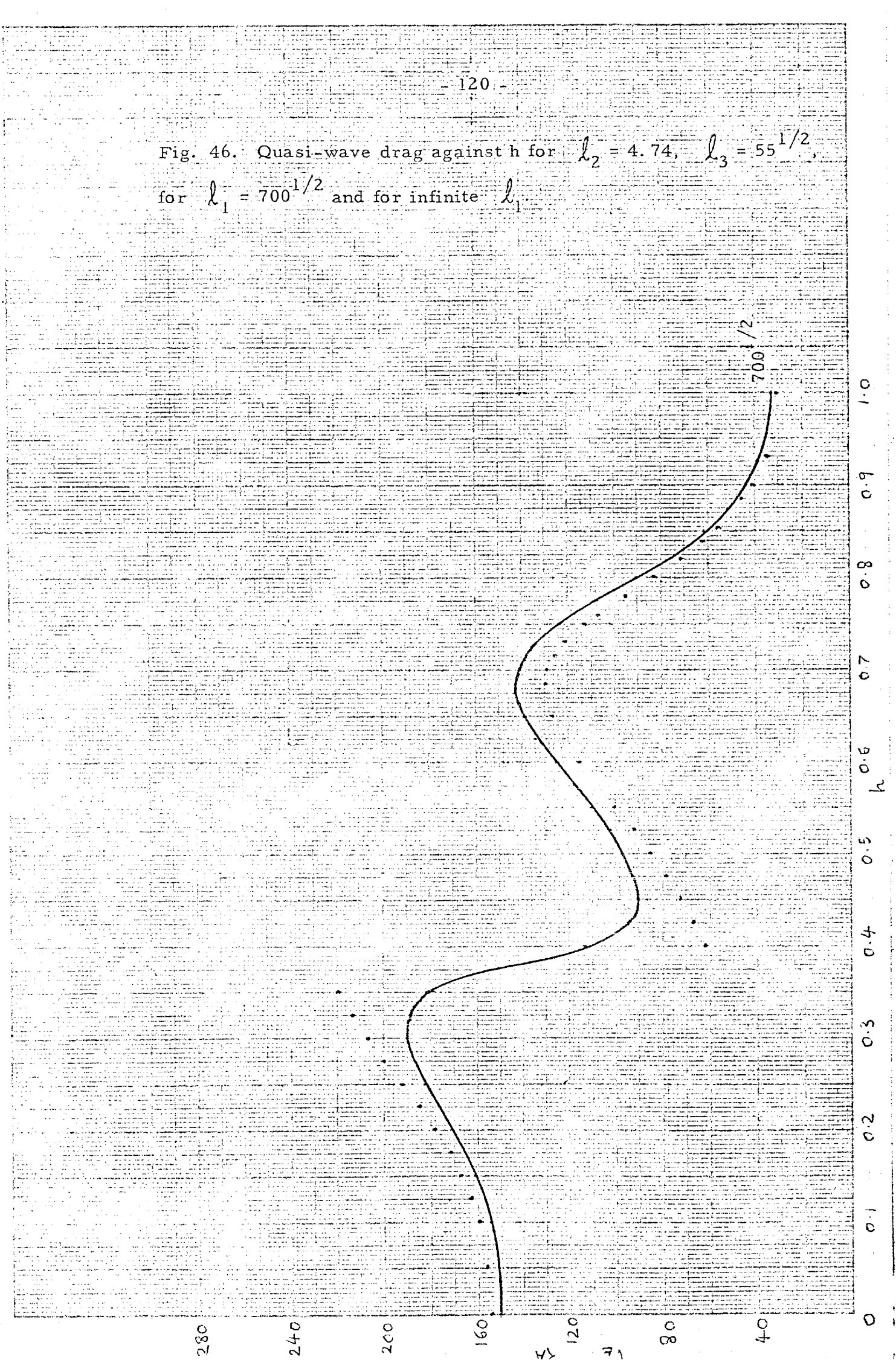

Fig. 47. Quasi-wave drag against h for $\ell_2 = 6.32$, $\ell_3 = 55^{1/2}$, for $\ell_1 = 700^{1/2}$ and for infinite ℓ_1.

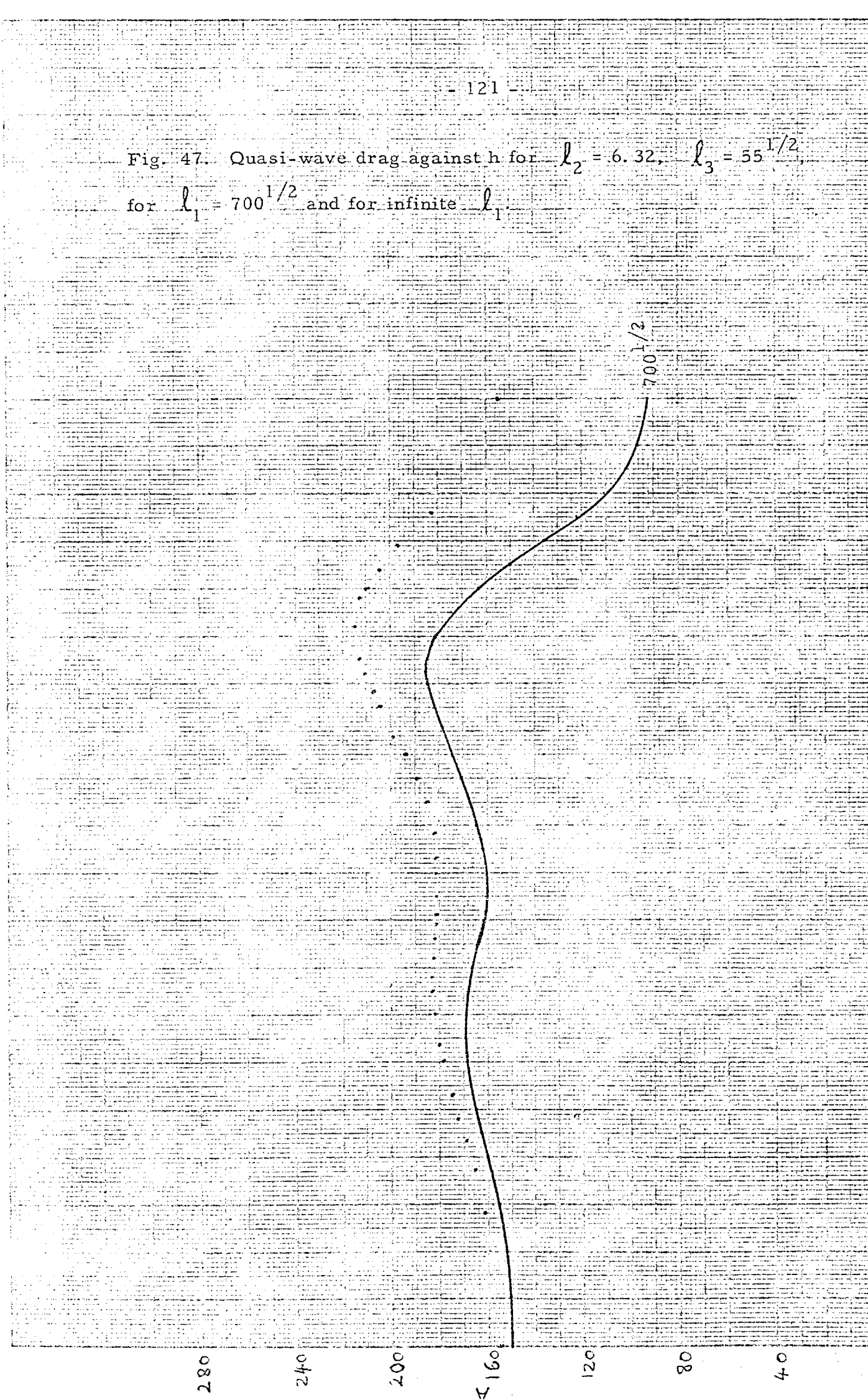

Fig. 48. Quasi-wave drag against h for $l_1 = 55^{1/2}$, $l_3 = 55^{1/2}$, as l_2 varies.

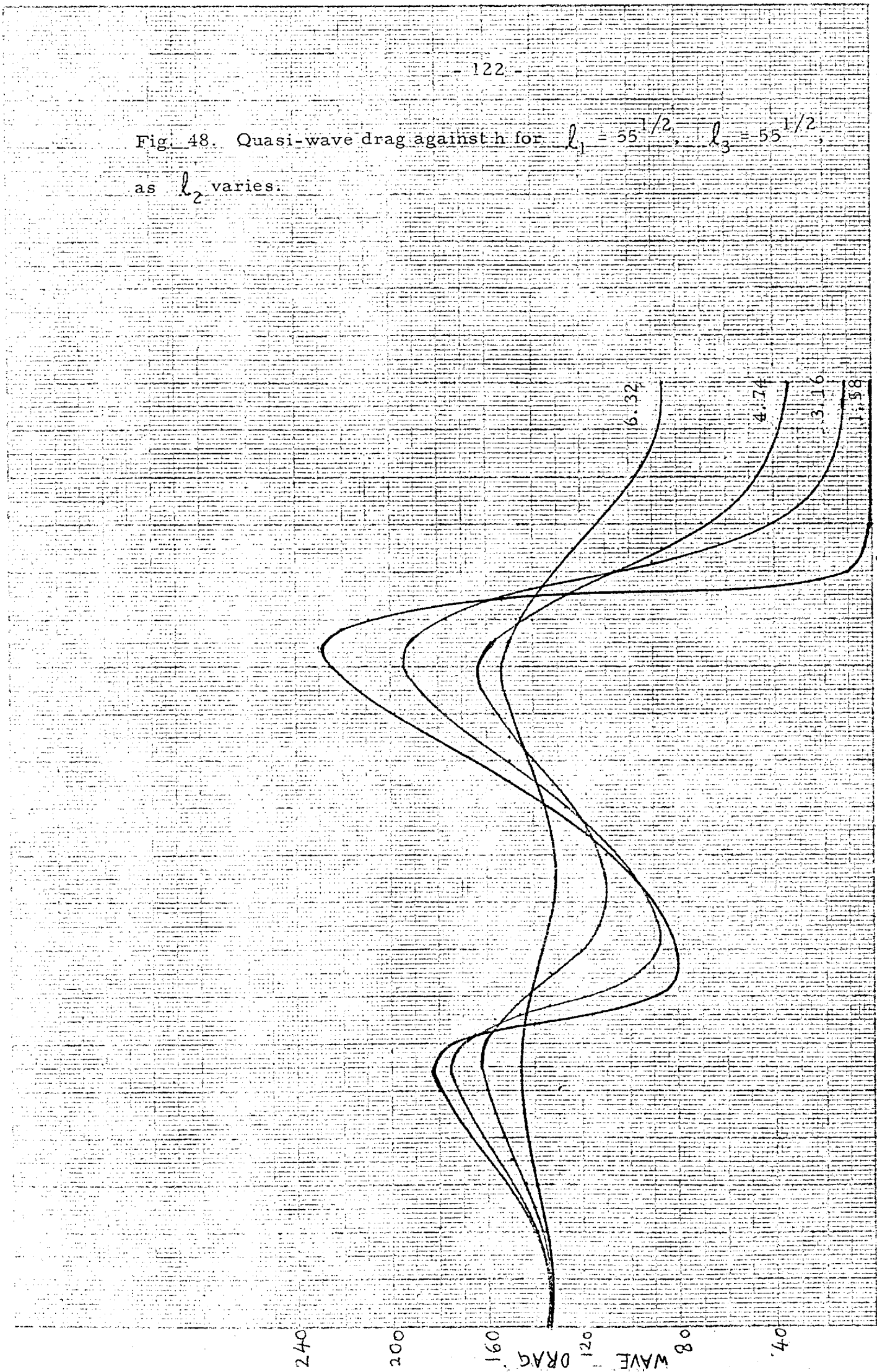

Fig. 49. Quasi-wave drag against h for $\ell_2 = 3.16$, $\ell_3 = 55^{1/2}$ as ℓ_1 varies

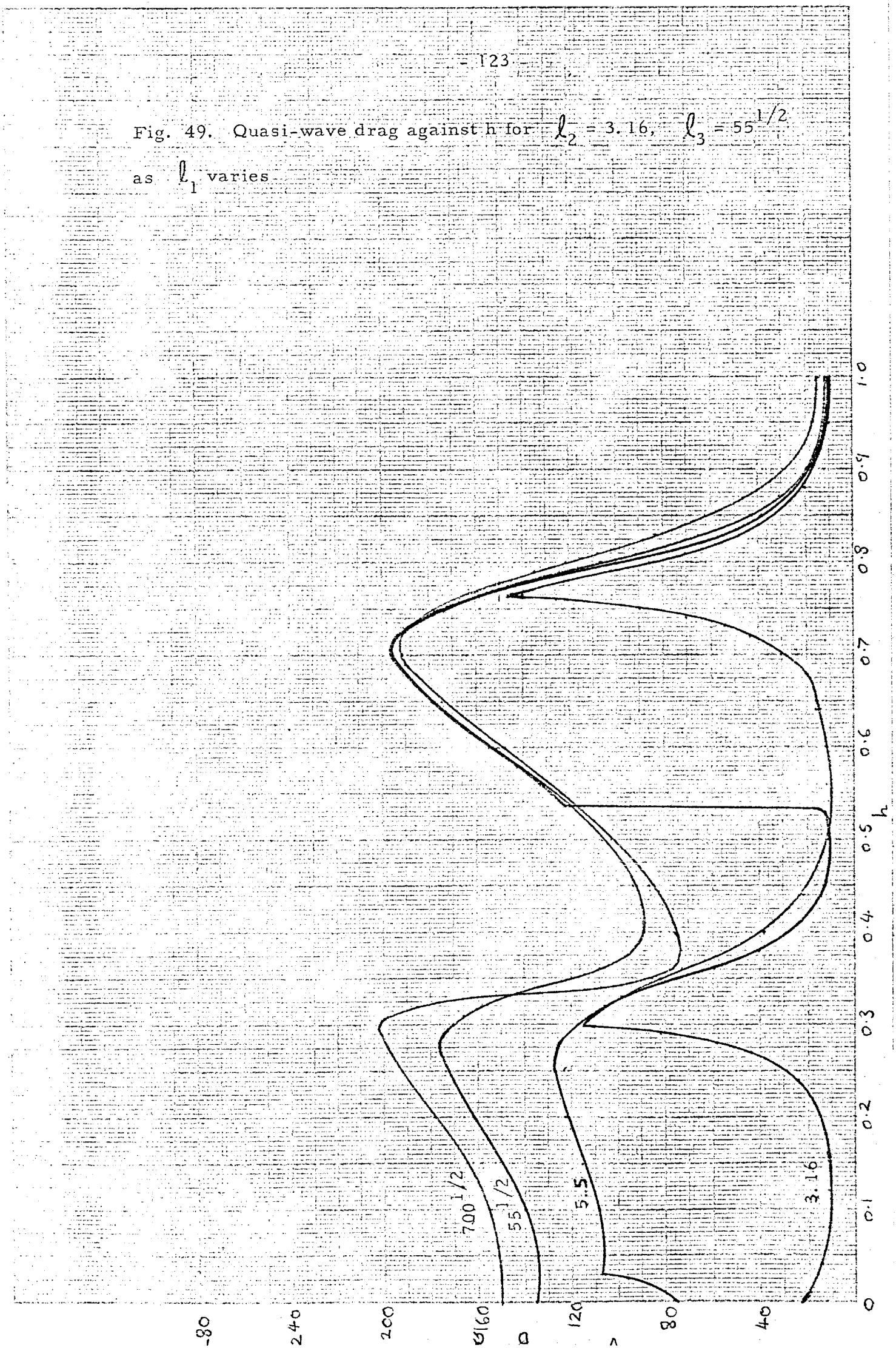

Fig. 50. Quasi-wave drag against h for $\ell_2 = 4.74$, $\ell_3 = 55^{1/2}$ as ℓ_1 varies.

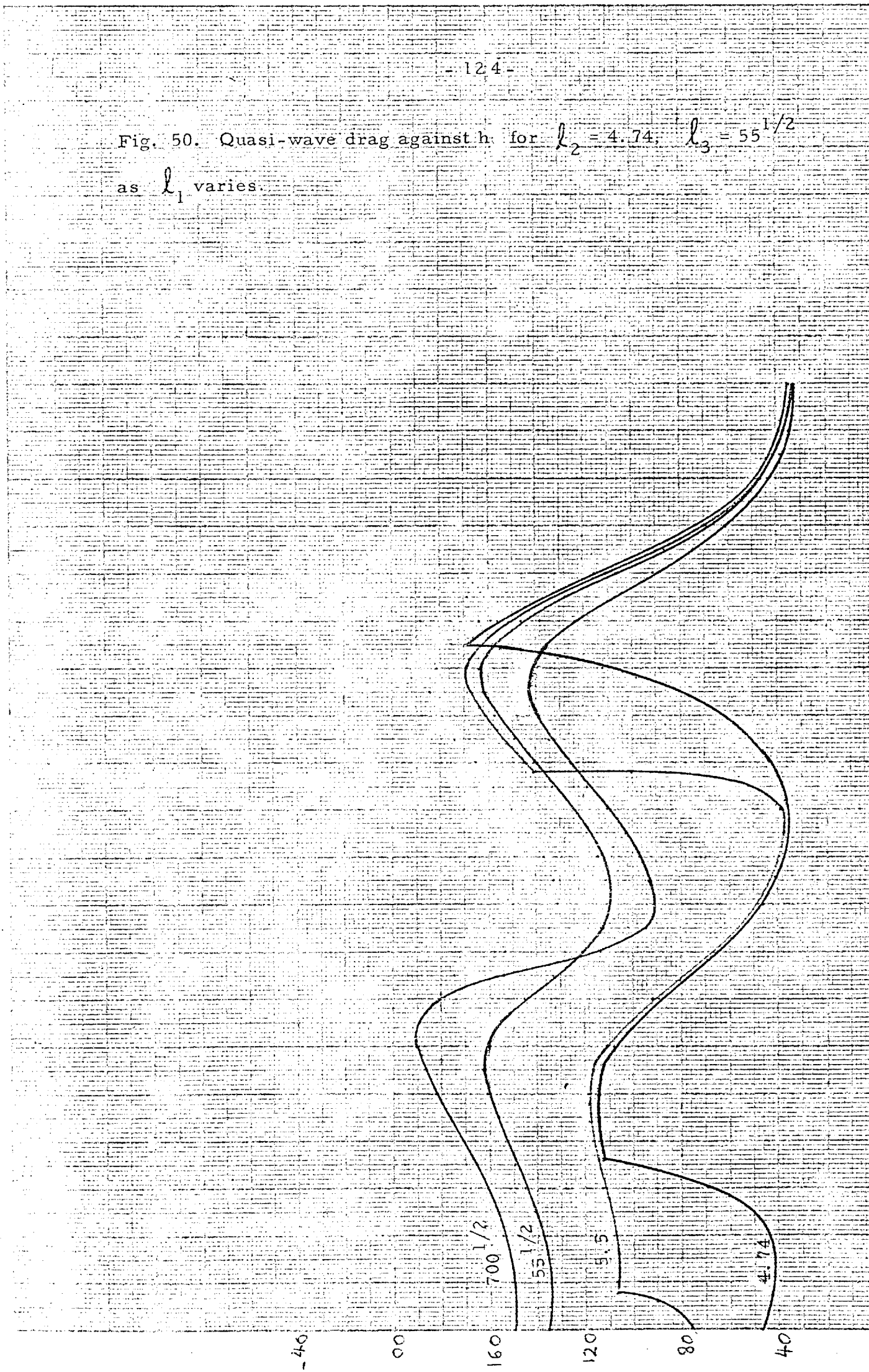

CHAPTER FOUR

A DISCUSSION OF THE ADAPTATION OF SOME REALISTIC ATMOSPHERIC PROFILES INTO LAYERS IN WHICH THE ℓ PARAMETER IS CONSTANT

1. Introduction

In this chapter we investigate some atmospheric profiles which have been observed and recorded on occasions when either a field study was in progress (section four), or when high winds caused considerable damage to ground structures, in regions close to the lee slopes of mountainous terrain (section two and three). It is of considerable interest to investigate whether these actual observed profiles of stability and wind speed (and hence the $\ell(z)$ profile), can be approximated by a more tractable model in which the Scorer parameter, ℓ, is constant in layers. If this is realistically feasible, then it is possible to predict which wavelengths can be expected under typical atmospheric conditions, and whether a critical wavelength which is in resonance with the mountain range will be produced.

An important feature of all three examples is the lee wavelength size which may be of order 40 Km. Another feature is the rate at which the waves decay downstream, so that only the front range lee slopes receive the full force of the gales experienced on critical days. The Rocky mountain range produce an almost two dimensional flow pattern in Colorado, although it is true that individual mountains and valleys in the range will produce distortion. This is slightly less true in Sheffield,

which is situated near the southern end of the Pennine chain. It is possible that edge effects distort the lee-wave picture which is discussed in the next section.

2. Gales in Yorkshire 1962

We consider as a first example gales which were present in Yorkshire, especially Sheffield, in 1962. Gales were present throughout the entire country in February, however, two gales on the twelfth and sixteenth were particularly severe to the east of the Pennines in the industrial West Riding. These gales were excpetionally strong in the vicinity of Sheffield on these two days. On the first day the winds averaged about 35 knots, with gusts of 69 knots, and on the second day gusts reached 84 knots. The gales were classed by C. J. M. Aanensen 1965 as being the once in fifty years case. However, wind speeds in other parts of the country away from the Pennine chain experienced gales which were considerably less severe than Sheffield.

The profiles of potential temperature and wind speed in the undisturbed airstream are shown in fig. 1, which is figure 31 in C. J. M. Aanensen. It is fortuitous that except for a shear layer near the ground, the velocity profile is nearly constant for all z. The condition that $U'(z)/U(z)$ is small was a necessary assumption in Chapter one in deriving the theory of Chapter two.

The gale of 12th February was less severe in the damage it caused than its counterpart on the 16th, when nearly two thirds of all the buildings in Sheffield had damage of one sort or another. In figure two, the l^2 profile is presented up to a height of 18 Km. (This appeared as fig. 32 in C. J. M. Aanensen.) The significant features of this l^2 profile are the pronounced maximum in the lower troposphere, the smaller values in the upper troposphere, and the assumed high-level stratospheric

values. We investigate the waves generated by two reduced three layer models in which the ℓ parameter is constant in each layer. These models are shown in figure two.

It must be noted that these parameters have dimensions of length (h) or length^{-1}, (ℓ), and it is necessary to non-dimensionalise these quantities, taking the height of the tropopause as a unit length. These values are shown in tables one and two. The first profile considers the tropopause to be at 14 Km with an intermediate tropospheric depth of 4 Km from the ground.

The lee wavenumbers are found by evaluating solutions to equation (1.6) of Chapter three which appear in the first quadrant of the complex wavenumber plane. A lee wavelength of 23.23 Km was obtained by this method. This is in good agreement with the calculation of Aanensen who predicted a lee-wavelength of 22.1 Km.

Aanensen's result was that an even longer wavelength of 38 km existed on 12th February when the ℓ profile was quite similar to that shown in figure two. A significant question can be asked which is: how sensitive is this model to small changes in the parameters? Figure three shows the locus of the principal Gamow pole for a change in h of about $10^{o}/o$. The importance of this figure is the increase of the imaginary part of the wavenumber which contributes to the decay rate of the wave, as h increases. When $h \approx 0.7$, corresponding to a lee-wavelength of 22.1 Km, the imaginary part of the wavenumber is about 1/7 of its value when h = 0.79 which corresponds to a lee-wavelength of 38 Km. This suggests that shorter wavelengths of the type observed on February 16th

will persist with greater intensity for distances downstream of the Pennines.

A second profile was taken to match the observed ℓ^2 profile. This is also shown in figure two. The tropopause is taken to be at 13 Km, and the tropospheric interface at 2.8 Km. A wavelength of 25.63 Km was computed for this model. Figure four shows the change in the Gamow pole as h changes by about $10^{o}/o$. Once again it was found that when h = 0.76, which corresponds to a lee-wavelength of 22.1 Km, the imaginary part of the Gamow pole is about 1/7 of its value when h = 0.86 which produces a wavelength of 38 Km.

The conclusion is that two differing models of an atmospheric profile predict results which are close to those observed to the east of the Pennines. The models also reveal how sensitive the parameters are to changes in the tropospheric profile.

3. Gales in Boulder 1972

Boulder, Colorado has many features in common with Sheffield. It is situated to the east of the continental divide which forms part of the Rocky Mountain chain, and is prone to strong, often hurricane force, winds. These winds usually substantially decrease only a few miles further downstream in the flat plane region near Denver.

On 11th January, 1972, a particularly severe windstorm hit northern Colorado and southern Wyoming. Peak gusts of over 100 mph were recorded in several districts of Boulder by anemometers. Luckily the development of this storm coincided with the readiness of two instrumented aircraft to fly over the windstorm region.

One of the aeroplanes took off on a mission to explore the lowest 10,000 feet of the atmosphere in the early afternoon, while the other took off at 5 pm. and explored the middle and upper troposphere. The resulting potential temperature field was plotted in Klemp and Lilly (1975) and Lilly and Zipser(1972). The significant feature of the temperature field is the existence of a heavily damped wave which has been compared with a hydraulic jump.

In figure five the ℓ profile is drawn as it was recorded on 11th January. The three layer approximation of constant ℓ in layers is also presented on this figure. It was found that two wavenumbers of importance existed in this layered model which were:

1. A non decaying real Scorer mode of wavenumber 10.249 with a wavelength of 6.74 Km. This is in good agreement with the observed result.
2. A heavily damped wave with a much longer wavelength of 48.10 Km.

The details of both these modes are summarised in table three.

Figure six reveals how sensitive the Gamow pole is to small changes in the depth of the lower troposphere, for the constant Scorer parameter values. As h changes from 0.55 to 0.62, the wavelength changes from approximately 15 Km to 138 Km. However, the Gamow pole imaginary part increases rapidly over the same range of h, and it is doubtful that the waves produced by this mode will have many oscillations, and can resemble a hydraulic jump, depending on whether the wave is in phase with the mountain or out of phase. A comparison of the hydraulic jump theory and the damped wave theory is discussed in Klemp and Lilly (1975). It was concluded that the dominant feature of the long downdraft region was caused by heavily damped waves.

4. The Colorado Lee-Wave Program 1968

A significant study of the lee-wave phenomenon was conducted at the National Centre for Atmospheric Research over a period of two winters. The zenith of this was reached in February 1968 when a joint flight program collected data on lee-waves and associated turbulence phenomena from the surface to 70, 000 feet above the Rocky Mountain terrain. The most significant result of the program was to find large amplitude standing gravity waves in the stratospheric levels.

Figure seven shows the atmospheric profile for ℓ recorded on February 15th, 1968. We approximate the profile by a two layer troposphere, and a stratosphere which is very stable. One would expect the wavenumbers for this ℓ profile to be near the real value obtained when ℓ_1 is infinite (the rigid tropopause model of Chapter two). The principal wavenumber is k = (3. 654, 0. 063) while the eigenvalue for the rigid lid case is 3. 631. This gives rise to a wavelength of 18. 23 kilometres. It would appear that this result is in some error, as Vergeiner (1971) and Lilly and Toutenhoofd(1969)have obtained a value of about 14 Km.

In figure eight the effect of changing the mid tropospheric depth by about $10^{o}/o$ is investigated. The Gamow pole changes less than its counterpart of section three, and in figure eight, the wavelength varies between about 17. 3 km and 19. 5 km. This suggests that an error may be introduced by taking ℓ_1 to be this large in figure seven as the atmospheric profile above 13 Km is undetermined. However, the significance of our investigation is that a long wavelength does exist in the simplified model of the atmosphere.

5. Conclusion

The three examples which have been described in sections two, three and four, reveal that long wavelengths of twenty or thirty km, can exist in an atmosphere with considerable amplitude close to the leeward slopes of the mountain ridge. These lee waves, when we identify them with their model counterpart, consist of waves internal to all three layers. In many cases these dominant wavelengths are critically dependent on the atmospheric parameters, so that a small change in the tropospheric profile can produce a large change in the lee-wavelengths. A significant feature of these waves is that they fail to penetrate to any great distance downstream of the mountain range, since their decay rate is large, and the most that can realistically be expected is two strips of land in which high surface winds exist, with a strip of relative calm in between. Such was the case of section two, as reported by C. J. M. Aanensen 1965. However, this second region of stronger winds was much less pronounced than the first.

A further consideration must be given to the mountain shape. Only wavelengths which are nearly multiples of resonant wavelengths will be excited to a large amplitude. In Sheffield (section two) a basic wavelength close to twenty km was observed to cause devastating damage on February 16th, whereas damage to a lesser extent was caused some days earlier by a wavelength which was nearly twice this size. It is reasonable to suppose that on a day which produces lee-wavelengths in between these two resonances, that their effects will be quite small.

TABLE 1

DIMENSIONALISED VALUES OF PARAMETERS FOR MODEL INTRODUCED IN FIG. 2

Wavelength	ℓ_1	ℓ_2	ℓ_3	Tropopause	h (above ground)
23.23 Km	$\sqrt{0.5}$ Km^{-1}	$\sqrt{0.05}$ Km^{-1}	$\sqrt{0.3}$ Km^{-1}	14 Km	4 Km

NON DIMENSIONALISED VALUES

Wavenumber	ℓ_1	ℓ_2	ℓ_3	Tropopause	h
(3.387, .035)	Sqrt(98.0)	Sqrt(9.8)	Sqrt(58.8)	1	0.714

TABLE 2

DIMENSIONALISED VALUES OF PARAMETERS FOR MODEL IN FIG. 2

Wavelength	ℓ_1	ℓ_2	ℓ_3	Tropopause	h (above ground)
25.63 Km	$\sqrt{0.5}$ Km^{-1}	$\sqrt{0.075}$ Km^{-1}	$\sqrt{0.4}$ Km^{-1}	13 Km	2.8 Km

NON DIMENSIONALISED VALUES

Wavenumber	ℓ_1	ℓ_2	ℓ_3	Tropopause	h
(3.187, .115)	$\sqrt{84.5}$	$\sqrt{12.665}$	$\sqrt{67.6}$	1	0.785

TABLE 3

DIMENSIONALISED VALUES OF PARAMETERS FOR MODEL OF FIG. 5

Wavelength	ℓ_1	ℓ_2	ℓ_3	Tropopause	h (above ground)
6.74 Km and 48.10 Km	0.68 Km^{-1}	1.755 Km^{-1}	1.1 Km^{-1}	11 Km	4.4 Km

NON DIMENSIONALISED VALUES

Wavenumber	ℓ_1	ℓ_2	ℓ_3	Tropopause	h
(10.249, 0) and (1.437, 0.374)	7.48	1.93	12.1	1	0.6

TABLE 4

DIMENSIONALISED VALUES OF PARAMETERS FOR MODEL OF FIG. 7

Wavelength	ℓ_1	ℓ_2	ℓ_3	Tropopause	h (above ground)
18.21 Km	1.0 Km^{-1}	0.2 Km^{-1}	0.5 Km^{-1}	10.6 Km	5.76 Km

NON DIMENSIONALISED VALUES

Wavenumber	ℓ_1	ℓ_2	ℓ_3	Tropopause	h
(3.654, 0.063)	10.6	2.12	5.3	1	0.4

Fig. 1

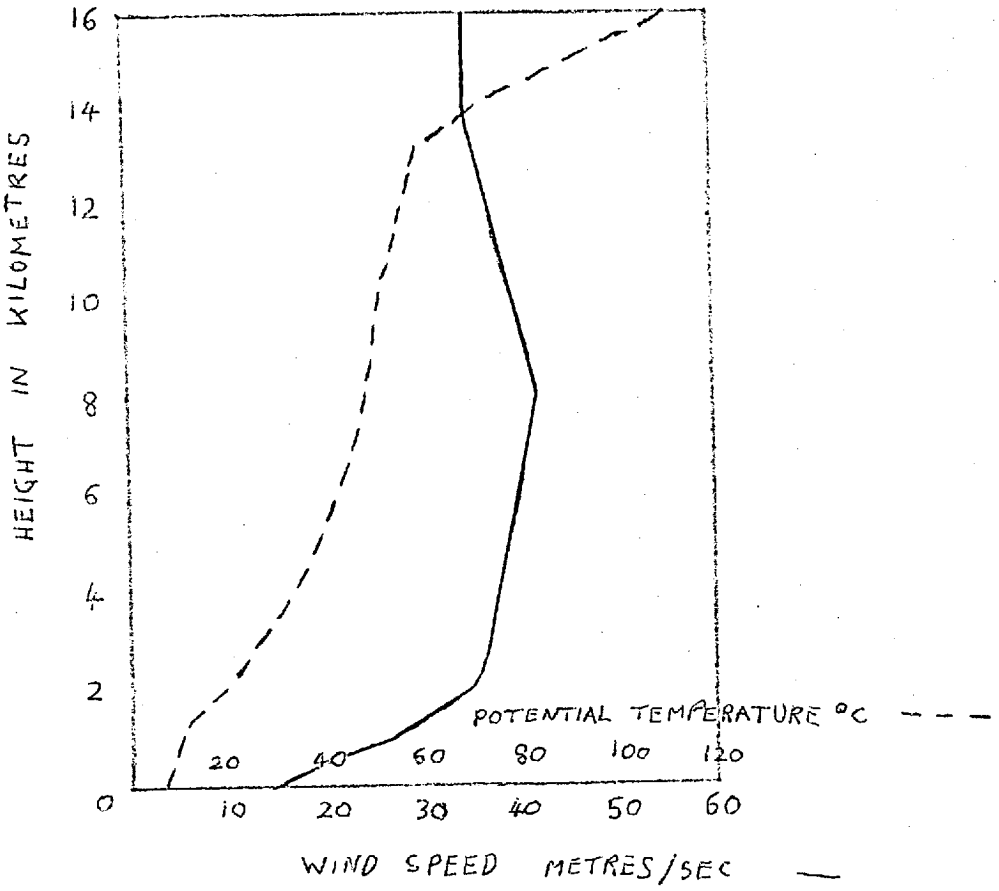

The profiles of potential temperature and wind speed in the undisturbed airstream appropriate to flow over the Pennines in the vicinity of Sheffield at about 0500 GMT, 16 February 1962.

Fig. 2

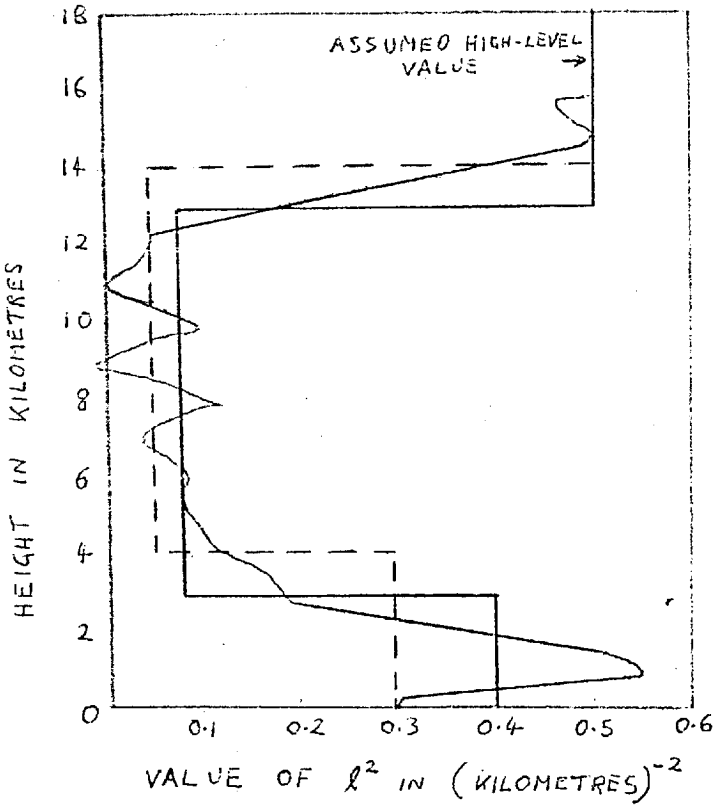

The profile of l^2 based on Aughton Radiosonde and wind data for 16th February, 1962, together with two layerwise constant profiles which approximate the solution.

Fig. 3. The locus of the Principal Gamow pole as h varies for the first layered model of fig. 2. See table I for details.

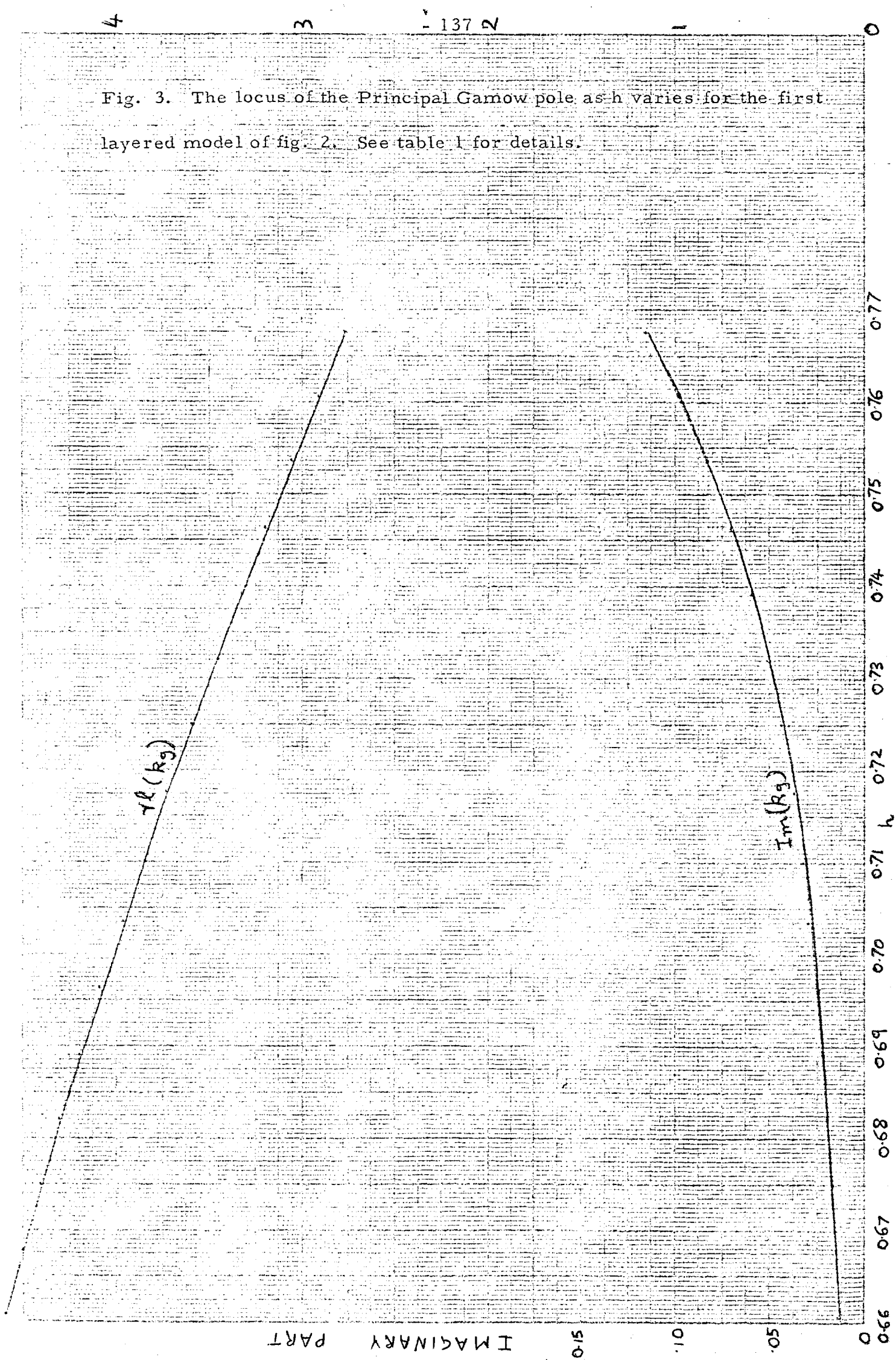

Fig. 4. The locus of the Principal Gamow pole as h varies for the second layered model of fig. 2. See table 2 for details.

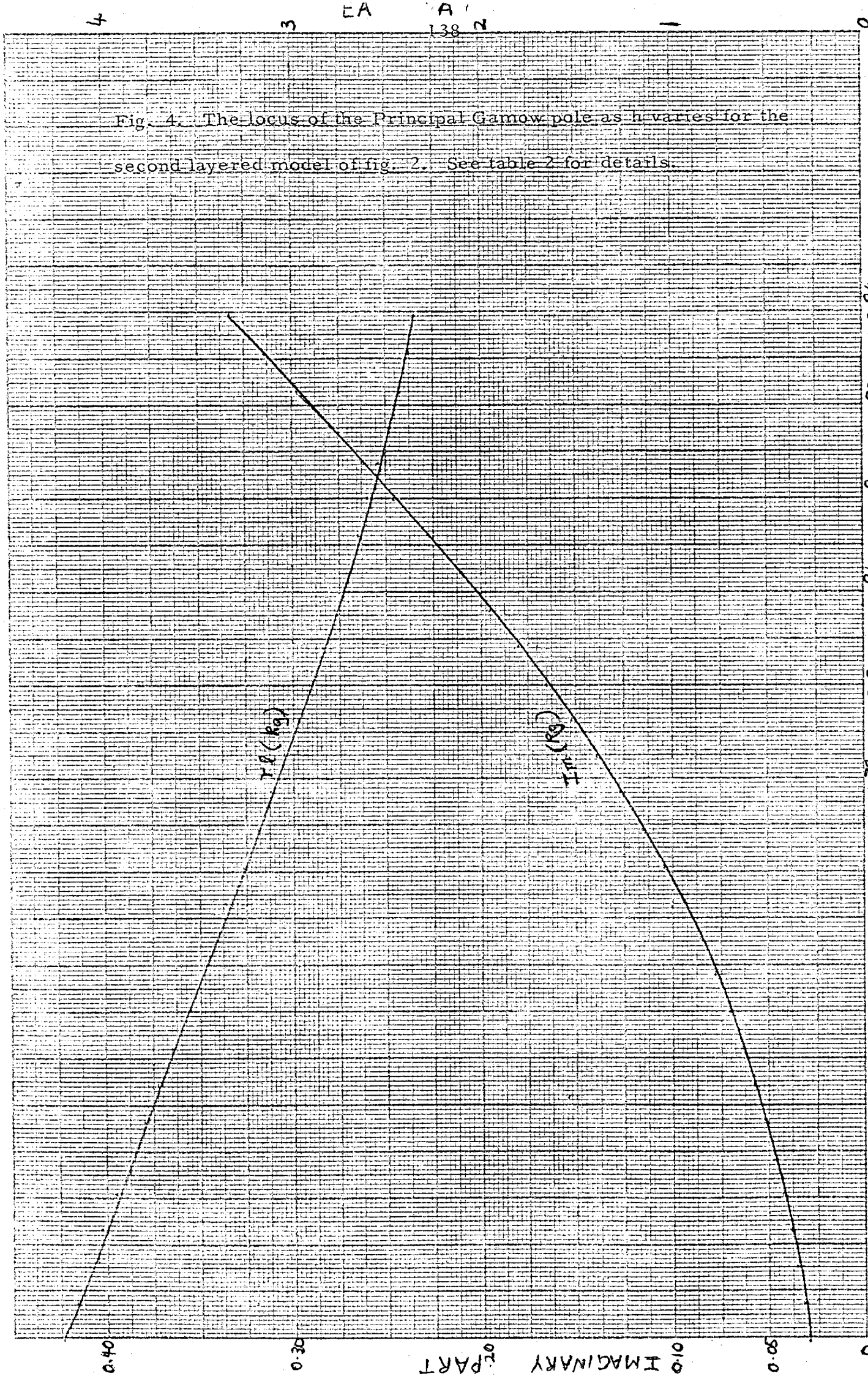

Fig. 5

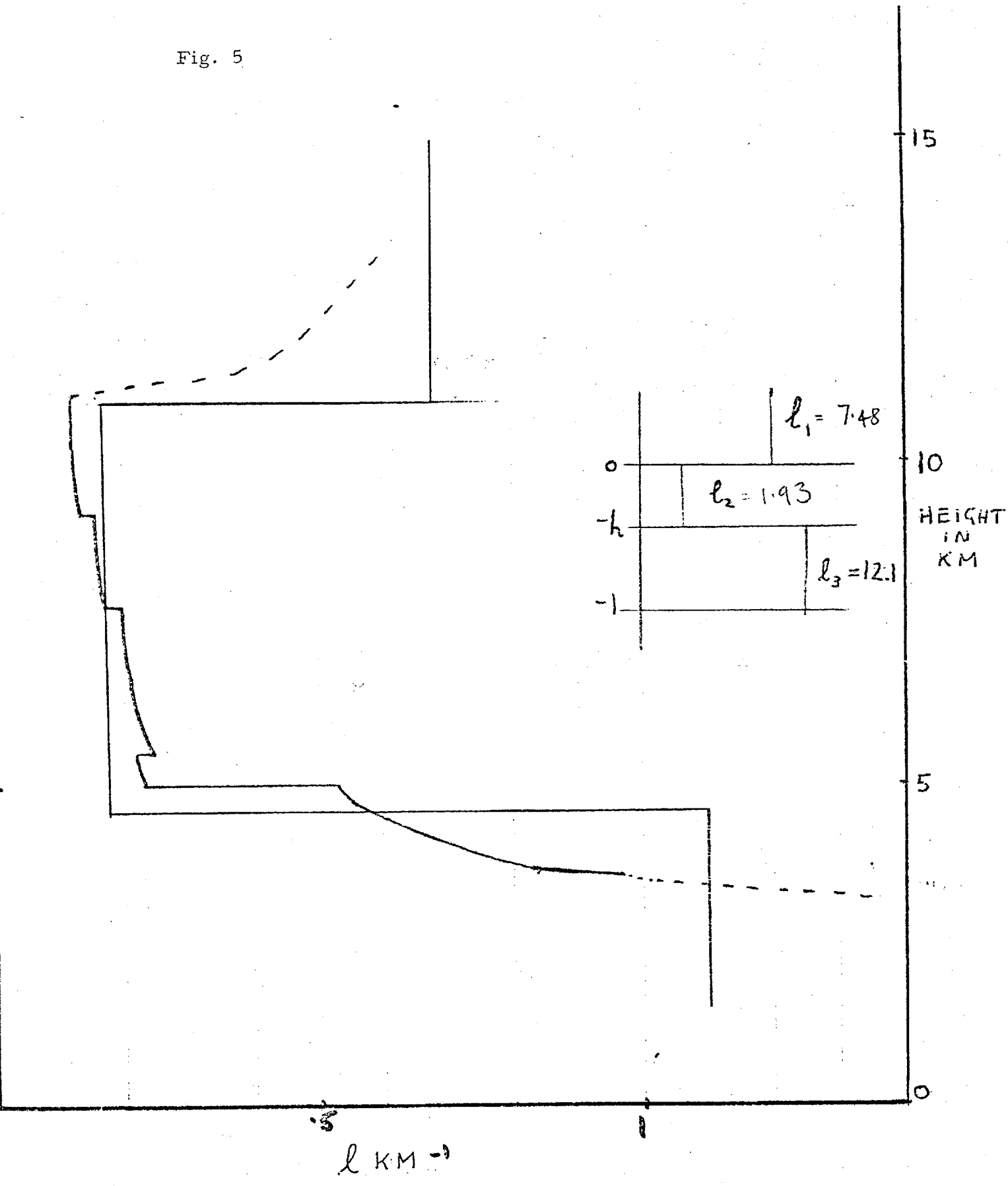

The ℓ profile for the conditions at Boulder on Jan. 11 1972, together with a layered approximation to the atmospheric profile.

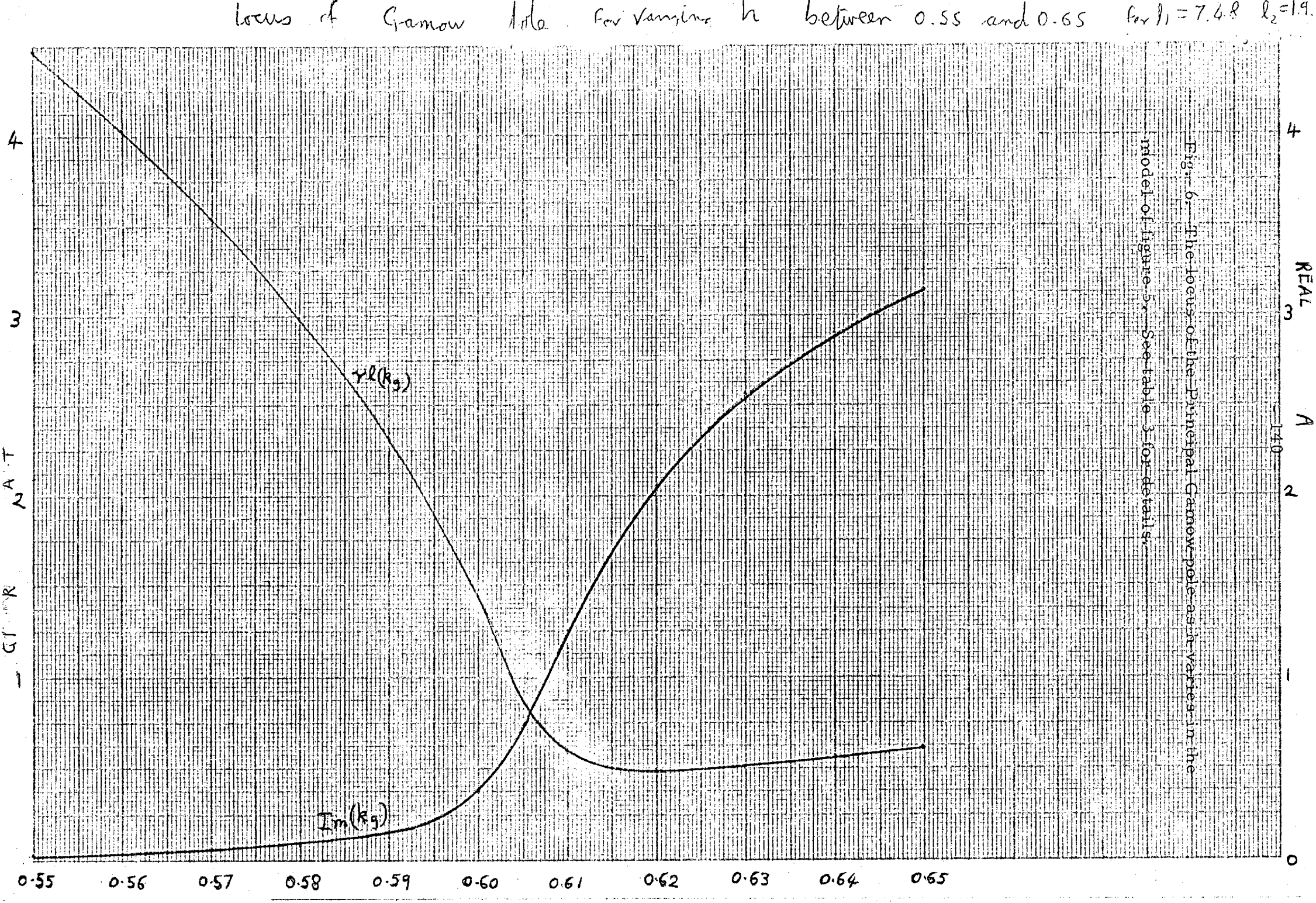

Fig. 6—The locus of the Principal Gamow pole as h varies in the model of figure 5. See table 3 for details.

Fig. 7. The ℓ profile for the conditions of Feb. 15th, 1968 in Colorado, together with an approximation to the atmospheric profile.

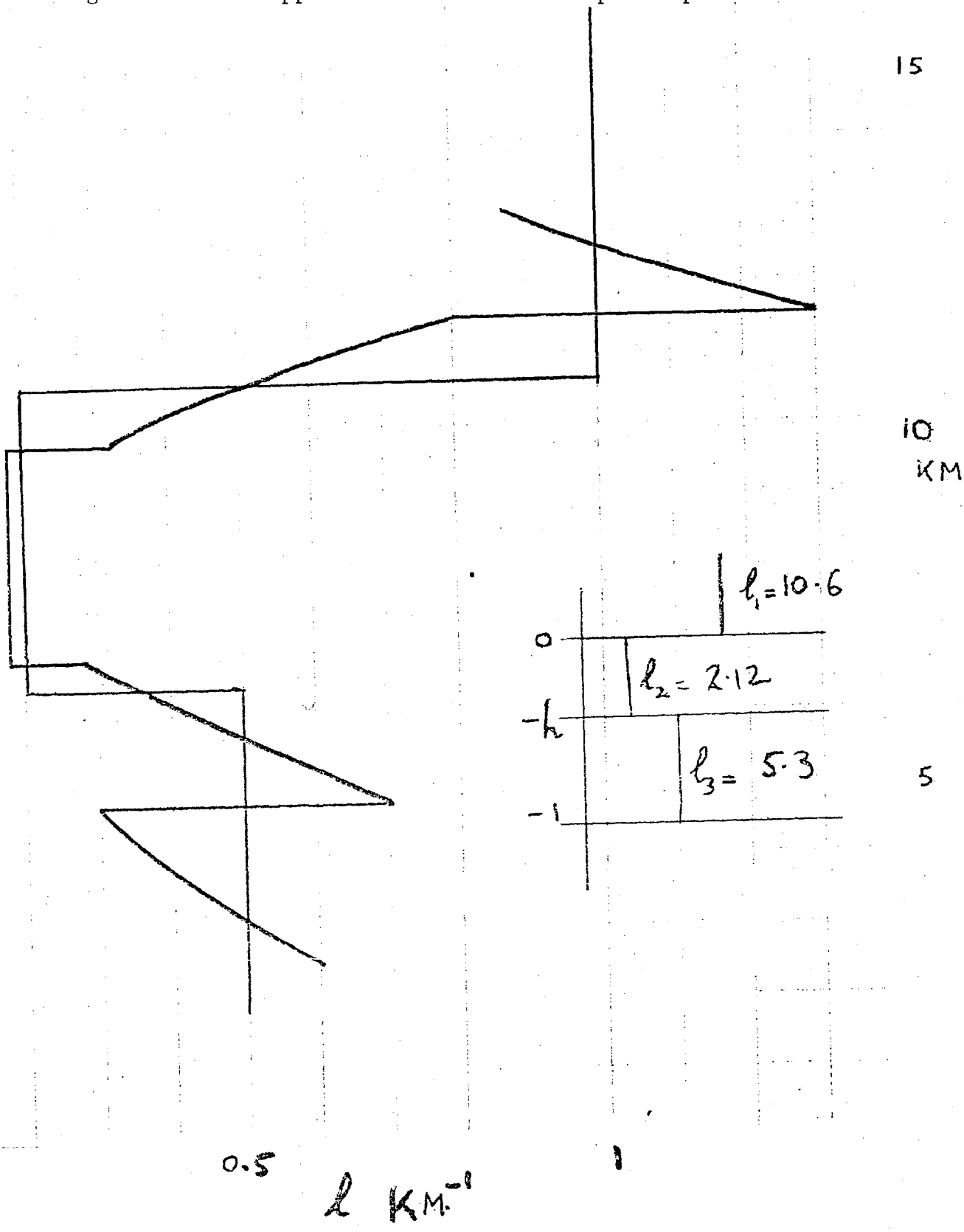

Fig. 8. The locus of the Principal Gamow pole as h varies in the model of figure 7. See table 4 for details.

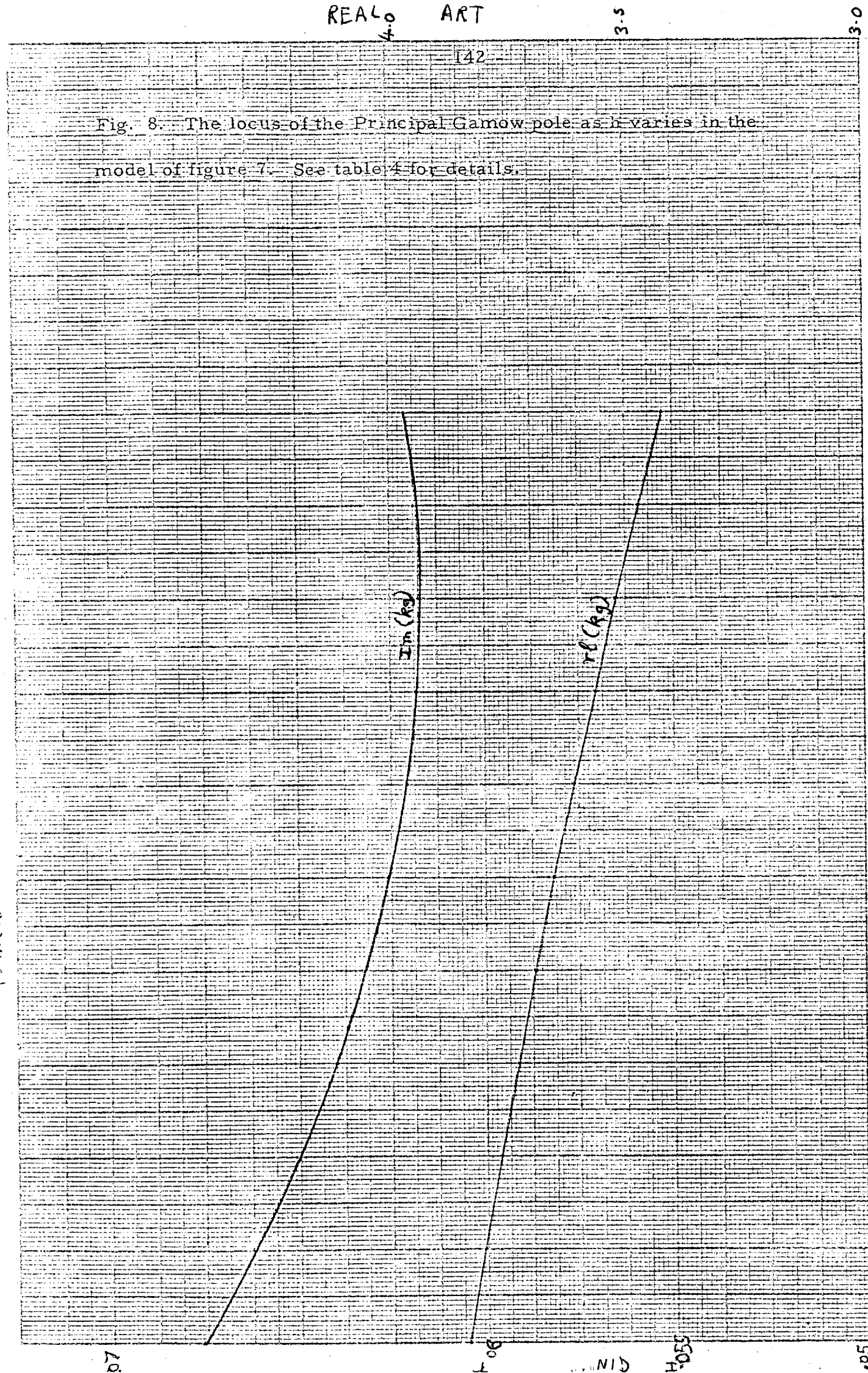

REFERENCES

Aanensen, C. J. M., 1965, Gales in Yorkshire in February 1962. Meteorological Office, Geophys. Mem., 14, pp1-44.

Berkshire, F. H. and Warren, F. W. G., 1970. Some aspects of linear lee wave theory for the stratosphere. Quart. J. R. Met. Soc. 96, pp50-66.

Berkshire, F. H., 1970. Lee waves in the stratosphere, Ph. D. Thesis, London University.

Berkshire, F. H., 1975. Two-dimensional linear lee wave modes for models including a stratosphere. Quart. J. R. Met. Soc. 101, pp259-266.

Corby, G. A. and J. S. Sawyer, 1958. The air flow over a ridge - the effects of the upper boundary and high level conditions. Quart. J. R. Met. Soc. 84 pp25-37.

Holmboe, J. and H. Klieforth, 1957. Investigation of mountain lee waves and the air flow over the Sierra Nevada, Department of Meteorology, University of California, Los Angeles.

Kelvin, Lord. 1886, 1887, On stationary waves in flowing water, Mathematical and Physical Papers Vol. IV, Cambridge University Press, 1910, pp270-302.

Klemp, J. B. and D. K. Lilly, 1975, The dynamics of wave-induced downslope winds, J. At. Sciences Vol. 32, number 2, pp320-339.

Lilly, D. K. and W. Toutenhoofd, 1969, The Colorado lee wave program, clear air turbulence and its detection edited by Yih-Ho Pao and A. Goldburg, pp232-245.

Lilly, D.K. and E. J. Zipser, 1972, The front range windstorm of 11th January 1972 - a meteorological narrative, Weatherwise, 25, pp56-63.

Lyra, G., 1943, Theorie der stationaren leewellenstromung in freier Atmosphare, Z. angew. Math. Mech. 23, pp1-28.

Miles, J. W., 1961, On the stability of heterogeneous shear, J. Fluid Mech. 10, pp496-508.

Miles, J. W., 1969, Waves and wave drag in stratified flows, Applied Mechanics. Proceedings of the Twelfth International Congress of Applied Mechanics, Stanford University, August 26-31, 1968.

National Bureau of Standards, 1964. Elementary transcendental functions, App. Mathematics Series, 55.

Nicholls, J. M., 1973, The airflow over Mountains, Research 1958-1972, Geneva. World Meteorological Organization Tech. Note 127.

Queney, P., 1947, Theory of perturbations in stratified currents with application to airflow over mountain barriers. The University of Chicago Press, Misc. Rept. No. 23.

Queney, P. and G. Corby, N. Gerbier, H. Koschmieder and J. Zierep, 1960. The airflow over mountains. Geneva: World Meteorological Organization, Tech. Note 34.

Rayleigh, Lord, 1883, The form of standing waves on the surface of running water, Scientific Papers Vol. II 1881-1887, Cambridge University Press 1900, pp258-267.

Sawyer, J. S. 1959, The introduction of the effects of topography into methods of numerical forecasting, Quart. J. R. Met. Soc. 85, pp31-43.

Sawyer, J. S. 1960, Numerical calculation of the displacements of a stratified airstream crossing a ridge of small height. Quart. J. R. Met. Soc. 86, pp326-345.

Scorer, R. S., 1949. Theory of waves in the lee of mountains, Quart. J. R. Met. Soc. 75, pp41-56.

Scorer, R. S., 1953, Theory of airflow over mountains II, The flow over a ridge. Quart. J. R. Met. Soc. 79, pp70-83.

Scorer, R. S., 1955, Theory of non-horizontal adiabatic flow in the atmosphere, Quart. J. R. Met. Soc. 81, pp551-561.

Scorer, R. S., 1954, Theory of airflow over mountains III - Airstream characteristics, Quart. J. R. Met. Soc. 80, pp417-428.

Scorer, R. S., 1956, Airflow over an isolated hill, Quart. J. R. Met. Soc. 82, pp75-81.

Scorer, R. S. 1958, Airflow over mountains: indeterminacy of solutions, Quart. J. R. Met. Soc. 84, pp182-183. and pp465-466.

Vergeiner, I. 1971, An operational linear lee wave model for arbitrary basic flow and two-dimensional topography. Quart. J. R. Met. Soc. 97, pp30-60.